

## ABSTRACT

Title of Document:

PROBABILISTIC MODELS FOR  
CREEP-FATIGUE IN A STEEL ALLOY

Fatmagul Ibisoglu, Master of Science, 2013

Directed By:

Professor Mohammad Modarres  
Department of Mechanical Engineering

In high temperature components subjected to long term cyclic operation, simultaneous creep and fatigue damage occur. A new methodology for creep-fatigue life assessment has been adopted without the need to separate creep and fatigue damage or expended life. Probabilistic models, described by hold times in tension and total strain range at temperature, have been derived based on the creep rupture behavior of a steel alloy. These models have been validated with the observed creep-fatigue life of the material with a scatter band close to a factor of 2. Uncertainties of the creep-fatigue model parameters have been estimated with WinBUGS which is an open source Bayesian analysis software tool that uses Markov Chain Monte Carlo method to fit statistical models. Secondly, creep deformation in stress relaxation data has been analyzed. Well performing creep equations have been validated with the observed data. The creep model with the highest goodness of fit among the validated models has been used to estimate probability of exceedance at 0.6% strain level for the steel alloy.

# PROBABILISTIC MODELS FOR CREEP-FATIGUE IN A STEEL ALLOY

By

Fatmagul Ibisoglu

Thesis submitted to the Faculty of the Graduate School of the  
University of Maryland, College Park, in partial fulfillment  
of the requirements for the degree of  
Master of Science  
2013

Advisory Committee:  
Professor Mohammad Modarres, Chair  
Professor Aris Christou  
Professor F.Patrick McCluskey

© Copyright by  
Fatmagul Ibisoglu  
2013

## Acknowledgements

Firstly, I would like to thank **Fulbright Program** for giving me the rare privilege of being sponsored for a second graduate degree in the United States.

I would like to thank the **Faculty of Graduate Studies, University of Maryland – College Park** for awarding me a graduate fellowship to pursue my graduate study in Reliability Engineering program.

I would like to express my sincere gratitude to my advisor **Prof. Mohammad Modarres**, for his invaluable guidance, academic support and financial assistance throughout my thesis work.

My sincere thanks to **M. Nuhi Faridani, Gary Paradee** and **Victor L. Ontiveros** for training me on instruments in the Modern Engineering Materials Instructional as well as in the Mechanics and Reliability Laboratory and providing me with valuable suggestions during the course of my thesis. I would like to thank **Mehdi Amiri** for his help during my testing. Additionally, I would like to thank my Fulbright Fellow **Sevki Cesmec**i for his technical help in my thesis work.

I would like to thank **Prof. Patrick. F. McCluskey** and **Prof. Aris Christou** for taking time off from their busy schedules and serving on my committee.

I duly acknowledge to all authors - especially to **Dr. Stefan Holmstrom** from VTT Technical Research Centre of Finland - whose literature has been cited in the study and to all those who have been referred to in the study. These references have been of immense help and provided in depth understanding of work.

Last, but not the least, my very special thanks to **my family and friends** for their constant support and encouragement during my graduate study.

# Table of Contents

Acknowledgements.....	ii
Table of Contents.....	iii
List of Tables .....	vi
List of Figures .....	vii
List of Symbols .....	xi
Chapter 1: Introduction .....	1
1.1 Background.....	1
1.2 The Scope of The Thesis.....	4
1.3 Thesis Organization .....	6
1.4 References.....	7
Chapter 2: Literature Review.....	9
2.1 Introduction.....	9
2.2 Factors Affecting CF Life of Materials .....	9
2.2.1 Microstructural Composition .....	9
2.2.1.1 Microstructural Composition .....	9
2.2.1.2 Carbon Content .....	10
2.2.1.3 Effect of Heat Treatments on Ductility.....	10
2.2.2 Waveform and Frequency.....	11
2.2.3 Environemntal/Service Factors .....	11
2.2.4 Complex Loading Path Histories .....	12
2.2.5 Classical Creep Damage (voidage).....	12
2.2.5.1 Creep Curve .....	13
2.2.5.2 Creep Characteristics .....	15
2.3 Published Studies on CF Expended Life Assesment of Materials.....	17
2.4 Published Studies on Creep in Cyclic Relaxation Response .....	24
2.5 Thesis Objective.....	26
2.6 References.....	27
Chapter 3: Models for CF and Creep in Cyclic Relaxation Response in a Steel Alloy..	29
3.1 Introduction.....	29
3.2 Models for CF in Steels and Alloys.....	31
3.2.1 Loading Sequence Dependent CF Expended Life Model.....	34
3.2.1.1 Sequential CF Loading .....	34
3.2.1.1.1 Linear damage summation .....	34
3.2.1.1.2 Strain range partitioning .....	36
3.2.1.1.3 Frequency modified approach.....	37
3.2.1.1.4 Damage rate model .....	38
3.2.1.1.5 Damage function method .....	39
3.2.1.1.6 Viscosity based model .....	41
3.2.1.1.7 Statistical thermal CF models .....	44
3.2.1.1.7.1 Low cycle thermal fatigue	
models .....	44
3.2.1.1.7.2 Leading creep rupture models	46

	3.2.1.1.7.3 Combining Fatigue and Creep .....	50
Damages		
	3.2.1.2 Simultaneous CF Loading.....	51
	3.2.1.2.1 Fii [ $\phi$ ] Model.....	51
Life Models	3.2.2 Case/Research Specific Alternate Approaches to CF Expended .....	52
	3.2.2.1 Generic Equation .....	53
	3.2.3 CF expended life models when cyclic material data is not available or not enough .....	58
	3.2.3.1 Sequential CF loading.....	58
	3.2.3.2 Simultaneous CF loading .....	58
	3.2.4 Modified Robust Models for CF.....	58
	3.2.4.1 Comparisons of Modified Leading Models .....	60
	3.3 Creep Models in Cyclic Relaxation Response under CF Conditions .....	62
CF Conditions	3.3.1 Applicable Creep Models in Cyclic Relaxation Response under .....	65
	3.3.2 Comparisons of Modified Robust Models .....	68
	3.4 References.....	69
Chapter 4: Experimental Details .....		75
	4.1 Introduction.....	75
	4.2 Experimental Details.....	75
	4.2.1 Material .....	79
	4.2.2 Tensile Test.....	82
	4.2.3 1D Uniaxial C Test .....	84
	4.2.3.1 Rationale for Selection of CF Parameters.....	87
	4.2.3.2 1D Uniaxial CF Test Results .....	93
	4.3 References.....	99
Chapter 5: Estimation of empirical Parameters using Bayesian Inference .....		101
	5.1 Introduction.....	101
	5.2 Estimation of Empirical Model Parameters Using Bayesian Inference.....	104
	5.2.1 Soviet Model.....	106
	5.2.2 Larson Miller Model .....	109
	5.2.3 Orr-Sherby Dorn Model.....	113
	5.2.4 Manson-Haferd Model .....	117
	5.2.5 Wilshire Model .....	121
	5.3 References.....	125
Chapter 6: Assessment of CF and Creep in Cyclic Relaxation .....		127
	6.1 Introduction.....	127
	6.2 CF Expended Life Curves.....	128
	6.2.1 Soviet Model.....	128
	6.2.2 Larson-Miller Model.....	130
	6.2.3 Orr-Sherby Dorn .....	131
	6.2.4 Manson Haferd Model .....	133
	6.2.5 Wilshire Model [Fii ( $\phi$ ) Model].....	134
	6.2.6 Comparisons of CF Life Models.....	136

6.3	Assessment of Creep Activation Energy of Test Material.....	138
6.4	Assessment of Creep under CF Condition.....	139
6.4.1	Creep in Cyclic Relaxation Response under CF Conditions .....	140
6.4.2	Probability of Exceedance Estimation at Strain 0.6% [mm/mm] ..	142
6.4.3	Damage Assessment in CF .....	144
6.4.4	Remaining Useful Life in Deterministic Framework .....	145
6.5	References.....	147
Chapter 7:	Conclusions and Recommendations for Future Work .....	147
7.1	References.....	152
Appendix A-I:	Thermocouple Clip Design Process .....	154
Appendix B-I:	Epoxy Mold Design Process.....	155
Appendix C-I:	WINBUGS Codes for Soviet Model .....	156
Appendix C-II:	WINBUGS Codes for Larson Miller Model .....	157
Appendix C-III:	WINBUGS Codes for Orr Sherby Dorn Model.....	158
Appendix C-IV:	WINBUGS Codes for Manson Haferd Model.....	159
Appendix C-V:	WINBUGS Codes for Wilshire Model .....	160
Appendix D-I:	WINBUGS Chain History for Soviet Model.....	161
Appendix D-II:	WINBUGS Chain History for Larson Miller Model .....	162
Appendix D-III:	WINBUGS Chain History for Orr Sherby Dorn Model .....	163
Appendix D-IV:	WINBUGS Chain History for Manson Haferd Model .....	164
Appendix D-V:	WINBUGS Chain History for Wilshire Model .....	165
Bibliography	.....	166

## List of Tables

Table 1.1: Survey indicated summary of wave form usage for creep-fatigue testing ..	5
Table 3.1: Review of creep-fatigue assessment methods in literature.....	33
Table 3.2: Relation between temperature and other parameters .....	45
Table 3.3: Robust creep rupture models in literature.....	46
Table 3.4: Published creep models that describe the whole creep curve from primary (P) to secondary (S) and tertiary part for 10Cr-Mo (9-10) steel alloys .....	66
Table 3.5: AIC values from comparison of different creep models for the given experimental data .....	68
Table 4.1: Standards used for specimen design and parameters of experimental tests	76
Table 4.2: EDS chemical composition results .....	80
Table 4.3: Expected time to failures based on the Larson-Miller and Wilshire formulas and equivalent test stress range.....	87
Table 4.4: Summary of test parameters for 3 Fatigue-Creep Tests .....	89
Table 5.1: Data used for prediction of Wilshire Model for the test material.....	122
Table 6.1: Soviet Model Bayesian parameters and their coefficient of variation.....	129
Table 6.2: Larson-Model Model Bayesian parameters and their coefficient of variation .....	130
Table 6.3: Orr-Sherby Dorn Bayesian parameters and their coefficient of variation	132
Table 6.4: Manson Haferd Model Bayesian parameters and their coefficient of variation .....	133
Table 6.5: Wilshire Bayesian parameters and their coefficient of variation.....	135
Table 6.6: Activation energies for different hold-times at 675.15°K(400°C).....	139
Table 6.7: Probability of exceedance at strain 0.6% [mm/mm] for different times at CF test#3 (21min hold time) .....	144
Table 6.8: Cumulative creep damage in each creep-fatigue for 21min hold time creep-fatigue test#3 .....	144
Table 6.9: Basic details of the service-aged secondary superheater .....	146

## List of Figures

Figure 1.1: Structure of thesis .....	6
Figure 2.1: Typical creep curves showing the 3-stages of creep .....	14
Figure 2.2: Effect of applied stress on a creep curve at constant temperature.....	16
Figure 3.1: Methodology for assessing integrity of structural components that operate at high temperatures. TMF, thermo-mechanical fatigue; NDE, nondestructive evaluation; LCF, low-cycle fatigue; HCF, high-cycle fatigue.....	30
Figure 3.2: Three classes of creep-fatigue life fraction models.....	31
Figure 3.3: Loading sequence dependent creep-fatigue expended life model.....	32
Figure 3.4: Case/research specific alternate approaches to creep-fatigue extended life models .....	32
Figure 3.5: Creep-fatigue extended life models when cyclic material data is not available .....	33
Figure 3.6: Normalized reference stress $\phi$ (Fii) as a function of $t_{CF}$ for 316FR at 550 °C .....	60
Figure 3.7: Creep-fatigue model $R^2$ for 316FR at 550 °C .....	61
Figure 3.8: Generic schematic of strain and stress history for a fully reversed strain cycle with hold time at maximum tensile strain .....	61
Figure 3.9: Stress relaxation curves at three test temperatures in a $\pm 2.5\%$ total strain range .....	65
Figure 3.10: $R^2$ results for creep deformation in stress relaxation curves at 813 °K test temperature temperatures in a $\pm 2.5\%$ total strain range .....	69
Figure 4.1: Dimensions by ASTM E8/E8M-11 .....	76
Figure 4.2: Rounded dog-bone sample and rounded dog-bone sample placed in particularly designed 316 stainless steel grips .....	77
Figure 4.3: (a) Designed 316 stainless steel grips for rounded dog-bone samples; (b) a view from tension testing of a rounded dog-bone sample which is fixed on 647 Hydraulic Grips together with the particularly designed 316 stainless steels .....	78
Figure 4.4: Creep furnace setup with thermocouples, and copper coil coolers; 316 stainless steel thermocouple clip attached to test specimen inside the creep furnace	78
Figure 4.5: Power supply unit of home-made creep furnace used to control the furnace temperature .....	79
Figure 4.6: Automated polishing to provide a mirror-like quality on encapsulated metal pieces .....	80
Figure 4.7: Encapsulated 7x7 mm piece for EDS analysis after polishing.....	80
Figure 4.8: (a) AFM picture of raw material surface in nanometer scale, (b) SEM picture (1000x) of raw material surface in micrometer scale .....	81
Figure 4.9: (a) Fractured tensile specimen, (b) Dispersion of elements on the fractured sample surface under SEM microscope.....	81
Figure 4.10: (a) SEM picture for surface topography of 5min immersed steel alloy, and (b) SEM picture of 15min immersed steel alloy .....	82
Figure 4.11: MTS 810 test machine software and tension test inputs .....	83

Figure 4.12: Tension test result in room temperature for the steel alloy .....	83
Figure 4.13: (a) Ruptured dog-bone sample, and (b) Ductile cup and cone form of ruptured cross-section of the steel alloy.....	84
Figure 4.14: SEM pictures of the fracture surface of the uni-axial tensile test sample (a) at 35x and (b) at 1000x showing the presence of surface pores.....	84
Figure 4.15: (a) ASTM E2714-09 creep-fatigue cycle shape: cycle with hold time at control parameter peak in tension; (b) Adjusted creep-fatigue cycle shape according to the available dog-bone sample design .....	86
Figure 4.16: Creep-fatigue test setting in Reliability and Mechanics lab.....	86
Figure 4.17: Strain controlled creep-fatigue test cycle with stress Ratio = 0, and Instron Dynamic Software Wave Matrix program steps. Step1 (tension), step2 (hold) and step 3(release) .....	90
Figure 4.18: Instron Dynamic Software WaveMatrix creep-fatigue test inputs: Step1.. .....	91
Figure 4.19: Instron Dynamic Software WaveMatrix creep-fatigue test inputs: Step2.. .....	91
Figure 4.20: Instron Dynamic Software WaveMatrix creep-fatigue test inputs: Step3.. .....	92
Figure 4.21: Instron Dynamic Software WaveMatrix test monitoring options .....	92
Figure 4.22: ASTM standard E2714-09 end-of-test criterion based on reduction of peak stress for softening materials.....	93
Figure 4.23: Stress-strain hysteresis diagram for all cycles in 600 seconds hold time creep-fatigue test in $673.15^{\circ}K(400^{\circ}C)$ .....	94
Figure 4.24: Strain-cycle to failure diagram for all cycles in 600 seconds hold time creep-fatigue test in $673.15^{\circ}K(400^{\circ}C)$ .....	94
Figure 4.25: Stress-cycle to failure diagram for all cycles in 600 seconds hold time creep-fatigue test in $673.15^{\circ}K(400^{\circ}C)$ .....	95
Figure 4.26: Strain-cycle to failure for all cycles in 840 seconds hold time creep-fatigue test in $673.15^{\circ}K(400^{\circ}C)$ .....	95
Figure 4.27: Stress-cycle to failure diagram for all cycles in 840 seconds hold time creep-fatigue test in $673.15^{\circ}K(400^{\circ}C)$ .....	96
Figure 4.28: Strain-cycle to failure diagram for all cycles in 1260 seconds hold time creep-fatigue test in $673.15^{\circ}K(400^{\circ}C)$ .....	96
Figure 4.29: Stress-cycle to failure diagram for all cycles in 1260 seconds hold time creep-fatigue test in $673.15^{\circ}K(400^{\circ}C)$ .....	97
Figure 4.30: Test sample before and after CF test showing the visual impact of CF deformation on the sample surface .....	97
Figure 4.31: Observed stress levels in each creep-fatigue test with respect to the stress-strain curve in room temperature.....	98
Figure 4.32: Observed number of cycles to failure with respect to the hold times in each creep-fatigue test.....	98
Figure 5.1: Bayesian inference framework.....	102
Figure 5.2: Normal distribution probability plot of failed creep-fatigue data .....	104
Figure 5.3: WinBUGS Bayesian Inference framework R2B results for each robust creep-fatigue models.....	105
Figure 5.4: WinBUGS node statistics for Soviet model.....	107

Figure 5.5: WinBUGS sample densities for parameters $b_0$ , $b_1$ and $b_4$ in Soviet Model .....	108
Figure 5.6: WinBUGS correlation tool result between parameters $b_0, b_1$ and $b_4$ in Soviet Model .....	108
Figure 5.7: WinBUGS autocorrelation tool results for parameters $b_0, b_1$ and $b_4$ in Soviet Model .....	109
Figure 5.8: WinBUGS node statistics for Larson-Miller Model .....	111
Figure 5.9: WinBUGS sample densities for $b_0, b_1$ and $b_2$ in Larson-Miller Model ..	111
Figure 5.10: WinBUGS correlation tool results between parameters $b_0, b_1$ and $b_2$ in Larson-Miller Model .....	112
Figure 5.11: WinBUGS autocorrelation results for parameters $b_0, b_1$ and $b_2$ in Larson-Miller Model .....	112
Figure 5.12: WinBUGS node statistics for Orr-Sherby Dorn Model .....	115
Figure 5.13: WinBUGS sample densities for $b_0, b_1$ and $b_2$ in Orr-Sherby Dorn Model. ....	116
Figure 5.14: WinBUGS correlation results between parameters $b_0, b_1$ and $b_2$ in Orr-Sherby Dorn Model .....	116
Figure 5.15: WinBUGS autocorrelation results for parameters $b_0, b_1$ and $b_2$ in Orr-Sherby Dorn Model .....	117
Figure 5.16: WinBUGS node statistics for Manson-Haferd Model .....	119
Figure 5.17: WinBUGS sample densities for $b_0, b_1$ and $b_2$ in Manson-Haferd Model... ..	120
Figure 5.18: WinBUGS correlation tool results between $b_0, b_1$ and $b_2$ in Manson-Haferd Model .....	120
Figure 5.19: WinBUGS autocorrelation results between parameters $b_0, b_1$ and $b_2$ in Manson-Haferd Model .....	121
Figure 5.20: WinBUGS node statistics for Wilshire Model .....	123
Figure 5.21: WinBUGS sample densities for $k$ and $u$ in Wilshire Model .....	124
Figure 5.22: WinBUGS correlation tool result between parameters $k$ and $u$ in Wilshire Model .....	124
Figure 5.23: WinBUGS autocorrelation results for parameters $k$ and $u$ in Wilshire Model .....	125
Figure 6.1: Soviet Model creep-fatigue expended life curve for steel alloy at $673.15^\circ K$ ( $400^\circ C$ ) .....	129
Figure 6.2: Soviet-Model creep-fatigue 3D life graph for the steel alloy at $673.15^\circ K$ ( $400^\circ C$ ) .....	130
Figure 6.3: Larson-Miller creep-fatigue expended life curve for the steel alloy at $673.15^\circ K$ ( $400^\circ C$ ) .....	131
Figure 6.4: Larson-Miller Model creep-fatigue 3D life graph for the steel alloy at $673.15^\circ K$ ( $400^\circ C$ ) .....	131
Figure 6.5: Orr-Sherby Dorn Model creep-fatigue expended life curve for the steel alloy at $673.15^\circ K$ ( $400^\circ C$ ) .....	132
Figure 6.6: Orr-Sherby Dorn Model creep-fatigue 3D expended life graph for the steel alloy at $673.15^\circ K$ ( $400^\circ C$ ) .....	133
Figure 6.7: Manson Haferd Model creep-fatigue expended life curve for the steel alloy at $673.15^\circ K$ ( $400^\circ C$ ) .....	134

Figure 6.8: Manson Haferd Model creep –fatigue 3D expended life graph for the steel alloy at 673.15 °K (400 °C ) .....	134
Figure 6.9: Wilshire Model creep-fatigue expended life curve for the steel alloy at 673.15 °K (400 °C ) .....	135
Figure 6.10: Wilshire Model creep-fatigue 3D expended life graph for the steel alloy at 673.15 °K (400 °C ) .....	136
Figure 6.11: Time to creep-fatigue failure comparison for the steel alloy .....	136
Figure 6.12: Predicted vs. observed creep-fatigue life for the steel alloy.....	137
Figure 6.13: R <sup>2</sup> results for Norton Bailey, Nuhi’s Empirical and Modified Theta Models.....	141
Figure 6.14: Creep curves in cyclic relaxation response under creep-fatigue conditions for 10min (CF Test#1), 14min (CF Test#2), and 21min (CF Test#3) hold times at 673.15 °K (400 °C ).....	142
Figure 6.15: Normal cdf at strain 0.006 [mm/mm] for creep in cyclic relaxation response under creep-fatigue conditions for 10min (CF Test#1), 14min (CF Test #2) and 21min (CF Test #3) hold times at 673.15 °K (400 °C ) .....	143
Figure 6.16: Acceleration factor graph with respect to the specified use level stress 17.3MPa.....	146
Figure A-I.1: (a) Thermocouple clip attached to test sample, and (b) thermocouple clip design dimensions .....	154
Figure B-I.1: (a) Epoxy mold produced, and (b) mounted sample using epoxy mold .....	155

## List of Symbols

$D$	total creep-fatigue damage
$n$	number of applied cycles at a particular loading condition
$N_f$	number of cycles to failure at a particular strain range
$t$	time duration at a particular load condition
$t_r$	time to rupture from isothermal stress-rupture curves for a given loading condition
$\Delta\varepsilon_{pp}$	plastic-plastic
$\Delta\varepsilon_{cp}$	creep-plastic
$\Delta\varepsilon_{pc}$	plastic-creep
$\Delta\varepsilon_{cc}$	creep-creep
$C$	material parameter
$\nu$	material parameter
$\nu_c$	compression-going frequency
$\nu_t$	tension-going frequency
$\beta, k, c$	material constants
$\beta_i$	creep-fatigue expended life model parameters $i=1,2,3,4,5$
$\tau$	cycle period
$\tau_0$	time per cycle of continuous loading
$\tau_c$	compression hold time
$\tau_T$	tension hold time
$\dot{\varepsilon}_m$	minimum creep rate
$t_f$	creep life
$\sigma$	stress

$T$	temperature
$Q_c$	activation energy
$D_f$	fatigue damage
$D_c$	creep damage
$\sigma_{ref}$	reference stress
$\Phi$	normalized reference stress
$S$	strain range parameter
$R$	strain rate parameter
$T$	temperature parameter
$H$	hold parameter
$t_h$	duration of hold time in hours
$\dot{\varepsilon}$	strain rate
$\varepsilon_e$	elastic strain
$\varepsilon_p$	plastic strain
$E$	Elastic modulus
$\dot{\varepsilon}_c$	stress relaxation rate
$t_{CF}$	time to creep-fatigue failure
$\Delta l$	change in initial length
$l_0$	initial length
$\alpha$	linear expansion coefficient
$\Delta t$	change in temperature
$t_0$	initial temperature

$t_1$	final temperature
$Q_c^*$	apparent activation energy
CF	creep-fatigue
LCF	low-cycle fatigue
HTLCF	high temperature low cycle fatigue
R2B	Bayesian Pearson coefficient of determination
R2	Pearson coefficient of determination
LS	loading sequence
MCMC	Markov Chain Monte Carlo

# **Chapter 1: Introduction**

## **1.1 Background**

Historically, the earliest attempts to evaluate combined creep and fatigue properties were made in Germany by Hempel and his coworkers [1, 2-4] during 1936-42 [1] focusing mainly on carbon steels. At about the same period, Tapsell and his coworkers [5,6] at the National Physical Laboratory studied the behavior of steels and extended their studies to develop methods of predicting combined creep and fatigue (CF) behavior [1].

Since the Second World War, a great deal of effort has been devoted in the United States to evaluate combined CF properties of a wide range of existing alloys in particular high temperature alloys. In the United Kingdom, commercial alloys have been examined at Bristol-Siddeley Engines Ltd., by Frith [7], with special reference to fatigue-rupture properties [1].

Perhaps the first attempt to apply basic structural theories to the problem of combined CF was made by Kennedy [8] at the British Iron and Steel Research Association, London. There is now an increased awareness of the importance of testing under combined CF conditions, and this is reflected by the number of testing and research programs at several alloy manufacturers and end-user facilities.

Meleka [1] presented some examples of cases where combined CF stresses are met with under service conditions. In almost all high-temperature applications, simultaneous CF may occur, even in normally static applications. Most of the following are suggested in Ref.[1] as examples of cases where combined CF are met under service conditions.

**a. Turbine Blades:** Turbine blades are subjected to severe service conditions and combined fatigue-creep is a major source of turbine failure. The blade is subjected to direct tensile stresses as a result of the centrifugal forces produced by the high speed rotation of the blade. Bending fatigue stresses are also present, mainly owing to the mechanical resonance of the blade. Turbine blades may fail by creep or by fatigue, depending on the relative severity of stresses. More combined CF data on turbine-blade materials exists than on any other, mainly because of the critical nature of the function of these components.

**b. Nuclear Power Applications:** Magnesium alloys are used extensively as cladding nuclear fuel elements, chiefly because of their low neutron-absorption. The cladding is exposed to temperatures up to 500°C and must exhibit sufficient creep strength and ductility to accommodate the dimensional changes of the uranium element and also to support its weight in a vertically stacked array. Similar conditions also apply to structural components inside the reactor. Creep stresses are obviously present because of the load-carrying function of the component, and fatigue stresses are produced by the vibrations resulting from gas flow. Separate CF have been conducted on a number of magnesium alloys separately, but very limited data exists for combined CF tests.

**c. Components in Power Generation Plants:** High temperature components in power generation are subjected to load cycles that involve gradually accumulating and life-limiting damage from cyclic (fatigue) and more steadily

progressing (creep) mechanisms of deformation and fracture. As a consequence, resistance of structural materials to combined CF is of considerable interest for both design and life assessment. In many applications of power generation, the loading rates and cycling frequencies are low, so that the combined CF damage could be creep dominated [10].

- d. The Supersonic Airliner:** One of the important factors to be considered in the design of a supersonic airliner is the effect of kinetic heating on the strength of the structure. Temperatures up to 150°C may be encountered, resulting in creep deformation. This will have to be limited to small values, say 0.1% over the life of airliner. So far, designers have based their calculations for present-day airliners on room-temperature fatigue data, but in the presence of kinetic heating creep considerations will also have to be taken into account.
- e. Jet and Rocket Engines:** Service conditions in jet and rocket engines are quite severe because of the high stress and temperatures encountered during service life. Under steady operating conditions the various components are subjected to essentially creep stresses, but severe vibration may be represented for short times which may affect the creep characteristics of the components.
- f. Pipes in Steam Power Plant:** These pipes are normally designed on the basis of creep, although from a study of fracture characteristics certain failures have been traced to fatigue. Large fatigue stresses are produced in power plant pipes by the vibrations in rotating machinery. During the design or service of such pipes, attention should be given to reducing the possibility of excessive vibrations.

**g. Relaxation of Internal Stresses:** The relaxation of internal stresses during service may lead to dimensional distortion of component concerned. Relaxation is, of course, another form of creep deformation, where the locked-in stresses give way to plastic deformation by creep. Relaxation under some circumstances can be initiated or accelerated by the presence of fatigue stresses.

**h. Thermal Fatigue:** It is clear that thermal-cycling conditions may have effects on creep properties similar to those caused by mechanical fatigue. One or two examples of this is given in Ref.[9].

## **1.2 The Scope of the Thesis**

The development of CF damage is influenced by temperature, strain amplitude, strain rate and hold time, and the creep strength and ductility of the material. With increasing hold time (and/or decreasing strain rate) and decreasing strain amplitude at high temperatures, the creep damage becomes more and more important. A survey was conducted using 57 high temperature fatigue testing specialists in 13 countries to study current CF testing practices concerning: the types of test employed, test piece machines and loading, strain measurement, temperature measurement and data acquisition.

CF damage may be generated in tests involving sequential blocks of CF loading. However, from the results of the survey, it was more common to apply a waveform shape responsible for the generation of both static and transient loading within the same cycle. CF tests were performed in both load and strain control, although more commonly in strain control (see, Table 1.1). The most commonly

adopted CF waveform was a cycle involving one or more hold times, where hold periods could be anything between 1 min and 24h (with an extreme case of 90 days).

**Table 1.1: Survey indicated summary of waveform usage for CF testing [11]**

Waveform	Load Control (User %)	Strain Control (User %)
Low frequency triangular (isothermal)	14	59
Saw tooth triangular (isothermal)	27	68
Cyclic hold (isothermal)	32	86
Thermo-mechanical fatigue (TMF) (without and with hold time)	14	68

The most widely used test specimen type was a uniform parallel gauge section specimen (without ridges for extensometer fixation), although other specimen types were used for special circumstances. Despite a uniform test specimen type, a range of gauge section dimensions and end connections were employed.

A range of failure criteria were adopted, varying between 2% and 25% reductions in steady state maximum stress. Notably, the most commonly adopted criteria was a 10% reduction in maximum stress (45%) compared with the anticipated outcome of a 2% reduction (22%).

In order to come up for a CF testing procedure for this thesis work, the worldwide survey results of current practices conducted by EPRI have been reviewed. These results have generated the motivation for this thesis work. Addressing the prediction feasibility of the all CF models identified in Chapter 3 is beyond the scope of this thesis. Hence, the *main focus in this study is isothermal CF tests under strain control with stress ratio  $R=0$  and hold periods in tension, and prediction feasibility of CF expended life models which do not need separation in CF damage.*

*Therefore, effective CF expended life was predicted utilizing the creep rupture properties of a material. Consequently, creep deformation produced by hold times in tension enabled this research to evaluate creep damage assessment in cyclic relaxation response in CF tests performed.*

### 1.3 Thesis Organization

The structure of this thesis is presented in Figure 1.1.:

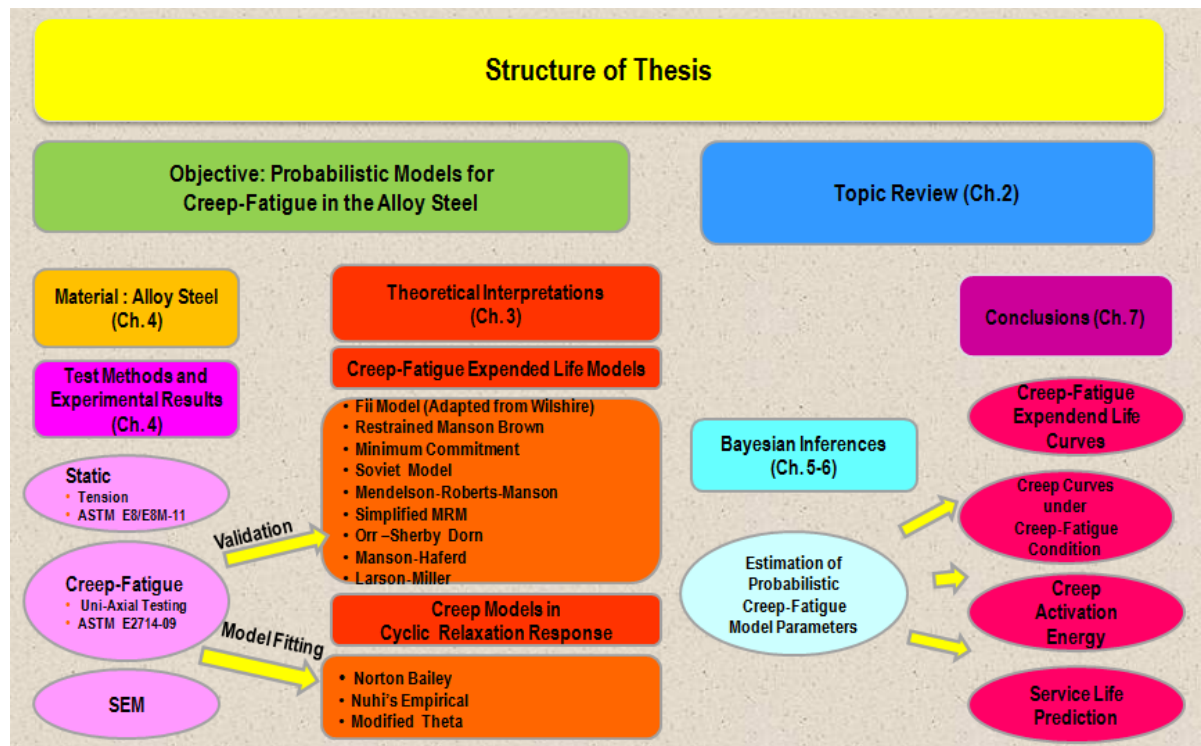


**Figure 1.1: Structure of thesis**

The thesis is organized as follows:

**In Chapter 2**, an introduction to factors influencing CF in steel materials such as metallurgical state, waveform and frequency, environment (e.g. oxidation), complex loading path histories, classical creep damage (voidage) is presented first, followed

by a literature review on CF in steels and alloys. Subsequently, a literature review on creep in cyclic relaxation response is presented.

**In Chapter 3**, models are adjusted into CF problem under uniaxial interaction. Best possible creep models are evaluated for creep deformation in cyclic relaxation response.

**In Chapter 4**, CF experiments are presented and experimental details are given.

**In Chapter 5**, experimental results are evaluated in Bayesian inference framework with respect to the models concerned in Chapter 3. Details of WinBUGS codes which uses MCMC to fit statistical models, and steps to reach correct posterior distributions are presented.

**In Chapter 6**, experimental results are presented by posterior distributions proposed in the previous Chapter 5, and compared to validate the models discussed in Chapter 3.

**In Chapter 7**, conclusions based on the results of this research are presented followed by future recommendations.

#### **1.4 References**

- [1] Meleka, A.H., “Combined creep and fatigue properties,” *Metallurgical Reviews*, Vol.7, Issue:25, 1962.
- [2] Hempel, M. and Tillmanns, H.E., *Mitt. K.-W.Inst.Eisenforsch*, Vol.18, Issue:163, 1936.
- [3] Hempel, M. and Ardelt, F., *ibid.*, Vol.21, Issue:115, 1939.
- [4] Hempel, H. and Krug, H., *ibid.*, Vo.24, Issue:77, 1942.
- [5] Tapsell, H.J., Forrest, P.G., and Tremain, G.R., *Engineering*, Vol.170, Issue:189, 1950.

- [6] Tapsell, H.J., "Symposium on High-Temperature Steels and Alloys for Gas Turbines" (Special Rep. No.43), p:169, London (Iron and Steel Inst.), 1952.
- [7] Frith, P.H., "Properties of Wrought and Cast Aluminum and Magnesium Alloys at Room and Elevated Temperatures," London (H.M. Stationery Office), 1956.
- [8] Kennedy, A.J., "Proceedings of the International Conference on Fatigue of Metals," p:401, London (Inst. Mech. Eng.), 1956.
- [9] A.S.T.M., "Symposium on the Effect of Cyclic Heating and Stressing on Metals at Elevated Temperatures," (Special Tech. Publ. No.165), Philadelphia, Pa. (Amer. Soc. Test. Mat.), 1954.
- [10] Holmstrom, S., Auerkari, P., "A robust model for creep-fatigue life assessment," *Mechanical Science and Engineering A*, Vol.559, pp:333-335, 2013.
- [11] Holdsworth, S.R., Gandy, D., "Towards a standard for creep-fatigue testing," *Advances in Materials Technology for Fossil Power Plants Proceedings from the Fifth International Conference*, In. Viswanathan, R., Gandy, D., and Coleman, K. (Eds.), pp: 689-701, 2008.

## **Chapter 2: Literature Review**

### **2.1 Introduction**

Chapter 2 presents four sub-sections linked to one another. Section 2.2 presents factors affecting creep-fatigue (CF) life of material. Section 2.3 and 2.4 present published studies on CF expended life assessment of materials, and creep in cyclic relaxation response. Section 2.5 specifies the thesis objectives in bullet points regarding the reasoning provided in Section 1.2 and reviews presented in Section 2.3.

### **2.2 Factors Affecting CF Expended Life of Materials**

Strain-controlled fatigue tests of annealed 2.25Cr-1Mo steel results from strain-controlled fatigue tests conducted in various environments from 370 to 593°C have shown that the time-dependent fatigue lifetime depends on the influence of (1) metallurgical state, (2) waveform and frequency, (3) environment (e.g. oxidation), (4) complex loading path histories, and (5) classical creep damage (voidage) [1]. In following sub-sections each of these influences is explained.

#### **2.2.1 Metallurgical State**

Metallurgical state is separated in to three sub-sections in this study. These are microstructural composition, carbon content, and effect of heat treatments on ductility. They are explained in following.

##### **2.2.1.1 Microstructural Composition**

Heat to heat variations has been reported in time-dependent fatigue properties of type 304 stainless steel. Small grain sizes and the presence of fine closely packed

intergranular precipitates have both improved the cyclic life. Intergranular precipitate restricts grain-boundary sliding and hence limits wedge cracking. Although grain size does not impact continuous-cycle fatigue life in the low-cycle regime, time-dependent fatigue behavior at the indicated temperature is improved as the grain size is decreased [1]. Qualitatively, the time dependent fatigue behavior of types 304 and 316 stainless steel are directly related to the creep ductility at strain rates similar to those that occur during stress relaxation [1].

#### **2.2.1.2 Carbon Content**

In Japan, type 304 stainless steel used in a prototype reactor, Monju is being replaced with low-carbon and nitrogen-controlled 316FR (fast reactor). The reduced carbon content of 316FR leads to considerably better creep strength than the conventional type 316 steel by reducing the Chromium Carbide precipitation along grain boundaries, which promotes initiation of creep cavities [2].

#### **2.2.1.3 Effect of Heat Treatments on Ductility**

Solution heat treatment (1250°C, 16h) prior to rolling reduces the possibility of carbide precipitation by homogenizing chromium distribution [2]. Consider 2 plates, A and B that were both produced using hot-rolling. The heat treatment of Plate A was 1050°C for 30 min followed by water quenching. Plate B had the same treatment as Plate A plus an additional treatment at 1250°C for 16h to homogenize chromium distribution. Under the same test conditions, plate A showed a shorter life than plate B. This trend coincides with the fact that ductility in creep tests has a strong correlation between creep ductility and CF life [2].

### **2.2.2 Waveform and Frequency**

It was reported in past studies that tensile loading leads to larger life reduction than compressive loading for austenitic stainless steel, and this was confirmed with several tests for the tested material [2].

At least two specific mechanisms can lead to intergranular crack formation and fracture in polycrystalline steels. These include formation of intergranular creep cavities and by grain-boundary triple-point nucleation of voidage as a result of localized grain-boundary sliding. The latter mechanism usually occurs at higher stresses (approaching the yield strength), which occur in low-to intermediate-cycle fatigue applications. Under tensile loads held at elevated temperatures high enough for creep to occur, intergranular voids form easily which in turn favors intergranular fatigue crack propagation. Increasing the temperature within the creep range or decreasing the cyclic frequency further weakens the grain boundaries with respect to the intragranular matrix material and promotes grain boundary sliding, resulting in decreased cyclic life for a given specimen geometry [1].

### **2.2.3 Environmental/Service Factors**

It is known that constant loading at high-temperature reduces the number of cycles to failure from pure-fatigue loading due to “creep damage” or other mechanisms such as oxidation [2]. Failure life at 600°C tended to be shorter than that at 550°C, but the difference was much smaller than observed in pure-creep tests. The difference of controlled parameters, i.e., stress-versus strain, is the reason for this [2].

#### **2.2.4 Complex Loading Path Histories**

For 304 stainless steel, previous studies have performed strain-controlled hold time tests with the strain held at the peak strain amplitudes. The following conclusions can be made from these results [1]:

1. Tensile hold times at peak strain values are more damaging than compressive hold times of equal duration.
2. Hold periods imposed at other locations on the hysteresis loops, such as at zero stress or zero relaxation points, degrade fatigue life but not as much as hold periods imposed at peak tensile strain values.
3. Hold periods imposed on the tension-going side of the loop tend to be more detrimental than those imposed on the compression-going side.
4. The rate of accumulation of a given amount of relaxation or creep strain is important in that lower creep rates favor intergranular cavitations and hence result in lower fatigue lives.

#### **2.2.5 Classical Creep Damage (voidage)**

Creep is modeled as time-dependent deformation, and thereby is mathematically distinct from elastic and plastic deformation. Elastic and plastic deformations are mathematically modeled as instantaneous deformations occurring in response to applied stresses. In reality, all deformations are time dependent, but the characteristic times for elastic and plastic deformations are orders of magnitude smaller than those for creep [7].

At elevated temperatures, most materials can fail at a stress which is much lower than its ultimate strength measured at ambient temperature. These failures are

time-dependent and are caused by creep rupture [7]. More generally, materials undergoing continuous deformation over time under a constant load or stress are said to be creeping. Elastic, plastic, visco-elastic and visco-plastic deformations can all be included in the creep process, depending on the material and the characteristic time of the deformation. However, creep deformation is often treated as plastic deformation because the failures associated with creep are similar to those due to yielding in plastic deformation of materials. There are various mechanisms of creep in materials at elevated temperatures and thus there are different creep models. These mechanisms are often be inter-related, depending on the material [7]. The measurement of phenomenological creep of materials is quite simple, although the mechanisms of creep are complicated [7].

#### **2.2.5.1 Creep Curve**

A creep curve shows time dependent deformation under constant load. When a constant load is applied to a tensile specimen at a constant temperature (usually greater than 0.4 ~ 0.5 of the absolute melting temperature of the specimen) the strain of the specimen is determined as a function of time. A typical variation of creep strain with time in a specimen at a constant load is schematically shown as curve A in Figure 2.1. The slope of the curve is the creep rate. Creep is usually characterized as having three distinct stages, as reflected by the creep curve. Stage 1 of curve A, follows after an initial instantaneous strain  $\epsilon_0$ , which includes elastic and plastic deformations. During phase 1, the creep rate decreases with time. This is termed primary creep. Stage 2 of curve A during which the creep rate approaches a stable minimum value, relatively constant over time, is secondary creep or steady-state

creep. The creep rate in the secondary creep stage, often termed the steady-state creep rate, is an important engineering property because most deformations involve this stage. In stage 3, termed tertiary creep, the creep rate accelerates with time and usually leads to failure by creep rupture. Although the three stages represent the creep behavior in most materials, the primary creep stage can be absent for some materials. The extension during the tertiary creep stage can be limited in brittle materials and very extensive in ductile materials [3].

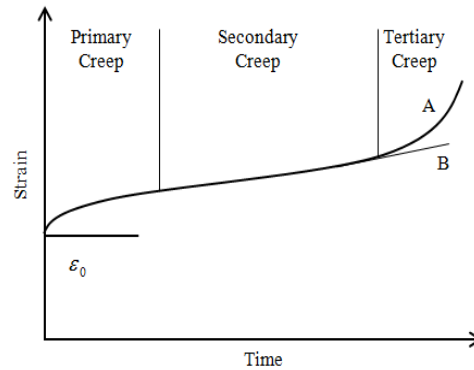


**Figure 2.1 Typical creep curves showing the 3-stages of creep [3]**

Curve B in Figure 2.1 is for a creep test with a constant stress. Under a constant load, the axial stress increases with time because the specimen decreases in cross-sectional area. The increasing stress thus accelerates creep and causes strains in the tertiary phase, as shown in curve A. In most engineering creep tests, it is often easier to maintain a constant load during the test because of instrumentation limitations. Under constant-stress, as shown in curve B, steady-state creep dominates over a much longer time period and thus greatly postpones tertiary creep [3].

### **2.2.5.2 Creep Characteristics**

Creep characteristics depend on several factors such as time, temperature, stress and the micro-structure [3]. These factors are explained in the following sections.

#### **a. Time**

A time scale is always involved in creep. For most engineering materials tested at low temperatures, the measured tensile properties are relatively independent of the test time, regardless of whether it is 5 minutes or 5 hours. If time dependence is observed in a tensile test, the material is by definition creeping. The main reason for this time dependence is the involvement of thermally activated time-dependent processes. Creep tests are designed to last hours, days or even years where the overall creep rate is usually controlled by a single dominant thermally activated process. For example, if the controlling process is diffusional, the creep rate is called diffusion controlled [3].

#### **b. Temperature**

Creep mechanisms involve mechanisms at the atomic scale. At higher temperatures, the mobility of atoms or vacancies increases rapidly with temperature so that they can diffuse through the lattice of the materials along the direction of the hydrostatic stress gradient, which is called self-diffusion. The self-diffusion of atoms or vacancies can also help dislocations climb. At low temperatures, creep becomes less diffusion-controlled. Diffusion can occur, but is limited in local porous areas, like grain boundaries and phase interfaces, which is called grain-boundary diffusion. Since creep is strongly temperature dependent, a measurement of this temperature

dependence is important. A temperature which is considered high for creep in one material might not be so high in another. To compensate for this difference, temperature is often expressed on a homologous scale, the ratio of the test temperature ( $T$ ), to the melting temperature ( $T_m$ ) of the material on an absolute temperature scale. Generally, creep becomes of engineering importance at  $T > 0.5T_m$ . This should be regarded as an approximate empirical guideline based on the observations that above  $0.5T_m$ , creep is most likely to be governed by mechanisms that depend on self-diffusion.

### c. Stress

Creep rate is also very sensitive to the applied stress level and stress state. Figure 2.2 schematically shows how the applied stress level affects creep rate at constant temperature. With increase of applied stress, the primary and secondary (steady-state) stages are shortened or even eliminated and the tertiary stage dominates the creep process. Practical measurements of creep are classified into creep and creep rupture tests according to the stress level [3].

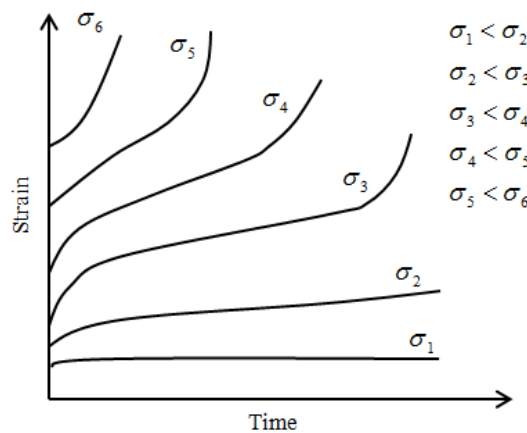


**Figure 2.2 Effect of applied stress on a creep curve at constant temperature [3]**

Creep tests are carried out at low stresses to avoid tertiary creep. The purpose of creep tests is mostly to determine the steady-state creep rate. The total strain is often less than 0.5% [3]. Creep rupture tests are similar to creep tests except that high loads are applied to precipitate failure of the material. Creep rupture tests are mostly used for obtaining the time-to-failure at a given stress and a given temperature. The total strain can be as high as 50% [3].

Different stress states such as, such as simple tension, simple compression, simple shear, simple torsion, and in some special cases, multi-axial stresses can be used for creep tests and creep rupture tests,. The difference in the results at the same stress level in simple tension and simple compression indicate the sensitivity of the creep rate to the direction of stress. The creep rate for lead and nickel, for example, is greater in tension than in compression. Cyclic stress also affects creep rate. At low creep temperatures, the steady-state creep rate is increased in many metallic materials by cyclic stresses while the opposite is often found at high creep temperatures [3].

### **2.3 Published Studies on CF Expended Life Assessment of Materials**

The literature review below covers peer reviewed articles from 1976 to 2013. Efforts in CF expended life models development are presented in chronological order.

Ostergren [4] developed an approach for predicting strain-controlled, low cycle fatigue life at elevated temperature using a proposed energy measure of fatigue damage. This measure of damage, defined as the net tensile hysteretic energy of the fatigue cycle, can be approximated by the damage function  $\sigma_T \Delta \epsilon_p$  where ( $\sigma_T$  is the maximum stress in the cycle and  $\Delta \epsilon_p$  is the inelastic strain range. The damage function was applied to predict the effects of hold time and frequency, when time

dependent damage occurs, through failure relations incorporating a variation of Coffin's frequency modified approach. Failure equations were developed for two postulated categories of time- dependent damage.

Halford et al. [5] presented procedures based on strain range partitioning (SRP) for estimating the effects of environment and other influences on the high temperature, low-cycle, CF resistance of alloys. It was proposed that the plastic and creep ductilities determined from conventional tensile and creep-rupture tests conducted in the environment of interest be used in a set of ductility normalized equations for making a first order approximation of the four (SRP) inelastic strain range-life relations. Different levels of sophistication in the application of the procedures were presented by means of illustrative examples with several high temperature alloys. Predictions of cyclic lives generally agreed with observed lives within factors of three.

Lloyd and Wareing [6] attempted to extend such models to cover the situations in which creep damage is introduced during periods of stress relaxation. Equations predicting fatigue life as a function of hold period are in good agreement with experimental data, for Type 316 stainless steel and Incoloy-800. Components operating at elevated temperature are often subjected to complex strain-time histories which include periods of cyclic strain, creep strain and relaxation strain resulting from the conversion of elastic strain to plastic strain. It has become increasingly apparent that one of the most damaging strain time patterns is when the strain is held constant at the maximum tensile strain part of a high strain fatigue cycle. To predict the life of a plant operating under such conditions is essential to understand the

mechanisms by which fracture development occurs. To this end, models have been developed which successfully describe the behavior of materials subjected to simple cycling at both room and elevated temperature. Wareing [6] described such cycles and extended it to cover cycles containing periods of stress relaxation. The predictions arising from such models were compared with experimental data on three austenitic steels at temperatures from 538 to 760°C.

Brinkman [1] reviewed the effects of various phenomena such as creep-induced intergranular cavitation, mean stress material condition, and environment on the fatigue life of several engineering structural alloys. Materials used to illustrate these effects when subjected to various loading conditions within the creep range included 2.25Cr-1Mo steel (annealed), modified 9Cr-1Mo steel (normalized and tempered), types 304 and 316 stainless steel, alloy 800H, Hastelloy X, and alloy 718. Several models were used to extrapolate available data to predict life were also discussed in terms of both their strengths and apparent shortcomings. No model was clearly superior in its ability to predict life for all alloys under all loading conditions envisioned, particularly at low strain ranges with long creep hold periods which occurs in many applications.

Fatemi and Yangth [7] provided a comprehensive review of cumulative fatigue damage theories for metals and their alloys, emphasizing the approaches developed between the early 1970s to the early 1990s. These theories were grouped into six categories: linear damage rules; nonlinear damage curve and two-stage linearization approaches; life curve modification methods; approaches based on crack growth concepts; continuum damage

mechanics models; and energy-based theories.

Goswami, [8] reviewed the dwell sensitivity behavior and mechanisms controlling deformation and failure under high-temperature low cycle fatigue (HTLCF) conditions for a range of materials. Dwell sensitivity maps were constructed utilizing normalized cycle ratio (NCR) and strain levels. The trends identified were summarized as follows:

1. Dwell cycles were beneficial to the creep-fatigue resistance only in isolated cases for copper alloys; AMZIRC and NARaloy-Z, and superalloys;
2. PWA 1480 and MA 754 an (ODS) alloy. Solders (96.5 Pb–3.5 Sn and 37 Pb–63 Sn), copper alloys; AMZIRC and NARaloy-Z, low steel alloys; 1 Cr-Mo-V, 1.25 Cr-Mo and 9 Cr-1 Mo, stainless steels; SS 304, SS 304L, SS 316, and SS 316L, superalloys; Mar M 002, Rene 80, Inconel 617, IN 100, PWA 1480 and MA 754 were observed to be tensile dwell sensitive.
3. Low steel alloy 2.25 Cr-Mo, titanium alloys Ti-6 Al-4V and IMI 829 and superalloys Mar M 002 below 1040°C, Waspaloy and Rene 95 were found to be compressive dwell sensitive.

Goswami [8] predicted the dwell sensitivity fatigue behavior empirically relating the strength ratios with ductility ratios. It was proposed that when the ductility ratio was equal to the strength ratio, compressive dwell sensitivity occurred and for unequal conditions, tensile dwell sensitivity occurred. These factors were determined and dwell sensitivity predicted. The mechanisms controlling deformation and failure were categorized as follows: Each cycle

type produced deformation in either transgranular (TG), mixed, or intergranular (IG) mode. Cyclic softening resulted in IG deformation as the stresses reduced. Grain boundary sliding, cavity formation and oxidation damage interacted and reduced life faster than TG modes, in which striations were observed. Depending upon the cycle time, stresses, and temperature, deformation in terms of precipitation, slip patterns, carbides, depletion of chromium carbides, Cr-Mo clusters occurred. These resulted in IG corrosion, oxidation and creep-fatigue interactions causing additional damage. Dynamic strain aging occurred depending upon the microstructure, temperature and material composition. Precipitates developed which enhanced HTLCF resistance, however, other competition mechanisms under dwell conditions were not known. The dwell sensitivity behavior and mechanisms controlling deformation and failure of numerous materials were summarized in this paper.

Goswami and Hannien [9] examined mechanisms controlling deformation and failure under high temperature CF conditions. The materials studied were pure alloys, solder alloys, copper alloys, low steel alloys, stainless steels, titanium alloys, tantalum alloys, and Ni-based alloys. The deformation and failure mechanisms, fatigue, creep, oxidation and their interaction, varied depending on the test and material parameters employed. Deformation mechanisms, such as cavity formation, grain boundary sliding, intergranular and transgranular damage, oxidation, internal damage, dislocation cell formation, and other damage mechanisms are very important in order to gain knowledge of fatigue behavior of materials. The observed mechanisms can be categorized as

follows:

1. Depending on the test parameters employed, a high NCR resulted in high strain levels. The damage was due to CF interaction by mixed TG and IG cracking, creep damage by cavity formation and surface damage by oxidation. Oxidation damage was found to depend on a critical temperature and compression and tension dwell periods in a cycle.
2. Dwell sensitivity was effective only below a certain strain range, and once this threshold was exceeded NCR value was not affected with a further increase in dwell time.
3. Microstructures changed depending on test temperature, dwell time, and strain range. Triple point cracking and cavities formed as a result. New precipitation occurred depending on temperature, strain range and dwell time. Some precipitates were beneficial in blocking the grain boundary damage, whereas other precipitates changed the dislocation substructure promoting more damage.
4. Depleted regions on the grain boundaries developed due to exposure at high temperatures resulting in the formation or propagation of IG cracks.
5. Dwell evolved mean stresses in tension and compression directions. Mean stress in tension was more detrimental and caused dwell sensitivity.
6. Dwell sensitivity was also dependent on material condition and defects present in the material.

Goswami [10] presented a data bank that was compiled from published and unpublished sources. Using this data, low cycle fatigue curves were generated

under a range of test conditions showing the effect of test parameters on the Coffin–Manson behavior of steel alloys. Phenomenological methods of creep–fatigue life prediction were summarized in a table showing number of material parameters required by each method and type of tests needed to generate such parameters. Applicability of viscosity method was assessed with creep–fatigue data on 1Cr–Mo–V, 2.25Cr–Mo and 9Cr–1Mo steels. Generic equations were developed in this paper to predict the creep–fatigue life of high temperature materials. Several new multivariate equations were developed to predict the creep–fatigue life of following alloy groups; (1) Cr–Mo steels, (2) stainless steels and (3) generic materials involving the materials from the following alloy groups, solder, copper, steels, titanium, tantalum and nickel-based alloys. Statistical analysis was performed in terms of coefficient of correlation ( $R^2$ ) and normal distribution plots and recommended these methods in the design of components operating at high temperatures.

Takahashi et al. [11, 12] developed a CF evaluation method for low-carbon, nitrogen-controlled 316 stainless steel, 316FR. To develop a CF evaluation method suitable for this steel, a number of uniaxial CF tests were conducted for three products of this steel. Long-term data up to about 35,000 h was obtained and the applicability of failure life prediction methods was studied based upon their results. Cruciform shaped specimens were also tested under biaxial loading conditions to examine the effect of stress multiaxiality on failure life under CF condition.

He [13] investigated the creep fatigue behavior of stainless steel materials. In the low cycle thermal fatigue life model, Manson’s Universal Slopes equation was

used as an empirical correlation which relates fatigue endurance to tensile properties. Fatigue test data was used in conjunction with different models to establish the relationship between temperature and other parameters. Then statistical creep models were created for stainless steel materials. In order to correlate the results of accelerated life tests with long-term service performance at more moderate temperatures, different creep prediction models, namely the Basquin model and Sherby-Dorn model, were studied. Comparison between the different creep prediction models were carried out for a range of stresses and temperatures. A linear damage summation method was used to establish life prediction model of stainless steels materials under fatigue creep interaction.

Holmström and Auerkari [14] stated high temperature components subjected to long term cyclic operation will acquire life-limiting damage from both creep and fatigue. A new robust model for CF life assessment was proposed with a minimal set of fitting constants, and without the need to separate creep and fatigue damage or life fractions. The model is based on the creep rupture behavior of the material with a fatigue correction described by hold time (in tension) and total strain range at temperature. The model is shown to predict the observed CF life of ferritic steel P91, austenitic steel 316FR, and Ni alloy A230 with a scatter band close to a factor of 2.

## **2.4 Published Studies on Creep in Cyclic Relaxation Response**

Jaske et al. [16] made a detailed analysis of data from low-cycle fatigue tests of solution-annealed nickel-iron-chromium Alloy 800 at 1000, 1200, and 1400 °F and of Type 304 austenitic stainless steel at 1000 and 1200 °F with hold times at maximum tensile strain. A single equation was found to approximate the cyclically stable stress

relaxation curves for both alloys at these temperatures. This equation was then used to create a linear time fraction creep damage analysis of the stable stress relaxation curves, and a linear life fraction rule was used to compute fatigue damage. CF damage interaction was evaluated for both alloys using the results of these damage computations. The strain range was found to affect the damage interaction for Type 304 stainless steel but not for the Alloy 800. With increasing hold times, both creep and total damage increased for the Alloy 800, decreased for the Type 304 stainless steel, and the fatigue damage decreased for both alloys. A method was developed to relate the length of hold time and fatigue life to total strain range. This method provides a simple and reasonable way of predicting fatigue life when tensile hold-times are known.

Lafen and Jaske [17] investigated the path and history dependence of elevated-temperature, time dependent deformation response for three steel alloys-2V.Cr-IMo steel, Type 304 stainless steel, and Type 316 stainless steel. The scope was limited to uni-axial loading under isothermal conditions. Relaxation data was evaluated for several prior cyclic (fatigue) loading histories. Results of these evaluations were compared with creep data for the same histories. In order to analyze the stress relaxation data, creep equations were chosen and integrated using the time-hardening rule to develop closed-form expressions for the relaxation response. Coefficients for these relaxation expressions were obtained using nonlinear least squares techniques. The appropriateness of using linearized transformations compared with direct nonlinear approaches was treated. For tensile hold-time CF tests, the dependence of the coefficients on initial stress level was

evaluated. Finally, the dramatic effects of both loading sequence and strain (both monotonic and cyclic) were discussed for one particular experimental case.

Jeong and Nam [18] conducted a quantitative analysis of the stress dependence on stress relaxation creep rate during hold time under CF interaction conditions for 1Cr-Mo-V steel. It was shown that the transient behavior of the Norton power law relation was observed in the early stage of stress relaxation in which the instantaneous stress is relaxed drastically, which occurs due to the initial loading condition. But after the initial transient response in a 5 hour tensile hold time, the relations between strain rate and instantaneous stress represented the same creep behavior, which was independent of the initial strain level. The value of stress exponent after transition was 17 which is the same as that of the typical monotonic creep suggested from several studies for 1Cr-Mo-V steel. Considering the value of the activation energy for the saturated relaxation stage, it was suggested that the creep rate was related to instantaneous stress and temperature by the Arrhenius type power law.

## **2.5 Thesis Objectives**

Regarding the reasoning provided in Section 1.2 and reviews presented in Section 2.3, specific objectives in this thesis, in this focus area, are listed below.

1. To modify well-known creep rupture models to CF life expense models.
2. To experimentally study the CF life expense models which do not need a separation in CF damage.
3. To validate models, developed in objective 1 using data in objective 2.
4. To study parametrically and develop an understanding of the effect of

different hold times on CF life expense of steel alloy.

5. To validate well-known creep models with highest goodness of fit on the creep data extracted from cyclic relaxation response of the steel alloy under CF condition.

## 2.6 References

- [1] Brinkman, C.R., "Hight-temperature time-dependent fatigue behaviour of several engineering structural alloys," *International Metals Review*, Vol.30, No.5, 1985.
- [2] Takahashi, Y., Shibamoto, H. and Inoue, K., "Study on creep-fatigue life prediction methods for low-carbon nitrogen-controlled 316 stainless steel (316FR)," *Nuclear Engineering and Design*, Vol. 238, pp. 322-335, 2008.
- [3] Li, J. and Dasgupta, A., "Failure mechanisms and models for creep and creep rupture," *IEEE Transactions on Reliability*, Vol.42, No.3, 1993.
- [4] Ostergren, W. J., "A Damage Function and Associated Failure Equations for Predicting Hold Time and Frequency Effects in Elevated Temperature, Low Cycle Fatigue," *Journal of Testing and Evaluation*, JTEVA, Vol. 4, No.5, pp.327-339, Sept. 1976.
- [5] Haford, G.R., Saltsman, J.F., and Hirschberg, M.H., "Ductility normalized strainrange-partitioning life relations for creep-fatigue life predictions," Conference on Environmental Effects and Degradation of Engineering Materials, Virginia, October 10-12, 1977.
- [6] Lloyd, G.J. and Wareing, J., "Life prediction methods for combined creep rupture," *IEEE Transactions on Reliability*, Vol.42, No.3, 1993.
- [7] Fatemi, A. and Yang, L., "Cumulative fatigue damage and life prediction theories: a survey of the state of the art for homogenous materials," *International Journal of Fatigue*, Vol.20, Issue: 1, pp:9-34, 1998.
- [8] Goswami, T., "Low cycle fatigue-dwell effects and damage mechanisms," *International Journal of Fatigue*, 1999.
- [9] Goswami, T. and Hanninen, H., "Dwell effects oh high temperature fatigue behavior Part I," *Materials and Design*, Vol.22, pp:199-215, 2001.

- [10] Goswami, T., "Development of generic creep-fatigue life prediction models," *Materials and Design*, Vol.25, pp:277-288, 2004.
- [11] Takahashi, Y., Shibamoto, H., Inoue, K., "Study on creep-fatigue life prediction methods for low-carbon nitrogen-controlled 316 stainless steel (316FR)," *Nuclear Engineering and Design*, Vol.238, pp:322-335, 2008.
- [12] Takahashi, Y., Shibamoto, H., Inoue, K., "Long-term creep-rupture behavior of smooth and notched bar specimens of low-carbon nitrogen-controlled 316 stainless steel (316FR) and their evaluation," *Nuclear Engineering and Design*, Vol.238, pp:310-321, 2008.
- [13] He, X., "Statistical thermal fatigue-creep modeling of stainless steel materials," *IEEE*, 2009.
- [14] Holmström, S. and Auerkari, P., "A robust model for creep-fatigue life assessment," *Materials Science & Engineering A*, Vol. 559, pp.333-335, 2013.
- [15] Jaske, C.E., Mindlin, H., and Perrin, J.S., "Combined Low-Cycle Fatigue and Stress Relaxation of Alloy 800 and Type 304 Stainless Steel at Elevated Temperatures," *Fatigue at Elevated Temperature, ASTM STP 520*, American Society for Testing Materials, pp:365-376, 1973.
- [16] Lafen, J.H. and Jaske, C.E., "Cyclic relaxation response under creep-fatigue conditions," *Stress Relaxation Testing, ASTM STP 676*, pp:182-206, 1976.
- [17] Jeong, C.Y. and Nam, S.W., "Stress dependence on stress relaxation creep rate during tensile holding under creep-fatigue interaction in 1Cr-Mo-V steel," *Journal of Materials Science*, Vol.34, pp:2513-2517, 1999.

## **Chapter 3: Models for Creep-Fatigue and Creep in Cyclic Relaxation Response in a Steel Alloy**

### **3.1 Introduction**

There are numerous applications in the modern engineering world that involve the use of metals under conditions of cyclic loading in operating conditions that can cause creep and/or environmental interactions with time-independent mechanical fatigue processes. The inter-relationships between the various damage mechanisms that occur under such severe service conditions are complex. Thus, the development of physics-based models to predict remaining life must be guided by experimental studies that are specifically aimed at the fundamental understanding of these mechanisms [1]. A number of standard and methods and guidelines exist for design and life assessment of structures subjected to cyclic loads at elevated temperatures. Most of these use methods where creep and fatigue life fractions of the loading history are evaluated separately, combined as additive quantities, and compared to case or material specific limits [2]. Figure 3.1 shows a schematic of a comprehensive methodology for ensuring structural integrity at elevated temperatures and it illustrates how crack growth can be interfaced with constitutive and crack initiation models to significantly impact the ability to predict component behavior during service and the design of better systems. In this chapter, such creep-fatigue (CF) life assessments models are reviewed in addition to the models which do not separate creep-fatigue damage. The CF models which do not need separate creep and fatigue damage are based on the creep rupture behavior of the material described by hold

time [2]. Well-known creep rupture models are reviewed in the end of the chapter, and some of them with highest performance are validated with the literature data from stress-relaxation tests under CF condition.

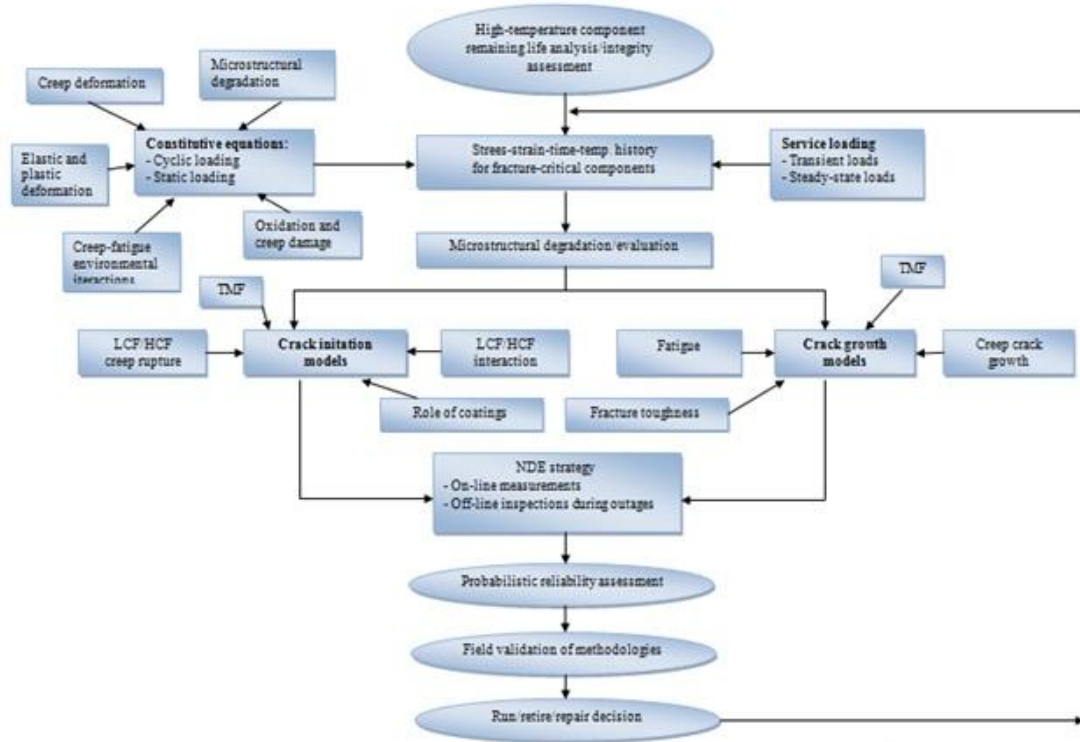


**Figure 3.1: Methodology for assessing integrity of structural components that operate at high temperatures. TMF, thermomechanical fatigue; NDE, nondestructive evaluation; LCF, low-cycle fatigue; HCF, high-cycle fatigue [1].**

Additionally, for high-temperature low-cycle fatigue, it is shown that fatigue life decreases as the hold time increases. This is a result of increased creep effect caused by stress relaxation. The exact reason for this reduction in fatigue life is suggested as the creep damage formation during stress relaxation [3-5]. Therefore, in the end of the chapter, cyclic relaxation response models under CF condition and relaxation creep damage models are reviewed. Finally, the models that were best suited for this CF study are defined.

### 3.2 Models for CF in Steels and Alloys

This section reviews published CF models which have been used for stainless steels, Cr-Mo steels, solder alloys, copper alloys, titanium alloys, tantalum alloys and super-alloys since 1970s. These models were separated according to the loading sequence in CF, case/research specific circumstances and availability of experimental data properties. Some of those categories were also separated into the other sub-categories such as loading sequence for the cases where it can affect the damage trend of interactions [2]. The parameters varied included temperature, strain rates, hold/dwell time and environment [2,3]. Figure 3.2 shows three classes of CF life fraction models. Figure 3.3 shows loading sequence dependent CF expended life models. Figure 3.4 shows case/research specific alternate approaches to CF expended life models, and Figure 3.5 shows CF expended life models when cyclic material data is not available.

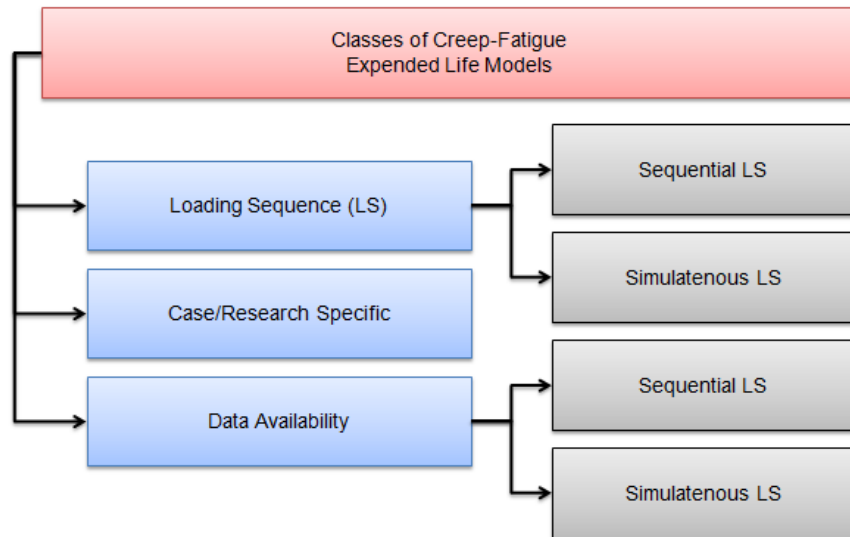


**Figure 3.2: Three classes of CF expended life models**

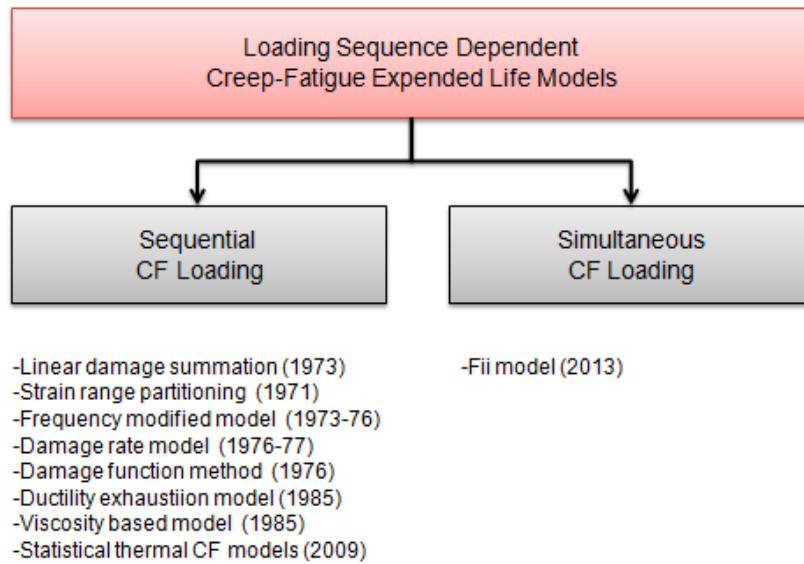


**Figure 3.3: Loading sequence dependent CF expended life model**

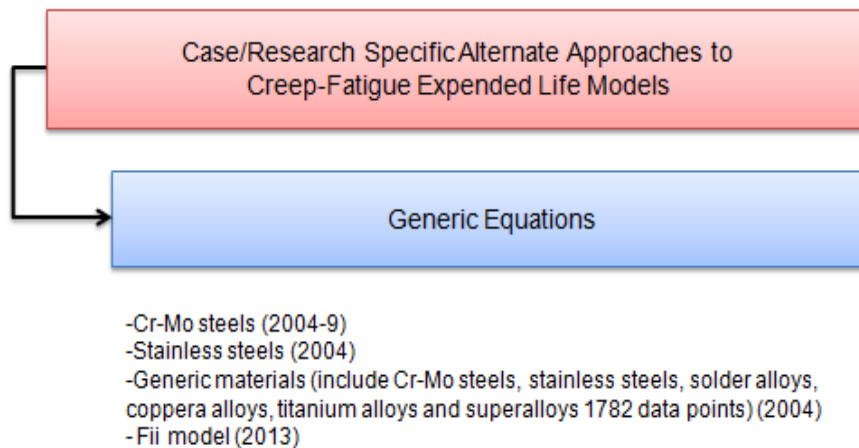


**Figure 3.4: Case/research specific alternate approaches to CF expended life models**

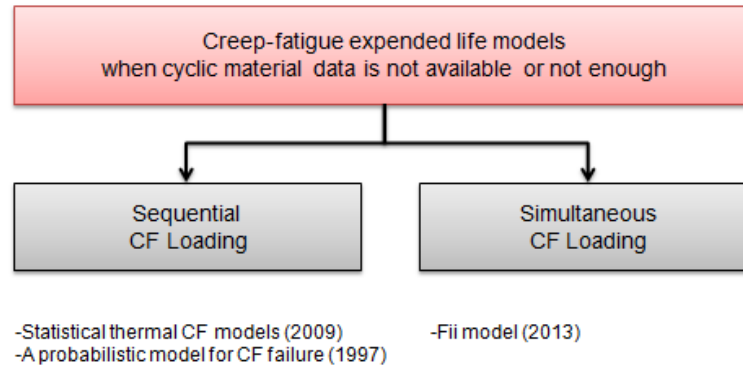


**Figure 3.5: CF expended life models when cyclic material data is not available**

**Table 3.1: Review of CF assessment methods in literature [6, 8]**

Method of life prediction	Life prediction equations	Material parameters needed (n)	Test requirements
Linear damage summation [9]	$1 = \sum N_i/N_f + \sum t_i/t_r$	Strain-life data (4) Creep-rupture (2-4)	0/0 tests ( $\epsilon_t - N_f$ ) creep rupture, stress relaxation
Strain range partitioning [10]	$N_{ij} = A_{ij} \Delta \epsilon_{ij}^{B_{ij}k}$ , ij represent PP, PC, CP and CC loops	Four inelastic strain vs. life relations (2x4)	Tests producing complex loops PP, PC, CP, and CC
Frequency modified approach [11]	$N_f = [F/\Delta \epsilon_p]^{1/B'} [v_z/2]^{1-k} [v_z/v_d]^d$	Strain-life data (4) Frequency vs. life (2) Stress-strain (2)	0/0 tests, hold time tests, frequency-life tests
Damage rate model [12]	$da/dN = a[T][\epsilon_p]^m [\dot{\epsilon}_p]^k$ $da/dN = a[C][\epsilon_p]^m [\dot{\epsilon}_p]^k$	Scaling factors (2)	0/0 tests, metallographic evidence, hold time tests
Damage function method [13]	$C = \sigma_T \Delta \epsilon_p N_f^B v^{B(K-1)}$	Strain-life (4)	0/0 data, frequency data, stress-life data, hold time data
Damage parameter approach [14]	$d\omega/dt = \left[ C \left\{ \frac{\sigma}{(1-\omega)} \right\}^{v_0} d\sigma/dt H(d\sigma) + C \left\{ \frac{\sigma}{(1-\omega)} \right\}^v \right] H(\sigma)$	Frequency-life (2) Stress-strain (2) Shape correction factor Material parameter (3) Fatigue damage (2) Creep damage (2)	Stress versus damage in creep and fatigue
Viscosity based model [15]	$N_f = K(\Delta \epsilon_p)^{m-1} (\Delta \epsilon_p / \text{strain rate})^m \sigma_{\text{act}}$	Total strain and life (2) Stress-strain (2)	Continuous fatigue

### 3.2.1 Loading Sequence Dependent CF Expended Life Models

In this category, models were separated into two groups of sequential and simultaneous CF loading. Nearly 90% of the published models are included in the sequential CF loading category. These life-prediction methods were all at different stages of development and these models are presented in the following section.

#### 3.2.1.1 Sequential CF Loading

Models presented in this category mostly depend on how cracks behave. They suffer from crack initiation effects and interaction effects which are unpredictable. Goswami [6, 8] summarizes empirical life prediction models developed since 1970 and found that only three of those methods received notable interest. They are: damage summation, strain range partitioning and damage approach [6, 8].

##### 3.2.1.1.1 Linear damage summation

Linear damage summation is widely known as the simplest of the many life-prediction methods [9, 15]. It is stated as [16]:

$$D_f + D_c = 1 \text{ (at failure)} \quad (3.1)$$

where  $D_f$  and  $D_c$  are the fatigue and creep damage ratios, respectively. The Summation method was employed by the American Society for Mechanical Engineers in Code Case N-47 [9], and used cycle and time ratios as follows:

$$\sum n/N_f + \sum t/t_r \leq D \quad (3.2)$$

where

$D$  = total CF damage

$n$  = number of applied cycles at a particular loading condition

$N_f$  = number of cycles to failure at a particular strain range

$t$  = time duration at a particular load condition

$t_r$  = time to rupture from isothermal stress-rupture curves for a given loading condition

The concept of simply summing creep and fatigue damage has been criticized for some reasons. The advantages and disadvantages of the cumulative linear damage summation technique was discussed by Brinkman [15] and a brief summary is shown below:

1. Compressive and tensile damage are treated equally by using tensile stress-rupture data for all creep-damage assessment.
2. Some materials such as type 304 stainless steel and alloy 800H show D-values that are considerably below 1 and tend to decrease with decreasing strain range and increasing hold time. For typical design situations that involve long hold periods at low strain rates, it is difficult to justify a given D-value.
3. Environmental interaction, which can influence both crack nucleation and growth, is not directly accounted for by this method. Therefore, when an apparent true CF interaction is indicated it actually may be due to environmental effects.
4. Materials such as 800H, 304 stainless steel or 2-25Cr-1Mo may cyclically harden or soften, depending on the material, heat treatment and strain range such that the stress-rupture properties determined from virgin material may not be appropriate. This problem may be corrected by using cyclic creep data if available.

### 3.2.1.1.2 Strain range partitioning

In this technique, the inelastic strain range is partitioned into four components:

$$\begin{aligned}\Delta\varepsilon_{pp} &= \text{plastic-plastic} & \Delta\varepsilon_{cp} &= \text{creep-plastic} \\ \Delta\varepsilon_{pc} &= \text{plastic-creep} & \Delta\varepsilon_{cc} &= \text{creep-creep}\end{aligned}$$

where the first subscript refers to the tensile and the second to the compressive deformation [10, 15]. Lifetime relationships for each of these strain ranges are experimentally established in the form of the Manson-Coffin equation [17]:

$$N_{jk} = A_{jk} \Delta\varepsilon_{jk}^{\theta_{jk}} \quad (3.3)$$

where j and k represent p or c. Damage fractions F are usually summed by the interaction damage rule,

$$\frac{F_{pp}}{N_{pp}} + \frac{F_{pc}}{N_{pc}} + \frac{F_{cp}}{N_{cp}} + \frac{F_{cc}}{N_{cc}} = \frac{1}{N} \quad (3.4)$$

where

$$\begin{aligned}\frac{\Delta\varepsilon_{pp}}{\Delta\varepsilon_{in}} &= F_{pp} & \frac{\Delta\varepsilon_{pc}}{\Delta\varepsilon_{in}} &= F_{pc}, \\ \frac{\Delta\varepsilon_{cp}}{\Delta\varepsilon_{in}} &= F_{cp}, & \frac{\Delta\varepsilon_{cc}}{\Delta\varepsilon_{in}} &= F_{cc}\end{aligned} \quad (3.5)$$

and  $\Delta\varepsilon_{in}$  is the inelastic strain range

$$\Delta\varepsilon_{in} = \Delta\varepsilon_{pp} + \Delta\varepsilon_{pc} + \Delta\varepsilon_{cp} + \Delta\varepsilon_{cc} \quad (3.6)$$

This method has been used extensively and is one of the easiest to manipulate. It has had good success in predicting failure of power plant components exposed to long-term service. It has also been modified to account for mean stress effects and changes in long-term ductility [15]. However, the disadvantages of this method are presented as follows:

1. It may be difficult to define the hysteresis loop and accurately partition the

inelastic strain range into the various components, particularly at low strain ranges

2. The method may be inaccurate in situations where the principal damaging mechanism is environmental rather than type of deformation.

### 3.2.1.1.3 Frequency modified approach

This method [18] modifies the original Coffin-Monson and Basquin law relationships between plastic (inelastic) strain range  $\Delta\varepsilon_p$  and cycles to failure  $N_f$  with a frequency factor  $v$  such that the plastic  $\Delta\varepsilon_p$  and elastic  $\Delta\varepsilon_e$  components of the total strain range  $\Delta\varepsilon_t$  can be expressed as follows:

$$\Delta\varepsilon_p = C_2(N_f v^{k-1})^{-\beta} \quad (3.7)$$

$$\Delta\varepsilon_e = A' N_f^{-\beta'} v^{k'_1} \quad (3.8)$$

where  $C_2$ ,  $k$ ,  $\beta$ ,  $A'$ ,  $\beta'$  and  $k'_1$  are material parameters for a given environment and are determined by regression analysis of available data [15]. Eq. (3.7) can be expressed as:

$$N_f = (C_2/\Delta\varepsilon_p)^{1/\beta} v^{1-k} \quad (3.9)$$

which was further modified to incorporate waveform effects:

$$N_f = (C_2/\Delta\varepsilon_p)^{1/\beta} v^{1-k} (v_c/v_t)^c \quad (3.10)$$

where

$c$  = material parameter

$v = 1/(1/v_t + 1/v_c)$  = frequency of cycling

$v_c$  = compression-going frequency

$v_t$  = tension-going frequency

This method has been used extensively to predict lifetimes for various materials. It has been criticized [15] for the following reasons:

- a) It does not contain a mean stress correction term.
- b) With decreasing frequency or increasing duration of a tensile hold time, this method predicts decreased fatigue life, which doesn't always occur because of metallurgical changes as seen in 316 stainless steel.
- c) Tensile hold times of equal duration are treated as being equally damaging irrespective of where they occur in the hysteresis loop, which is not always the case.

#### **3.2.1.1.4 Damage rate model**

This model [19] was developed from observations of the behavior of 304 stainless steel, and assumes that in the low-cycle regime most of the fatigue life is associated with the growth of cavities and crack growth [15]. It is manipulated on a differential form of damage with time and employs several equations appropriate for various waveforms characterizing cavity and crack growth. These growth laws are integrated over the specimen life, with critical crack and cavity size determined by an interaction damage rule [15]. However, Brinkman [15] indicates that various problems have been identified depending on waveform, duration of hold time, and whether or not a mean stress was present. Crack-nucleation phenomena such as oxide cracking are ignored. This method needs greater time-dependent fatigue interaction.

### 3.2.1.1.5 Damage function method

Ostergren [19] suggested that the time dependent damage associated with hold time for a material at a given temperature level can be separated into the two categories as independent or dependent of waveshape.

#### a. Time-dependent damage is independent of wave-shape

Ostergren [19] conducted a hold time test on the cast nickel-base “superalloy” IN738 at 871°C. On a uniform gage specimen with axial extensometer and total strain control, Ostergren defined failure by a change in the character of stress and inelastic strain, indicative of the presence of a crack of some magnitude.

As far as the method is concerned, since no additional correction for wave shape beyond using measure of damage  $\sigma_T \Delta \epsilon_p$  appears necessary, this would suggest a frequency modified failure relation similar to Coffin’s frequency modified equation [19]:

$$\begin{aligned} \sigma_T \Delta \epsilon_p N_f^\beta v^{\beta(k-1)} &= C \\ v = (1/\tau) &= 1/(\tau_0 + \tau_T + \tau_c) \end{aligned} \quad (3.15)$$

where

$\beta, k, C$  = material constants,  
 $v$  = frequency,  
 $\tau$  = cycle period,  
 $\tau_0$  = time per cycle of continuous cycling,  
 $\tau_T$  = tension hold time,  
 $\tau_c$  = compression hold time.

When comparable  $\sigma_T \Delta \epsilon_p$  life reduction is dependent only on cycle period, one would conclude that time-dependent damage is independent of wave shape and that Eq. (3.15) is the appropriate failure criterion [19]. Further reduction of Eq. (3.15) to the conventional frequency modified approach is not possible because of the mean

stresses which arise from hold times [12]. Additionally, the Coffin-Manson [20] equation is:

$$\begin{aligned}
 \sigma_T \approx (\Delta\sigma/2) &= C_0 \left[ (\Delta\epsilon_p)^{n'/2} \right] \\
 \left[ C_0 (\Delta\epsilon_p)^{n'/2} \right] (\Delta\epsilon_p N_f^\beta) &= C \\
 \Delta\epsilon_p N_f^{\beta/(1+n')} &= (2 C/C_0)^{1/(1+n')} \\
 \Delta\epsilon_p N_f^{\beta^*} &= C^*
 \end{aligned} \tag{3.16}$$

where  $n'$  is the cyclic strain hardening exponent and  $C_0, \beta^*$  and  $C^*$  are material constants. For constant strain rate isothermal cycling without hold times, significant mean stresses do not generally occur [19]. Therefore similar to Eqns (3.15) and (3.16):

$$\begin{aligned}
 \sigma_T \approx \frac{\Delta\sigma}{2} &= \frac{C_0 (\Delta\epsilon_p)^{n'}}{2} v^{k_1} \\
 \left( \frac{C_0 (\Delta\epsilon_p)^{n'}}{2} v^{k_1} \right) (\Delta\epsilon_p N_f^\beta v^{\beta(k-1)}) &= C \\
 \Delta\epsilon_p N_f^{\beta/(1+n')} v^{[\beta(k-1)+k_1]/(1+n')} &= (2 C/C_0)^{1/(1+n')} \\
 \Delta\epsilon_p N_f^{\beta^*} v^{\beta^*(k^*-1)} &= C^*
 \end{aligned} \tag{3.17}$$

where  $\Delta\sigma$  is the frequency modified stress range and  $C_0, k_1, \beta^*, k^*$ , and  $C^*$  are material constants. For nickel-base superalloy materials (for example, IN738),  $k \approx 1$  because they can be correlated without the frequency term [19]. Therefore, there is very little time-dependent damage in these alloys.

#### **b. Time dependent damage is dependent on wave shape**

Similar to the failure criterion of Eq. (3.15), the failure relation can be written as:

$$\begin{aligned}
 \sigma_T \Delta\epsilon_p N_t^\beta v^{\beta(k-1)} &= C \\
 v &= 1/(\tau_0 + \tau_T - \tau_c) \text{ for } \tau_T > \tau_c
 \end{aligned} \tag{3.18}$$

$$\nu = 1/\tau_0 \text{ for } \tau_T \leq \tau_c$$

where

$\beta, k, C$  = material constants,

$\nu$  = effective frequency,

$\tau_0$  = time per cycle of continuous cycling,

$\tau_T$  = time for which creep occurs in tension (tension hold time), and

$\tau_c$  = time for which creep occurs in compression (compression hold time).

The effective frequency term  $\nu$ , which considers the increase in cycle period by taking the tensile hold time minus the compressive hold time, is an empirical approach for including the time-dependent damage of tensile creep and beneficial effects of compressive creep [12]. The effective frequency is equal to the actual frequency when hold times occur only in tension; other than it is greater than actual frequency [19].

#### 3.2.1.1.6 Viscosity based model

Goswami [6] developed a new CF life prediction model with the premise that deformation under CF test conditions can be represented in terms of viscous behavior, which is dissipative and irreversible. In an LCF test below  $T_m$  (where  $T_m$  is melting temperature of a material in absolute scale), the cyclic damage can be represented by viscous flow [6]. In modeling steady-state creep behavior, this concept has been applied. Material parameters used in Goswami's analysis [6] were analogous to the dashpot parameters in terms of force and displacement. Steady-state creep behavior is in terms of linear dashpot process, where velocity is proportional to force. It assumes constant value of force to give a constant velocity resulting in a linear displacement versus time behavior. When the force is removed, the motion stops, so that the deformation is permanent. These concepts were extended in a dwell fatigue situation

in which creep and fatigue processes interact. Since these tests are conducted at a strain level where total strain range exceeds the elastic strain range, the cyclic deformation is permanent. In order to simulate fatigue, a dynamic velocity term was used in the model development. It may be noted that fundamental viscosity and dynamic viscosity concepts are analogous [6]. Goswami [6] presented the dynamic viscosity as the following Eq.(3.19):

$$\text{Dynamic viscosity at failure} = \Delta\sigma/\dot{\epsilon} \quad (3.19)$$

Since the deformation in a dwell fatigue cycle depends upon the strain range and time, the rate of damage is in terms of strain rate of a cycle. Therefore, the total strain range, which has no units, has been multiplied in Eq. (3.19) to account for strain range effects [6]. The resulting term has the same units as dynamic viscosity and is referred to as dynamic viscosity (DV):

$$\text{DV at failure} = \Delta\sigma\Delta\epsilon_t/\dot{\epsilon} \quad (3.20)$$

When the ability of a material to accommodate viscosity ceases as the dynamic viscosity reaches a critical value, failure occurs [6]. The ability of a material to accommodate permanent deformation was assumed in terms of material toughness. The toughness of a material is a product of ductility and strength:

$$\text{Material toughness} = \text{ductility} \times \text{strength} \quad (3.21)$$

Since strength in a cyclic fatigue test is in terms of saturated stress range ( $\sigma_{\text{sat}}$ ) at a particular strain range, it was used in Eq. (3.21). It may be noted that this stress value can be determined from actual low cycle fatigue test and depending on cyclic stress-strain behavior under a particular failure criterion such as 10-50% load drop

used in testing. Ductility was determined using drop Edmund and White equation as follows:

$$\text{Ductility} = \Delta \varepsilon_p N_f \quad (3.22)$$

Therefore, Eq. (3.22) was substituted in Eq. (3.21) with multiplier  $\sigma_{sat}$  giving material toughness. Therefore, Goswami [6] derives a new CF life prediction equation by equating these two terms: dynamic viscosity Eq. (3.21) and toughness Eq. (3.22) and deriving a new life prediction equation as follows:

$$\Delta \sigma \Delta \varepsilon_t / \dot{\varepsilon} = \Delta \varepsilon_p N_f \sigma_{sat} \quad (3.23)$$

Since CF life is a dependent on a variety of test parameters [6], Goswami [2] developed a scaling relationship by plotting strain range vs. strain rate ratios and cycles to failure on log-log scales. This produced a linear equation with a slope of m and this slope m was combined with the cyclic stress-strain equation Eq. (3.24) to develop the following life prediction equation:

$$N_f = K(\Delta \varepsilon_p)^{n-1} (\Delta \varepsilon_t / \dot{\varepsilon})^m \sigma_{sat} \quad (3.24)$$

An empirical correction factor was used to account for dwell times in the above equation, which was determined by data fitting as shown below in Eq. (3.25).

$$\text{Dwell time correction factor} = \frac{\text{strain rate}}{(1 + \log (\text{dwell time in s}))} \quad (3.25)$$

The dwell time correction factor used in Eq. (3.24) and dwell fatigue life predicted by the CF data bank, material parameters, e.g., parameters of Coffin-

Manson equation, cyclic stress-strain parameters, m and other parameters can be derived by appropriate data fitting for each material and test.

### 3.2.1.1.7 Statistical thermal CF models

He [21, 22] investigated the CF behavior of stainless steel materials. He [21, 22] focused on low cycle thermal fatigue life models, and then evaluated statistical creep models for stainless steel materials. In the low cycle thermal fatigue model, He [21, 22] used Manson's universal slopes equation [23], as an empirical relation relating fatigue endurance to tensile properties. Afterwards, He [21, 22] studied creep prediction models of Basquin [24] and Sherby-Dorn [24] in order to correlate the results of short-time elevated temperature tests with long-time service performance at more moderate temperatures. In this section, the creep prediction models are evaluated a little bit more in detail, in addition to He's [21,22] experimental study.

#### 3.2.1.1.7.1 Low cycle thermal fatigue life models

The low cycle thermal fatigue life can be obtained from the total strain range vs. life curve. When the cyclic material data is insufficient or unavailable, Manson's universal slopes equation [23] can be used as an empirical correlation which relates fatigue endurance to tensile properties:

$$\Delta\varepsilon = 3.5 \frac{UTS}{E} (N_f)^{-0.12} + \varepsilon_f^{0.6} (N_f)^{-0.6} \quad (3.26)$$

where  $\Delta\varepsilon$  is the total strain range, UTS is the ultimate tensile strength, E is the Young's modulus,  $N_f$  is the number of cycles to failure and  $\varepsilon_f$  is the true ductility which can be obtained by following equation:

$$\varepsilon_f = \ln \left( \frac{100}{100-RA} \right) - \varepsilon_H \quad (3.27)$$

where RA is the percentage reduction in area at tensile failure and  $\varepsilon_H$  is the pre-strain [21, 22].

**Table 3.2: Relation between temperature and other parameters [21, 22]**

T (°C)	450	600	700
Ultimate Tensile Stress, UTS (MPa)	465	405	326
Elastic Modulus, E (GPa)	168.5	151	142
% Reduction in Area, RA (%)	70	70	68

To find the relationship between temperature T and other parameters, He [21, 22] used the data in Table 3.2 in conjunction with different modes. The results showed that the polynomial model provided the best fit ( $R^2 = 1$ ) for the relationship between temperature T and UTS, and a model of the following type was expected:

$$UTS(T) = -0.0016T^2 + 1.238T + 223.8 \quad (3.28)$$

The natural logarithmic model provided a relative better fit ( $R^2 = 0.9999$ ) for the relationship between temperature T and E.

$$E(T) = -60.068 \ln(T) + 535.53 \quad (3.29)$$

It can be seen from Table 3.2 that for AISI316 stainless steel, % RA only changes slightly as the temperature increases. Thus, %RA = 70 was used in the study of He [20, 21]. The true ductility  $\varepsilon_f$  was obtained by following equation:

$$\varepsilon_f = 1.20 - \varepsilon_H \quad (3.30)$$

Substituting Eqns (3.28), (3.29) and (3.30) into Eq. (3.31) gives:

$$\Delta \varepsilon = 3.5 \frac{-0.0016T^2 + 1.238T + 223.8}{-60.086 \ln(T) + 535.53} (N_f)^{-0.12} + (1.20 - \varepsilon_H)^{0.6} (N_f)^{-0.6} \quad (3.31)$$

**Table 3.3: Leading creep rupture models in literature\***

Model	Trend Eq. (T in °K) ( $t_r$ in sec)	Material Parameters needed (n)	REF
Restrained Manson-Brown (RMB) <sup>a</sup>	$\log t_r = \log t_a \cdot T^{-a_1-1} + (T - T_a \cdot (q))^{a_2} (a_0 + a_1 \cdot \log \sigma + a_2 \cdot \log^2 \sigma)$	6	Seruga and Nagode (2011) [25]
Wilshire Equation	$\log(t_r) = \left( \frac{\ln(\frac{\sigma}{\sigma_{UTS}})}{-k} \right)^{1/w} \cdot \frac{1}{\exp(\frac{-Q_a}{R \cdot T})}$	3	Wilshire et al. (2009) [26]
Minimum commitment	$\log(t_r) = \beta_0 + \beta_1 \cdot \log[\sigma_c] + \beta_2 \sigma_c + \beta_3 \sigma_c^2 + \beta_4 T + \frac{\beta_5}{T}$	6	Manson and Muraldihan (1983) [27]
Soviet Model 1&2	$\log(t_r) = \beta_0 + \beta_1 \cdot \log[T] + \beta_2 \cdot \log[\sigma_c] + \frac{\beta_3}{T} + \beta_4 \cdot \frac{\sigma_c}{T}$	5	Trunin et al. (1971)
Mendelson-Roberts-Manson (MRM) <sup>a</sup>	$\log(t_r) = \{\sum_{k=0}^n \beta_k (\log[\sigma_c])^k\} (T - T_c)^r / \sigma_c^{-n} + \beta_2$ (n=2,3,4)	min.4-max.6	Mendelson et al. (1965) [29]
Simplified MRM <sup>a</sup>	$\log(t_r) = \{\sum_{k=0}^n \beta_k \log([\sigma_c])^k\} / (T - T_c) + \beta_2$ (n=2,3,4)	min.4-max.6	Mendelson et. al. (1965) [29]
Orr-Sherby-Dorn <sup>a</sup>	$\log(t_r) = \{\sum_{k=0}^n \beta_k (\log[\sigma_c])^k\} + \beta_2 / T$	min.4-max.6	
Manson-Haferd <sup>a</sup>	$\log(t_r) = \{\sum_{k=0}^n \beta_k (\log[\sigma_c])^k\} (T - T_c) + \beta_2$ (n=2,3,4)	min.4-max.6	Manson and Haferd (1953) [29]
Manson-Haferd with $T_c = 0^a$	$\log(t_r) = \{\sum_{k=0}^n \beta_k (\log[\sigma_c])^k\} T + \beta_2$ (n=2,3,4)	min.4-max.6	Manson and Haferd (1953) [29]
Larson-Miller <sup>a</sup>	$\log(t_r) = \{\sum_{k=0}^n \beta_k (\log[\sigma_c])^k\} / T + \beta_2$ (n=2,3,4)	min.4-max.6	Larson and Miller, 1952 [29]

a: Models derived from Restrained Manson-Brown

\* Adapted from Holdsworth and Daviel [36]

### 3.2.1.1.7.2 Leading creep rupture models

In order to design reliable systems, accurate information for the elevated-temperature tensile, creep and rupture test data for stainless steel is required and has been collected for a number of different steel manufacturers [20, 21]. In this section, leading creep rupture models as seen in Table 3.3 are discussed.

#### a. Restrained Manson Brown

The Manson-Brown parameter in particular, given by:

$$MB = \frac{\log t_r - \log t_a}{(T - T_a)^q} \quad (3.34)$$

is numerically unstable due to the coefficients  $T_a$  and  $q$ . The set of equations used to determine the coefficients can be non-linear and cannot be solved trivially. The restrained Manson-Brown (RMB) parameter is proposed as:

$$RMB = \frac{\log t_r - \log t_a \cdot T^{|q|-1}}{(T - T_a \cdot \langle q \rangle)^q} \quad (3.35)$$

where  $\log t_a$ ,  $T_a$  and  $q$  are the coefficients obtained by the least squares method [25]. The value of  $\langle q \rangle$  is if  $q > 0$  and 0 if  $q \leq 0$ . The MB parameter (Eq.(3.34)) is hard to solve numerically due to the unrestrained coefficients  $q$  and  $T_a$ . Therefore, the RMB parameter is introduced as a substitute resembling all of the properties of the MB parameter. This is numerically friendlier to solve because the coefficients can be determined by solving a set of linear equations and not nonlinear, as in the case of MB parameter [25]. The states of the RMB parameter represent the Larson-Miller (LM), Orr-Sherby-Dorn (OSD) and Manson-Haferd (MH) parameter. If  $q = 1$ , the RMB parameter represents the MH parameter, given by Eq. (3.34). If  $q = 0$ , the RMB parameter represents the OSD parameter, given by:

$$OSD = \log t_r - \frac{\log t_a}{T} \quad (3.36)$$

and if  $q = -1$ , the RMB parameter represents the LM parameter, given by:

$$LM = T(\log t_r - \log t_a) \quad (3.37)$$

If  $q \neq 1, 0$  or  $1$ , the RMB parameter examines whether or not it is possible to describe the test data more accurately than with LM, OSD and MH parameters. Every

time-temperature parameter is also a function of the stress and this function is usually a second degree polynomial especially in the case of limited test data [25].

$$\text{RMB} = \text{LM} = \text{OSD} = \text{MH} = f(\sigma) \quad (3.38)$$

$$\text{RMB} = \text{LM} = \text{OSD} = \text{MH} = a_0 + a_1 \cdot \log \sigma + a_2 \cdot \log^2 \sigma \quad (3.39)$$

Considering only the RMB parameter (Eq.(3.35)), the relation between the time to rupture, temperature and stress is thus given by [25]:

$$\frac{\log t_r - \log t_a \cdot T^{|q|-1}}{(T - T_a \cdot \langle q \rangle)^q} = a_0 + a_1 \cdot \log \sigma + a_2 \cdot \log^2 \sigma \quad (3.40)$$

This yields Eq. (3.64).

$$\log t_r = \log t_a \cdot T^{|q|-1} + (T - T_a \cdot \langle q \rangle)^q (a_0 + a_1 \cdot \log \sigma + a_2 \cdot \log^2 \sigma) \quad (3.41)$$

The coefficients  $\log t_a$ ,  $T_a$ ,  $q$ ,  $a_0$ ,  $a_1$  and  $a_2$  are obtained for the existing creep rupture test data by the least squares method.

## b. Wilshire Equation

It has become common practice to describe creep and creep fracture behavior in terms of the dependencies of the minimum creep rate ( $\dot{\epsilon}_m$ ) and creep life ( $t_f$ ) on stress ( $\sigma$ ) and temperature ( $T$ ) using power law expressions of the form [26]:

$$\frac{M}{t_f} = \dot{\epsilon}_m = A \sigma^n \exp\left(\frac{-Q_c}{RT}\right) \quad (3.42)$$

where  $R=8.314\text{Jmol}^{-1}\text{K}^{-1}$ ,  $M(= \dot{\epsilon}_m t_f)$ , the parameter ( $A$ ), the stress exponent ( $n$ ) and the activation energy for creep ( $Q_c$ ) are themselves functions of stress and temperature.

In contrast to parametric methods, the stress/creep life plots are easily superimposed by normalizing the applied stress thorough the measured values of yield stress  $\sigma_{YS}$  or tensile stress  $\sigma_{TS}$ . With this approach,  $\sigma_{TS}$  is preferred to  $\sigma_{YS}$ , because property sets can be considered over the full stress range from  $\sigma/\sigma_{TS}=1$  to  $\sigma/\sigma_{TS}=0$  for  $\sigma_{TS}$ . Eq. (3.42) can then be re-written as:

$$\frac{M}{t_f} = \dot{\epsilon}_m = A^* \left( \frac{\sigma}{\sigma_{TS}} \right)^n \exp \left( \frac{-Q_c}{RT} \right) \quad (3.43)$$

where  $A^* \neq A$  and  $Q_c^* \neq Q_c$ . Eq. (3.43) avoids the large and variable  $Q_c$  values observed using Eq.(3.43), but does not avoid fluctuating  $n$  values. In seeking to quantify creep life behavior over broad stress ranges,  $t_f$  must approach zero as  $(\sigma/\sigma_{TS}) \rightarrow 1$ , with points of inflection in the stress rupture plots ensuring that  $t_f \rightarrow \infty$  as  $(\sigma/\sigma_{TS}) \rightarrow 0$  [26].

$$\left( \frac{\sigma}{\sigma_{TS}} \right) = \exp \left\{ -k_1 \left[ t_f \exp \left( \frac{-Q_c^*}{RT} \right) \right]^u \right\} \quad (3.44)$$

With this relationship, the coefficients ( $k_1$  and  $u$ ) are evaluated simply from plots of  $\ln[t_f \exp(-Q_c^*/RT)]$  vs.  $\ln[-\ln(\sigma/\sigma_{TS})]$  [26]. However, a distinct change in  $k_1$  and  $u$  occurs as  $(\sigma/\sigma_{TS})$  decreases. Inserting the derived values of  $k_1$  and  $u$  into Eq. (3.44) over the appropriate  $(\sigma/\sigma_{TS})$  ranges leads to the sigmoidal ‘master curve’. Eq. (3.44) provides a clear indication of the high-stress  $t_f$  measurements which should not be included when determining long-term performance [26]. This decision can be made in an unambiguous manner by discarding results for  $\sigma > 0.5\sigma_{TS}$ , but this approach requires the completion of many long term tests, whereas reasonable estimates can be produced by applying Eq. (3.44) to data sets with  $t_f < 5000h$ . An

additional advantage is then gained by using Eq. (3.44), because no decision is required on whether the durations of tests which have not failed after long times should be included when estimating long-term rupture strengths [26].

### c. Minimum Commitment

Rupture data were analyzed using Manson's Minimum Commitment Methods [27]. All of the data available (264 test results) was used in this analysis by Brinkman et al. [28]. The Minimum Commitment Method (MCM) equation developed [28] is as follows:

$$\log t_r + \left[ R_1(T - T_{\text{middle}}) + R_2 \left( \frac{1}{T} - \frac{1}{T_{\text{middle}}} \right) \right] = B + C \log \sigma + D \sigma + E \sigma^2 \quad (3.45)$$

where all logarithms are base 10.

$t_r$ =rupture life (h)

$\sigma$ =stress (MPa)

$T$ =temperature (K)

$T_{\text{middle}}$ =867°K

#### 3.2.1.1.7.3 Combining Fatigue and Creep Damages

If there is only one level of fatigue loading and creep loading in the study, the fatigue damage  $D_f$  and creep damage  $D_c$  can be identified as follows:

$$D_f = \frac{N}{N_f} \text{ and } D_c = \frac{N t_h}{t_r} \quad (3.46)$$

where  $N_f$  represents the number of cycles to failure in continuous fatigue tests,  $N$ , is the number of cycles to failure in CF test,  $t_r$  is the rupture time for a pure creep test and  $t_h$  is the hold time [21, 22].

Different damage summation methods were considered by researchers for comprising both fatigue and creep damage. The linear damage summation rule is still

widely used for its simplicity when  $D_f + D_c \geq 1$  failure is predicted. Then the linear damage summation method can be described as follow [21, 22]:

$$N \geq \frac{N_f t_f}{t_f + N_f t_h} \quad (3.47)$$

### 3.2.1.2 Simultaneous CF Loading

#### 3.2.1.2.1 Fii [ $\Phi$ ] Model

Holmström and Auerkari [2] proposed a new CF (CF) model based on the creep rupture behavior of the material with a fatigue correction described by hold time and total strain range at temperature. This model does not need separation of creep and fatigue damage or life fractions, and can be applied with a minimum of input data. The model is shown to predict the observed CF life with a scatter band close to a factor of 2 for austenitic steel 316FR, ferritic steel P91 and the Ni alloy A230 [2]. Holmström and Auerkari [2] included only isothermal CF tests under strain control, with stress ratio  $R=-1$  and hold periods in tension.

The proposed CF model by Holmström and Auerkari [2] aims to predict the expected life under tensile-compressive loading cycles combined with hold periods of relaxation. The effective CF lifetime ( $t_{CF}$ ) and corresponding number of cycles to failure ( $N_{CF}$ ) are predicted utilizing the creep rupture properties of a material. To assess CF data, Holmström and Auerkari [2] summed up the hold times for each test ( $\sum t_h$ ). The proposed Holmström and Auerkari creep rupture model was used to determine the stress required to produce rupture in this time  $t_{CF} = \sum t_h$ . This reference stress ( $\sigma_{ref}$ ) was divided with the ultimate tensile strength (UTS) at temperature to obtain the normalized reference stress (Fii)  $\Phi = \sigma_{ref} / \sigma_{UTS}$ .

Holmström and Auerkari [2] applied the proposed CF approach on the creep rupture model by Wilshire [26]. Measured values of normalized reference stress  $\Phi_m$  for each point of CF test data can be calculated from:

$$\Phi_m = \exp \left\{ -k \left[ t_{CF} \exp \left( -\frac{Q_c^*}{RT} \right) \right]^u \right\} \quad (3.48)$$

where  $k$  and  $u$  are material constants from creep-rupture data,  $Q_c^*$  is the apparent activation energy and  $R$  is the gas constant. The required constants are acquired from fitting  $\Phi = \sigma_{ref} / \sigma_{UTS}$  with the  $\sigma_{UTS}$  taken at the same temperature as the creep test and preferably from the same material batch [2]. The predicted number of cycles to the “end criterion” is simply calculated as:

$$N_{CF} = \frac{t_{CF}(\Phi_{CF})}{t_h} \quad (3.49)$$

To apply this CF model, any other well performing creep rupture models can be used (see, Table 3.3).

### 3.2.2 Case/Research Specific Alternate Approaches to CF Expended Life Models

It was observed that the models in this category are mostly material and path dependent. Section 3.2.2.1 reviews statistical equations developed for Cr-Mo steels, stainless steels, generic materials including solder alloys, copper alloys, titanium alloys and superalloys. Their goodness of fit has been evaluated according to  $R^2$  statistics.  $R^2$  is used in the context of statistical models whose main purpose is the prediction of future outcomes on the basis of other related information.  $R^2$  is most often seen as a number between 0 and 1, used to describe how well a regression line

fits a set of data. An  $R^2$  near 1 indicates that a regression line fits the data well, while an  $R^2$  close to 0 indicates a regression line does not fit the data very well. It is the proportion of variability in a data set that is accounted for by the statistical model [29].

### 3.2.2.1 Generic Equations

Generic equations [30-33] were originally derived to predict the low-cycle fatigue response curves of SS304, 316, 321 and recommended in design by American Society of Mechanical Engineers (ASME). Goswami [6, 8] developed a methodology to derive a new multi-variate and generic equations according to the coefficient of correlation ( $R^2$ ) value. Furthermore, Goswami [6-8] examined the following alloy groups and derived a particular model for each case.

- a) Cr-Mo steels
- b) Stainless steels
- c) Generic materials (includes Cr-Mo steels, stainless steels, solder alloys, copper alloys, titanium alloys, tantalum alloys and superalloys 1782 data points).

Goswami [6, 8] studied the effect of several variables during testing, while ignoring the effects of composition, microstructure, grain size, heat treatment and other material parameters to develop general life prediction models. Goswami [6, 8] utilized only four independent variables as strain range, strain rate, dwell time and temperature. The transformation functions used were [6, 8].

$S$  = Strain range parameter ( $S = \log(\Delta \epsilon_f / 100)$ )

$R$  = Strain rate parameter ( $R = \log \dot{\epsilon}$ )

$T$  = Temperature parameter ( $T = T / 100$ ) and

$H$  = Hold parameter  $\{H = \log(1 + t_h)\}$

$\Delta \varepsilon_t$  = % total strain range

$\dot{\varepsilon}$  = Strain rate (1/s)

$T_c$  = Test temperature ( $^{\circ}\text{C}$ )

$N_f$  = Predicted cyclic life ( $N_f = \sqrt{\log(N_f)}$ )

$t_h$  = Duration of hold time in hours

The use of transformation functions reduced the scatter in the residual data, which was the difference between the predicted and observed cyclic life. It is desired that the data scatters through the scale and does not show the typical trends such as funnel, double bow and residual non-linear [6-8].

#### **a. Generic Model for Cr-Mo Steels**

Goswami [6-8] used a total of 479 data sets for the following low steel alloys: 0.5Cr-Mo, 1Cr-Mo-V, 1.25 Cr-Mo, 2.25Cr-Mo-V and 9Cr-1Mo to derive a multivariate equation. The dwell times ranged from a few seconds to 48h and the temperature varied from room temperature to  $600^{\circ}\text{C}$ . The total strain range varied from 0.1% to as high as 2.5% and strain rate, though not specified for each test, varied from  $5 \times 10^{-3}$  to as low as  $5 \times 10^{-3}/\text{s}$ . The four independent variables identified earlier were used and a best fit equation was derived for fourth power optimized for maximum  $R^2$  value. It is shown that higher power terms do not contribute to further improvement in the  $R^2$  value. The analysis of variance involved a corrected total degree of freedom of 473 terms, sum of squares of 13.50, mean square = 0.14955 and F value of 18.99. A 69-variable, multivariate equation was developed which gave a  $R^2$  value of 76.43%. Thus, 23.57% of the total variations remain unexplained. This could be due to random samples that were collected, test run out, premature failures, or to an additional variable, which has not been considered [6-8].

$$\begin{aligned}
N_f = & -2081.00004 - 96.58004S^2 - 157.18380R^2 - 33.27409T^2 - 34.18196S^3 - 6.81706R^3 + \\
& 5.12091H^3 + 0.99174T^3 - 3.97033S^4 + 0.09245R^4 - 4.36154H^4 - 0.00567T^4 + 7.03397S^2H + \\
& 91.06390S^2T + 76.69415S^3R + 24.38854RH + 173.20087RT - 1.41757HT - 1.41757R^2S - \\
& 1.90162R^3H - 0.23208R^4H - 3.91813R^3T - 0.21865R^4T - 1.48672R^3S - 0.08994R^4S + \\
& 6.89747H^2T - 4.13082H^3T + 3.79652H^4T + 11.04750H^2R + 1.19693H^4R - 14.18916H^2S + \\
& 8.76843H^3S - 0.04130H^4S + 4.71022S^2R^2 + 1.94284S^3R^2 + 0.18897S^4R^2 + 0.09321R^3S^3 + \\
& 0.00457R^4S^3 + 5.29123R^2H^2 + 1.84380R^3H^2 + 0.18912R^4H^2 - 0.01721R^3H^4 - 0.02016R^4H^3 - \\
& 0.00026564R^4H^4 + 4.31392R^2T^2 + 0.59154R^3T^2 + 0.03438R^3T^3 + 0.00497R^4T^3 + \\
& 0.00003261R^4T^4 - 0.51238H^2T^2 + 0.33980H^3T^2 - 0.49672H^4T^2 + 0.00254H^4T^4 - 6.49058S^2H^2 - \\
& 0.98987S^3H^2 + 4.97361S^2H^3 + 1.21784S^3H^3 + 0.10385S^4H^3 - 0.00003761S^4H^4 - \\
& 0.00034935S^4R^4 - 0.61685S^2T^2 - 0.40559S^3T^2 - 0.07365S^4T^2 + 0.13386S^3T^3 + 0.02383S^4T^3 - \\
& 0.00164S^4T^4 - 0.00929S^3T^4 - 0.01461S^2T^4 + 0.20819S^2T^3 + 1.05891R^2H^3
\end{aligned} \tag{3.50}$$

## b. Generic Model for Stainless Steels

Goswami [6-8] used a total of 612 data sets from the following stainless steels, SS304, SS304L, SS316, SS321 and SS348, to derive a multivariate equation. The dwell times ranged from a few seconds to several hours and temperature varied from room temperature to 700°C. Total strain range varied from 0.2% to as high as 2.5% and strain rate, though not specified for each test, varied from  $5 \times 10^{-3}$  to as low as  $5 \times 10^{-3}$  /s. These four independent variables identified earlier were used, and a best-fit equation was derived for maximum  $R^2$  value. The analysis of variance involved a correct total degree of freedom 611 terms, sum of squares of 26.7411, mean square of 0.30243 and F value of 27.91. A 69-variable, multivariate equation was developed which gave a  $R^2$  value of 78.04%. Thus, 21.96% of the total variations remained unexplained. This could be due to random test samples that were collected, test run out, premature failures, or to an additional variable, which has not been considered [6-8].

$$\begin{aligned}
N_f = & 163.39883 + 64.20992S^2 + 7.01704R^2 + 25.13215T^2 + 41.65816S^3 - 0.38332R^3 - \\
& 3.26665T^3 + 7.57208S^4 - 0.23007R^4 - 36.86686H^4 + 0.15386T^4 + 23.85942SH + 1.85719S^4R - \\
& 23.61841RH - 12.08030RT + 0.02434HT - 0.13906R^2S - 4.66900R^2T + 0.99592R^3H + \\
& 0.09961R^4H + 0.49319R^3T + 0.16143R^4T + 0.02522R^4S + 17.33993H^2T - 8.96337H^3T - \\
& 33.69973H^4R - 20.80409H^4R + 6.24712H^2S - 23.99468H^3S + 1.26908H^4S + 0.96278S^2R^2 + \\
& 0.73930S^3R^2 + 0.13531S^4R^2 + 0.01450R^3S^3 - 0.00620R^4S^3 - 25.82372R^2H^2 - 5.53079R^3H^2 - \\
& 0.37609R^4H^2 + 0.13917R^3H^3 - 0.21810R^3H^4 + 0.01970R^4H^3 - 0.31492R^2T^2 - \\
& 0.08381R^3T^2 - 0.03459R^4T^2 + 0.00313R^4T^3 - 0.00012748R^4T^4 - 3.15001H^2T^2 + 1.67298H^3T^2 - \\
& + .16910H^4T^2 + 0.18640H^2T^3 - 0.09993H^3T^3 - 0.04251H^4T^3 + 0.00287H^4T^4 - 2.87564S^2H^2 - \\
& 2.71987S^3H^2 - 0.44970S^4H^2 - 8.92880S^2H^3 - 0.91209S^3H^3 + 0.04629S^4H^4 - 0.00192S^4R^4 - \\
& 10.48912S^2T^2 - 6.82999S^3T^2 - 1.24378S^4T^2 + 1.34692S^3T^3 + 0.24474S^4T^3 - 0.01345S^4T^4 -
\end{aligned} \tag{3.51}$$

$$0.07416S^3T^4 - 0.11433S^2T^4 + 2.07277S^2T^3 - 3.72231R^2H^4$$

### c. Generic Model for High Temperature Materials

Goswami [6-8] used a total of 1782 data sets from the following high temperature alloys:

- a) Solder alloys
- b) Copper alloys
- c) Steel alloys
  - 1. Cr-Mo low steel alloys
  - 2. Stainless steels
- d) Titanium alloys
- e) Tantalum alloys
- f) Ni-based alloys

Goswami [6-8] varied the dwell times from a few seconds to several hours and temperature from room temperature to 1100°C. In this experimental study [6-8], the total strain range varied from 0.1% to as high as 5% and strain rate, though not specified for each test, varied from  $5 \times 10^{-3}$  to as low as  $5 \times 10^{-5}$ /sec. The four independent variables identified earlier were used and a best fit equation was derived for fourth power optimized for maximum  $R^2$  value. It is shown that higher power terms do not contribute to further improvement in the  $R^2$  value. The analysis of variance involved a corrected total degree of freedom 1776 terms, sum of squares of 105.53, mean square of 0.82897 and F value of 34.44. A 78-variable, multivariate equation was developed which produced a  $R^2$  value of 61.27%. Thus, 38.73% of the total variations remained unexplained. This could be due to random test samples that were collected on so many different materials ranging from solder alloys, test run out, premature failures, or to an additional variable, which has not been considered.

$$\begin{aligned}
N_f = & 0.08317 + 1.09592S^2 + 0.28803R^2 - 3.92644H^2 + 0.11683T^2 + 0.12602S^3 + 0.08337R^3 + \\
& 0.48073H^3 - 0.02490T^3 - 0.01410S^4 + 0.00427R^4 - 0.07199H^4 + 0.00136T^4 + 0.05327SR - 0.00292S^3T + \\
& 0.99189RH + 0.00582RT + 0.09628HT + 0.07534R^2S + 0.02614R^2H - 0.07225R^3H - 0.00807R^4H + \\
& 0.01471R^3T + 0.00271R^4T + 0.04763R^3S + 0.00489R^4S - 0.23417H^2T + 0.15182H^3T + 0.03809H^4T - \\
& 0.78985H^2R + 0.20922H^3R - 0.01827H^4R - 6.30474H^2S + 1.05744H^3S + 0.01944H^4S - 0.07108S^2R^2 - \\
& 0.00131S^4R^2 - 0.01761R^2S^3 - 0.00089565R^3S^3 - 0.00019713R^4S^3 + 0.15444R^2H^2 + 0.10979R^3H^2 + \\
& 0.01101R^4H^2 - 0.04600R^3H^3 + 0.00573R^3H^4 - 0.00438R^4H^3 + 0.00052764R^4H^4 - 0.00126R^2T^2 - \\
& 0.00209R^3T^2 - 0.00041344R^4T^2 + 0.00006870R^3T^3 + 0.00002351R^4T^3 - 4.70403E - 7R^4T^4 + \\
& 0.01583H^2T^2 - 0.01689H^3T^2 - 0.00899H^4T^2 - 0.00059596H^2T^3 + .00076001H^3T^3 + 0.00087790H^4T^3 - \\
& 0.00003188H^4T^4 - 3.79717S^2H^2 - 0.95991S^3H^2 - 0.08619S^4H^2 + 0.68806S^2H^3 + 0.17249S^3H^3 + \\
& 0.01406S^4H^3 + 0.00026628S^4H^4 - 0.00001764S^4R^4 + 0.06530S^2T^2 + 0.05116S^3T^2 + 0.00915S^4T^2 - \\
& .00887S^3T^3 - 0.00163S^4T^3 + 0.00007714S^4T^4 + 0.00040737S^3T^4 + 0.00043237S^2T^4 - 0.01039S^2T^3 - \\
& 0.09279R^2H^3 + 0.01364R^2H^4
\end{aligned} \tag{3.52}$$

#### d. Generic Fii [ $\Phi$ ] Model

Holmström and Auerkari [2] proposed a new CF (CF) model based on the creep rupture behavior of the material with a fatigue correction described by hold time and total strain range at temperature. This model does not need to separate creep and fatigue damage or life fractions, and can be applied with a minimum of input data. The model is shown to predict the observed CF life with a scatter band close to a factor of 2 for austenitic steel 316FR, ferritic steel P91 and the Ni alloy A230 [2]. Holmström and Auerkari [2] included only isothermal CF tests under strain control, with stress ratio  $R = -1$  and hold periods in tension. The values of  $\Phi_m$  from Eq. (3.54) can then be fitted with multi-linear regression as a function of total strain range  $\Delta\epsilon$ , hold time  $t_h$  and temperature (T) as:

$$\Phi_{CF}(\Delta\epsilon, t_h, T) = c_1 + \frac{c_2}{\Delta\epsilon} + c_3 \log(t_h) + c_4 T \tag{3.53}$$

$\Phi$  was shown in Eq.(3.55) have a multi-linear relationship in the total strain range, hold time and temperature against the logarithm of  $t_{CF}$  [2].

### 3.2.3 CF expended life models when cyclic material data is not available or not enough

#### 3.2.3.1 Sequential CF loading

In this category, one model (Statistical thermal CF loading [21]) was included. Statistical thermal CF loading [21] is presented in subsection 3.2.1.1.7 Statistical thermal CF models.

#### 3.2.3.2 Simultaneous CF loading

In this category, one model (Fii model [2]) was included. Fii model [2] is presented in subsection 3.2.1.2.1 Fii Model.

### 3.2.4 Modified Robust Model(s) for CF

The modifications made are merely for the rupture time variable. As Holmström and Auerkari [2] suggested, any creep rupture model may be of concern to assess CF life in materials under elevated temperature as long as  $t_{CF} = \sum t_h$  is assumed instead of creep rupture time. Also,  $\sigma_0$  is assumed to be the maximum relaxation stress observed in each strain controlled tensile hold CF test data. Among these models, only Fii model was modified previously by Holmström and Auerkari [24]. The rest of the models have been converted according to the approach presented in this publication.

- Fii Model [2] (Adapted from Wilshire Equation [26])

$$\log(t_{CF}) = \left( \frac{\ln \left( \frac{\sigma_{max}}{\sigma_{UTS}} \right)}{-k} \right)^{1/u} \cdot \frac{1}{\exp \left( \frac{-Q_c^*}{R \cdot T} \right)} \quad (3.54)$$

- Restrained Manson Brown (RMB) [25]

$$\log t_{CF} = \log t_a \cdot T^{|q|-1} + (T - T_a \cdot \langle q \rangle)^q (a_0 + a_1 \cdot \log \sigma_{max} + a_2 \cdot \log^2 \sigma_{max}) \quad (3.55)$$

- Minimum Commitment [Manson and Muraldihan [27]]

$$\log(t_{CF}) = \beta_0 + \beta_1 \cdot \log[\sigma_{max}] + \beta_2 \sigma_{max} + \beta_3 \sigma_{max}^2 + \beta_4 T + \frac{\beta_5}{T} \quad (3.56)$$

- Soviet Model 1& 2 (1971)

$$\log(t_{CF}) = \beta_0 + \beta_1 \cdot \log[T] + \beta_2 \cdot \log[\sigma_{max}] + \frac{\beta_3}{T} + \beta_4 \cdot \frac{\sigma_{max}}{T} \quad (3.57)$$

- Mendelson-Roberts-Manson [29]

$$\log(t_{CF}) = \left\{ \sum_{k=0}^n \beta_k (\log[\sigma_{max}]^k) \right\} (T - T_0)^r / \sigma_{max}^{-q} + \beta_5 \quad (n=2,3,4) \quad (3.58)$$

- Simplified MRM [29]

$$\log(t_{CF}) = \left\{ \sum_{k=0}^n \beta_k \log([\sigma_{max}])^k \right\} / (T - T_0) + \beta_5 \quad (n=2,3,4) \quad (3.59)$$

- Orr-Sherby Dorn [29]

$$\log(t_{CF}) = \left\{ \sum_{k=0}^n \beta_k (\log[\sigma_{max}]^k) \right\} + \beta_5 / T \quad (3.60)$$

- Manson-Haferd [29]

$$\log(t_{CF}) = \left\{ \sum_{k=0}^n \beta_k (\log[\sigma_{max}]^k) \right\} (T - T_0) + \beta_5 \quad (n=2,3,4) \quad (3.61)$$

- Manson-Haferd with  $T_0 = 0^a$  [29]

$$\log(t_{CF}) = \left\{ \sum_{k=0}^n \beta_k (\log[\sigma_{max}]^k) \right\} T + \beta_5 \quad (n=2,3,4) \quad (3.62)$$

- Larson-Miller [29]

$$\log(t_{CF}) = \{\sum_{k=0}^n \beta_k (\log[\sigma_{max}])^k\} / T + \beta_5 \quad (n=2,3,4) \quad (3.63)$$

### 3.2.4.1 Comparisons of Modified Leading Models

Comparison of the prediction performance for the modified CF models above has been conducted with the experimental data provided by Holmstrom and Auerkari [2] for 316FR. Figure 3.6 shows the experimental data used to evaluate the prediction performance of the well-known creep-rupture models which were converted into CF life fraction. Figure 3.7 shows for 316FR at 550°C, the  $R^2$  statistics for each of the CF models that were converted into CF life fraction models. It was observed that all the presented a prediction performance greater than 0.90  $R^2$ .

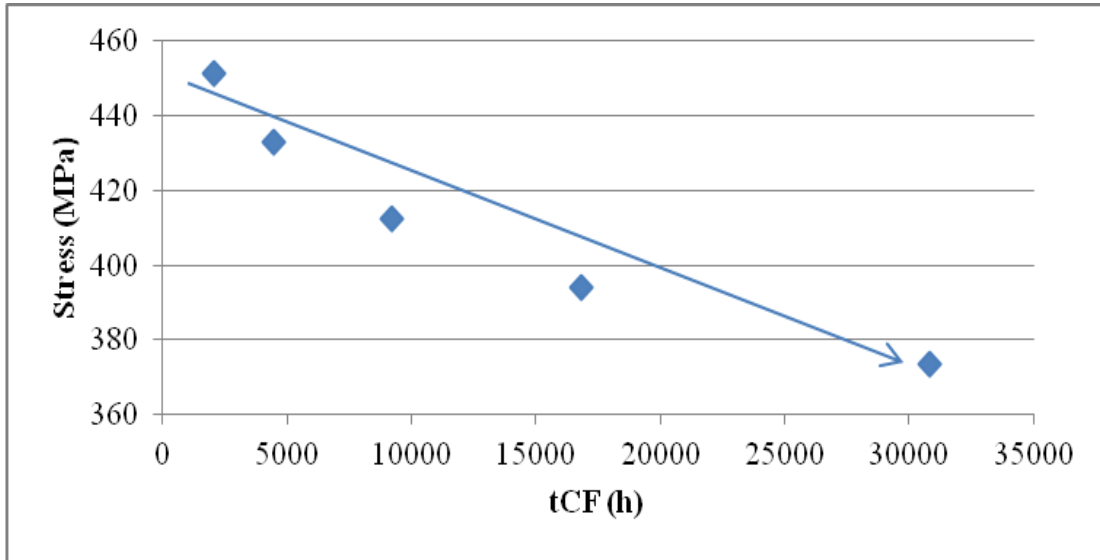


**Figure 3.6: Normalized reference stress  $\Phi$  (Fii) as a function of  $t_{CF}$  for 316FR at 550°C [2]**



**Figure 3.7: CF model R<sup>2</sup> for 316FR at 550C**

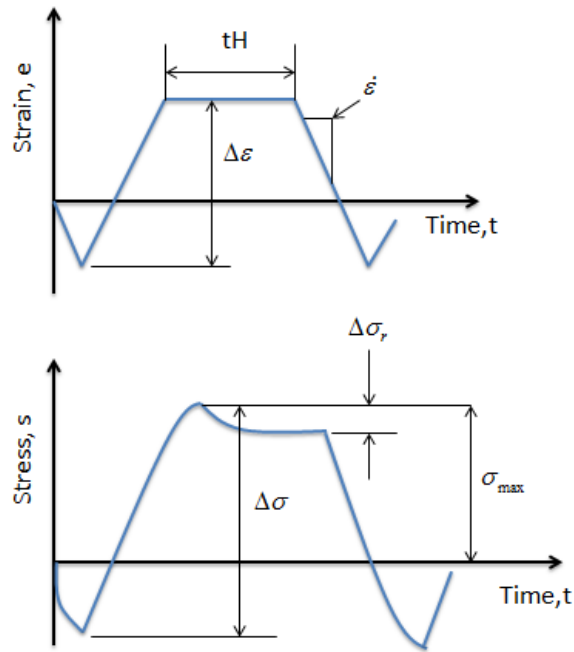


**Figure 3.8: Generic schematic of strain and stress history for a fully reversed strain cycle with hold time at maximum tensile strain**

### 3.3 Creep Models in Cyclic Relaxation Response under CF Conditions

It is known that the creep mechanisms of stress relaxation are the main reasons for fatigue life reduction under CF interactions after a long enough time are the same as that of long-term monotonic creep. The benefit of this is that a large amount of creep information can be obtained from a short term relaxation test [34]. Since relaxation during most of the tests occurred in cyclically hardened materials, it would have been more appropriate to relate creep damage to stress-rupture curves for materials that had been cyclically hardened, if such information had been available [34] (see, Figure 3.8)

To determine the form of the relaxation curve, it is assumed that the total strain  $\varepsilon$  is composed of elastic, plastic and creep components [5]:

$$\varepsilon = \varepsilon_c + \varepsilon_p + \left(\frac{\sigma}{E}\right) \quad (3.65)$$

Under the tension condition of total strain controlled LCF with hold, the elastic ( $\varepsilon_e$ ) and plastic ( $\varepsilon_p$ ) strain components remain constant during hold time [4]. Hence the sum of the each strain rate is given by,

$$\dot{\varepsilon}_e + \dot{\varepsilon}_p = 0 \quad (3.66)$$

$$\dot{\varepsilon} = \dot{\varepsilon}_c + \dot{\varepsilon}_p + \dot{\varepsilon}_e = \dot{\varepsilon}_c \quad (3.67)$$

where  $\dot{\varepsilon}_e$  and  $\dot{\varepsilon}_p$  represent the elastic and plastic strain respectively. Thus, the time dependent creep strain rate can be expressed in terms of elastic modulus ( $E$ ) and a stress relaxation rate by,

$$\dot{\varepsilon}_c = -\frac{1}{E} \frac{d\sigma_r}{dt} \quad (3.68)$$

where  $\sigma_r$  and  $t$  are the instantaneous relaxation stress and time, respectively and the value of  $d\sigma_r$  is negative during stress relaxation. Thus, the plastic strain rate is determined from the rate of change in stress during stress relaxation, and therefore its value changes throughout the hold time [4].

By analyzing the value of activation volume for initial transient relaxation behavior in which the stress is relaxed drastically, it has been suggested that the rate controlling dislocation mechanisms is either cross slip, or overcoming Peierls-Nabarro stress [4]. Thus, the temperature dependence of creep rate was identified during stress relaxation. It was shown that the creep mechanism is identical to steady state monotonic creep after a long enough hold time which is diffusion controlled dislocation climb [4].

For most solid materials, it has been shown that the steady state creep rate  $\dot{\epsilon}$  is related to the applied stress and temperature by,

$$\dot{\epsilon} = A\sigma^n \exp\left(-\frac{Q_{app}}{RT}\right) \quad (3.69)$$

where  $Q_{app}$  is the apparent activation energy for creep,  $T$  is the absolute temperature, and  $A$  and  $n$  are the structure factor and the creep exponent, respectively. Therefore, the stress dependence of the creep rate after transient inelastic behavior due to the initial loading can be represented by,

$$\dot{\epsilon} = A_0\sigma^n \quad (3.70)$$

So if dislocation creep is considered, the strong dependence of creep rate on the applied stress is observed. Stress dependence on creep rate can also have a hyperbolic sine equation form:

$$\dot{\varepsilon}_c = K'' \sinh(\beta\sigma) \quad (3.71)$$

Nevertheless, these equations model only secondary creep, whereas real creep curves exhibit a nonlinear (in time) primary creep stage that can be modeled as follows [5]:

$$\dot{\varepsilon}_c = mK\sigma^n t^{m-1} \quad (3.72)$$

$$\dot{\varepsilon}_c = mK' \sinh(\beta\sigma) t^{m-1} \quad (3.73)$$

The main difference is that total strain is constant in tensile hold test and the stress is changed with time, whereas the stress is constant in monotonic creep. Therefore, it may be possible to interpret the stress dependence of the rate change as a function of the hold time [4].

Applying the linear damage fraction rule to determine the creep damage term  $\left(\frac{\Delta t}{t_r}\right)$  requires numerical integration of stable stress relaxation curves. To simplify the integration process, relaxation curves were approximated by the function [34]:

$$\ln(\sigma_{\max}/\sigma) = \frac{A}{1+m} t^{1+m} \quad (3.74)$$

or

$$\ln\left(\frac{\sigma_{\max}}{\sigma}\right) = EKt^m \quad (3.75)$$

Best fit values of A and m were obtained by least squares regression of each stable relaxation curve (see, Figure 3.9).

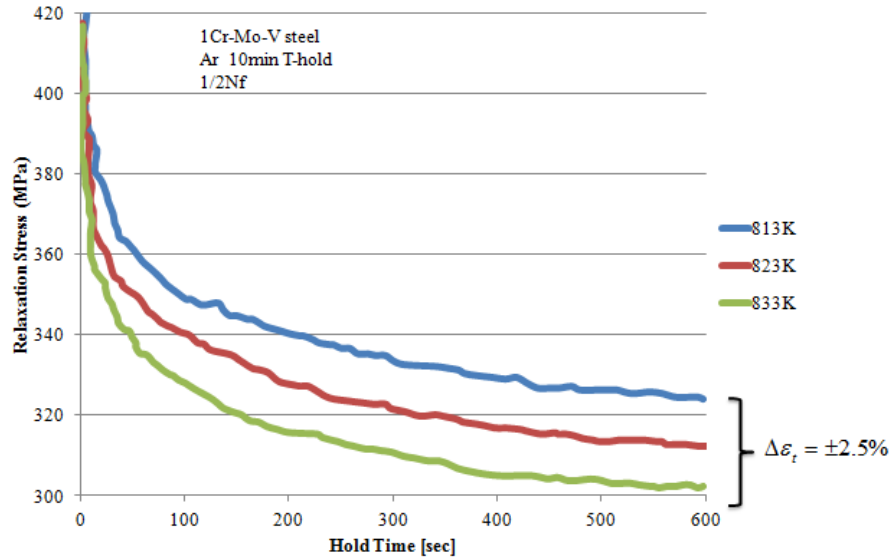


**Figure 3.9: Stress relaxation curves at three test temperatures in a  $\pm 2.5\%$  total strain range [4]**

### 3.3.1 Applicable Creep Model(s) in Cyclic Relaxation Response under CF Conditions

Since hold periods contain only creep deformation, using all the CF hold times from all of CF cycles to the end criterion, it is possible to look for a creep deformation curve that covers all three regions in addition to the suggestion provided by Lafen [5]. Lafen proposed that a creep curve including time dependencies could be used to predict the primary and secondary regions of the creep curve.

Long-term constant loading at elevated temperatures leads to the development of creep behavior as a material is damaged and eventually leads to the failure of engineering structures or components [49]. Creep properties of materials form the basis to analyze the high-temperature structural strength and life of materials under constant applied stresses. There exist some creep-damage equations, such as Kachanov–Rabotnov (K–R) creep-damage formula [50-52],

theta projection [53-59] model, and modified Theta-Omega model [52] that have been widely used to predict the creep damage and the residual strength of different materials. These models are briefly explained below.

**Table 3.4: Published creep models that describe the whole creep curve from primary (P) to secondary (S) and tertiary part for 10Cr-Mo (9-10) steel alloys [35-36]**

Model Equation	Model	Creep Range	References
Graham-Walles (1995)	Power law	P/S/T	[37]
Evans and Wilshire Theta Model (1985)	Exponential	P/S/T	[38]
Modified Theta model (1985)	Power law	P/S/T	[39]
Kachkanov-Robotnov (1986)	Power law	P/S/T	[40-43]
Bolton (1994)	Power law	P/S/T	[44-45]
Dyson-McLean (1998)	Exponential	P/S/T	[46]
Modified Garofalo (2001)	Exponential	P/S/T	[47]
Holmström-Auerkari-Holdsworth (LCSP)	Power law	P/S/T	[48]
Nuhi's Probabilistic Model (2011)	Power law	P/S/T	[35]

- Kachkanov-Rabotnov (K-R) constitutive [40-43]:

$$\dot{\varepsilon}_e = B \frac{(\sigma_e)^n}{(1 - \omega)^n} \quad (3.76)$$

$$\dot{\omega} = D \frac{(\lambda \sigma_1 + (1 - \lambda \sigma_e))^x}{(1 - \omega)^\phi} \quad (3.77)$$

Integration of  $\dot{\omega}$  and substitution in the relation for  $\dot{\varepsilon}_e$  and further

integration results to the following simplified strain time equation:

$$\varepsilon = \varepsilon_R \left[ 1 - \left( 1 - \frac{1}{t_R} \right)^{1/\lambda} \right] \quad (3.78)$$

where  $\varepsilon_e$  and  $\sigma_e$  are, respectively equivalent creep strain and stress.  $\sigma_1$  is the maximum principal stress,  $\omega$  is the damage variable can be ranged from 0 (no damage) to 1 (full damage ), and  $\varepsilon_R$  and  $t_R$  are strain and time to rupture. The terms D, B, n,  $\phi$ ,  $\chi$  and  $\lambda$  are material parameters which are obtained from uniaxial tensile creep curves.

- Theta-projection model [39]:

$$\varepsilon_c = \theta_1 \{1 - \exp(-\theta_2 t)\} + \theta_3 \{\exp(\theta_4 t) - 1\} \quad (3.79)$$

where t is the time,  $\theta_1, \theta_2, \theta_3$  and  $\theta_4$  are parameter constants determined by fitting the equation to experimental data.

- Theta-Omega model [38]:

$$\varepsilon_c = X(1) \{1 - \exp(-\theta_2 t)\} + \left( \frac{-1}{X(3)} \right) \ln(1 - X(4)t) \quad (3.80)$$

where X(1), X(2), X(3) and X(4) are parameters constants characterizing creep curve shapes.

- Nuhi's empirical model [35]:

$$\varepsilon_c = at^n + ct^m \exp(pt) \quad (3.81)$$

where a,n,c,m and p are parameter constants describing the creep curve.

Faridani [35] performed an akaike evaluation on the data from experimental and damage simulation of creep damage for duralumin alloy 2A12, given in the literature [60], and fitted into all above-mentioned models. The results are given in Table 3.5.

**Table 3.5: AIC values from comparison of different creep models for the given experimental data [35]**

	<b>Empirical – model</b>	<b>Theta – model</b>	<b>Theta – Omega-model</b>	<b>K-R-model</b>
<b>n</b>	39	39	39	39
<b>k</b>	5	4	4	6
<b>AIC</b>	-432.3 <	-422 <	-363 <	-357

AIC was computed from the results of least-square estimation or a likelihood- based analysis. Akaike’s approach allows identification of the best model in a group of models and allows ranking the rest of the models easily. The best model has the smallest AIC value. In Table 3.5, the AIC-values are ranked in ascending order as follows: Empirical Model, Theta Model, Theta-Omega Model and the K-R Model respectively, which indicates that the proposed empirical model is a superior model for describing the creep- damage process. It should be mentioned that K-R model which has the highest number of parameters (variables), has the worst ranking.

### **3.3.2 Comparisons of Modified Robust Models**

Comparison of the creep models for steel data in terms of highest goodness of fit on the was evaluated here once more on the data provided in Figure 3.10. It was observed that in addition to the model suggested by [5]-[34]. Faridani’s [35] empirical equation and the modified theta model could be good candidates to predict the creep deformation behavior in cyclic relaxation response under CF.  $R^2$  results can be seen in Figure 3.10 for 1Cr-Mo-V steel CF data.

In addition to CF expended life models, these creep models are validated on the same experimental CF data.

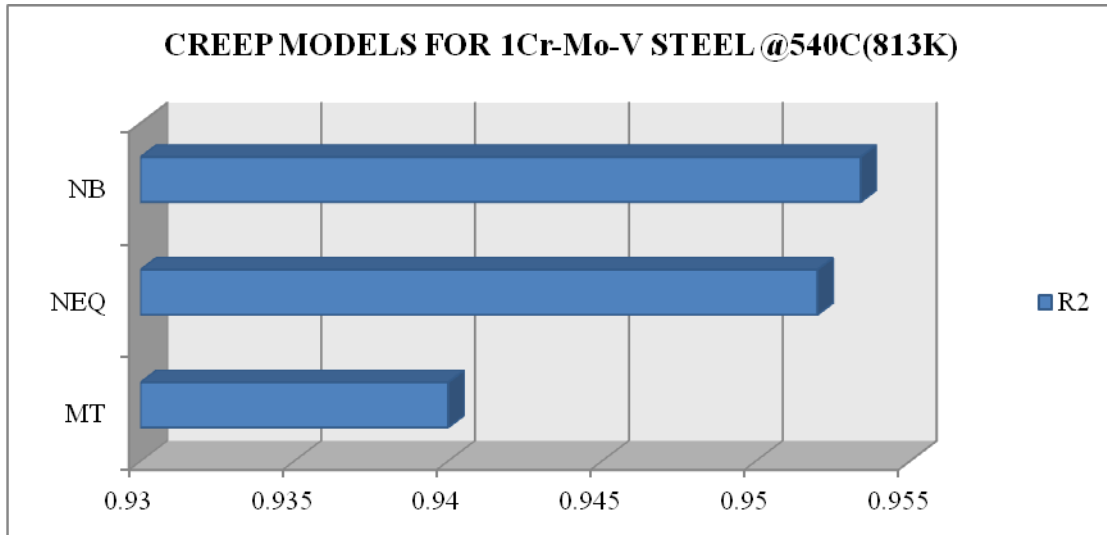


**Figure 3.10:  $R^2$  results for creep deformation in stress relaxation curves at 813°K test temperature in a  $\pm 2.5\%$  total strain range**

### 3.4 References

- [1] Evans, J.L. and Saxena, A., “Modeling Creep Fatigue,” In. Furrer D.U. and Semiatin, S.L. (Eds.), *ASM Handbook*, Vol.22A: Fundamentals of Modeling for Metals Processing, pp:419-428, 2009
- [2] Holmstörn, S. and Auerkari, P., “A robust model for creep-fatigue life assessment,” *Materials Science & Engineering A*, Vol. 559, pp.333-335, 2013.
- [3] Asayama, T. and Tachibana, Y., “Collect Available Creep-Fatigue Data and Study Existing Creep-Fatigue Evaluation Procedures for Grade 91 and Hastelloy XR,” DOE/ASME Generation IV Materials Project, Japan Atomic Energy Agency, September 30, 2007.
- [4] Jeong, C.Y. and Nam, S.W., “Stress dependence on stress relaxation creep rate during tensile holding under creep-fatigue interaction in 1Cr-Mo-V steel,” *Journal of Materials Science*, Vol.34, pp:2513-2517, 1999.
- [5] Lafen, J.H. and Jaske, C.E., “Cyclic relaxation response under creep-fatigue conditions,” *Stress Relaxation Testing*, ASTM STP 676, pp:182-206, 1976.
- [6] Carden, A.E., McEvily, A. and Wells, C.H., *Fatigue at elevated*

*temperatures*, American Society for Testing and Materials, 1974.

- [7] Goswami, T., "Development of generic creep-fatigue life prediction models," *Materials and Design*, Vol.25, pp.277-288, 2004.
- [8] Toland, J. and Goswami, T., "General creep-fatigue life prediction models," *Journal of the Mechanical Behavior of Materials*, Vol.15, Issue 1-2, 2004.
- [9] Anon. Code Case N-47, ASME boiler and pressure vessel code, "Criteria for design of elevated temperature," Class 1 Components in section III, division 1, *American Society of Mechanical Engineers*, 1976.
- [10] Halford, G.R., Saltsman, J.F. and Hirschberg, M.H., "Ductility normalized strain range partitioning life relations for creep-fatigue life predictions," NASA Report TMX 67838, 1971.
- [11] Majumdar, S., Maiya, P.S., "Wave shape effects in elevated temperature low-cycle fatigue of type 304 stainless steel," *ASME/CSME Pressure Vessel and Piping Conference*, PVP-PB 028, 1978.
- [12] Maiya, P.S., "Effects of wave shape and ultrahigh vacuum on elevated temperature low cycle fatigue in type 304 stainless steel," *Material Science and Engineering*, Vol.47, pp.13-21, 1981.
- [13] Chrzanowski, M., "Use of the damage concept in describing creep-fatigue interaction under prescribed stress," *International Journal of Material Sciences*, Vol.18, Issue 2, pp.69-73, 1976.
- [14] Goswami, T., "Low-cycle fatigue life prediction - a new model," *International Journal of Fatigue*, Vol. 19, Issue 2, pp:109-115, 1997.
- [15] Brinkman, C.R., "High temperature time-dependent fatigue behavior of several engineering structural alloys," *International Metal Reviews*, Vol.30, Issue 5, pp:235-258, 1985.
- [16] Coffin, L.F., "Methods for predicting life in fatigue," *American Society of Mechanical Engineers*, pp:1-24, New York, 1979.
- [17] Manson, S.S., Halford, G.R. and Hirschberg, M.H., "Creep-fatigue analysis by strain-range partitioning," *1<sup>st</sup> National Pressure Vessel and Piping Conference Sponsored by the American Society of Mechanical Engineers*, pp: 12-24, New York, 1971.
- [18] Coffin, L.F., "Fatigue at high temperature – prediction and interpretation," *Inst MechEng*, Vol.188 9, Issue 74, pp.109-127, 1974.

- [19] Ostergren, W.J., "A damage function and association failure equations for predicting hold time and frequency effects in elevated temperature, low cycle fatigue," *Journal of Testing and Evaluation*, Vol.4, Issue 5, pp. 327-339, 1976.
- [20] Manson, S.S., Thermal stress and low cycle fatigue, McGraw-Hill, p:171, New York, 1966.
- [21] He, X., "Statistical thermal fatigue-creep modeling of stainless steel materials," *IEEE*, 2009.
- [22] He, X., Li, G. and Ding, Y., "Statistical thermal creep-fatigue modeling of 316 stainless steel materials," *Scientific Research Essays*, Vol.6, Issue 20, pp:7172-7178, 19 September, 2011.
- [23] Manson, S.S., "A complex subject – some simple approximations," *Experimental Mechanics*, Vol.5, Issue 7, pp:193-326, 1965.
- [24] Truman, R.S. et al., "Elevated-temperature tensile, creep and rupture properties of 18%Cr-8%Ni, 18%Cr-12%Ni-Mo, 18%Cr-10%Ni-Ti, and 18%Cr12%Ni-Nb steels," *Proceedings of Joint Conference Organizaed by the British Iron and Steel Research Association and the Iron and Steel Institute*, pp:265-300, Eastbourne, UK, 1966.
- [25] Seruga, D. and Nagude, M., "Uniform of the most commonly used time-temperature creep parameters," *Material Science and Engineering A*, Vol.528, pp:2804-2811, 2011.
- [26] Wilshire, B., Scharming, P.J. and Hurst, R., "A new approach to creep data assessment," *Material Science and Engineering A*, Vol.510-511, pp:3-6, 15 June 2009.
- [27] Manson, S.S. and Muralidharan, U., "Analysis of creep-rupture data for five multi-heat alloys by the minimum commitment method using double heat term centering," *Progress in Analysis of Fatigue and Stress Rupture MPC-23*, ASME, pp:43-60, 1984.
- [28] Brinkman, C.R., Booker, M.K. and Ding, J.L., "Creep and creep-rupture behavior of Alloy 718," *Special Emphasis Symposium on Superalloys 718, 625, and Various Derivatives*, Pittsburg, PA (USA), 23-26 Jun 1991.
- [29] Steel, R. G. D. and Torrie, J. H., *Principles and Procedures of Statistics*, New York: McGraw-Hill, pp:187-287, 1960.
- [30] Diercks, D.R. and Raske, D.T., "A statistical analysis of elevated

temperature, strain controlled fatigue data on type 304 stainless steel,”  
*ASME Annual Winter Meeting*, New York, December 5-10, 1976.

- [31] Sonoya, K., Nonaka, I. and Kitagawa, M., “Prediction of creep-fatigue lives of Cr-Mo steels with Direcks Eq.,” *ISIJ International*, Vol. 1, No.12, pp.1424-1430, 1991.
- [32] Langer, B.F., “Design of pressure vessels for low-cycle fatigue,” *J Basic Eng*, Vol.84, Issue 3, pp.389-402, 1962.
- [33] Goswami, T., “Creep-fatigue life prediction of Cr-Mo steel alloys,” In. Laiw, P.K., Bunchanan, R.A., Klarstrom, D.L., Wei, R.P., Harlow, D.G., Tortorelli, P.F. (Eds.), *Material lifetime science and engineering*, pp.43-50, 2003.
- [34] Jaske, C.E., Mindlin, H., and Perrin, J.S., “Combined Low-Cycle Fatigue and Stress Relaxation of Alloy 800 and Type 304 Stainless Steel at Elevated Temperatures,” *Fatigue at Elevated Temperature, ASTM STP 520*, American Society for Testing Materials, pp:365-376, 1973.
- [35] Faridani, M.N. and Modarres, M., “Classification and probabilistic model development for creep failures of structures: study of X-70 carbon steel and 7075-T6 aluminum alloys,” Thesis, In partial fulfillment of the requirements of the degree of Master of Science, Fall 2011.
- [36] Holdsworth, S.R., Merckling, G., “ECCC developments in the assessment of creep rupture data,” In: Proceedings of sixth international Charles Parsons Conference on engineering issues in turbine machinery, power plant and renewable, Trinity College Dublin, 16-18 September, 2003.
- [37] Graham, A. and Walles, K.F.A. ; NGTE Reports Nos.R.100(1952), R.137 (1953), R.189 and R.190 (1956); *J. Iron and steel Inst.*179,105, 1955.
- [38] Moles, M. D. C. and Westwood, H. J.; “ Residual life estimation of high temperature superheater and reheater tubing, CER RP, 78-66, Final report of Ontario Hydor Research Dev., Toronto, for the Canadian Electrical Assn., Montreal, pp: 67-82, Mar. 1982.
- [39] Johnson, G.R.; Cook, W.H., "A constitutive model and data for metals subjected to large strains, high strain rates and high", 1983.
- [40] Johnson,G. R.,Cook, W.H. ; Fracture characteristics of three metals subjected to various strain rates, temperatures and pressures, *Eng. Fracture Mechanics*, Vol.21, Issue:1, pp:31-48, 1985.
- [41] Modified Theta model in: R.W. Evans and B. Wilshire, *Creep of*

metals and alloys, Institute of Metals, 1985.

- [42] Rabotnov, Y.N. ; Some problems of the theory of creep, NACA., TM, 1353, 1953.
- [43] Rabotnov, Y. N. ; On the equation of state of creep, ASME/ASTM/IMEchE Proceedings Conference on creep, Inst. Mech. E., New York/London, 1963.
- [44] Maruyama, K. et al. ; Long-term creep curve prediction based on the modified  $\theta$  projection concept. J. Pressure Vessel Technol., 112, 1990.
- [45] Brinkman, C.R.; Booker, M.K.; and Ding, J.L.: Creep and Creep-Rupture Behavior of Alloy 718. Proceedings of the International Symposium on the Metallurgy and Applications of Superalloys 718, 625, and Various Derivatives, Minerals, Metals & Materials Society, Warrendale, PA, 1991.
- [46] Prager, M. 'Development of the MPC Omega method for life assessment in the creep range', ASME J. Pressure Vessel Technology, 117, May, 95-103, 1995.
- [47] BJF-model: Jones, D.I.G, French, R.M. and Bagley, R.L.; A Renewal Theory of Inelastic Thermo-Mechanical Behavior of Metal Alloys; ASME AD-Vol. 50, Fatigue and Fracture at Elevated Temperatures, A. Nagar and S. Mall, ed.; Book No. H01013 1995.
- [48] Baker and Cane model: Baker AJ, O'Donnell MP. R5 high temperature structural integrity assessment of a cracked dissimilar metal weld vessel test. In: Proceedings of second international conference on integrity of high temperature welds, London, 10–12 November 2003.
- [49] Zhao, Bin, et.al., “Experiment and simulation of creep damage for duralumin alloy” 2A12, Material Science and Engineering A 513-514, 91-95, 2009.
- [50] Lin, J., Kowalewski, Z. L. and Cao, J., Int. J. Mech. Sci. 47, pp. 1038–1058, 2005.
- [51] Kachanov, L. M., *Izv. AN SSSR, OTN* 8, pp. 26–31, 1958.
- [52] Kachanov, L. M., *The Theory of Creep*, British Library, Boston Sp, Wetnerley, 1960.

- [53] Rabotnov, Y. N., *Creep Problems in Structural Members*, Amsterdam, North-Holland 1969.
- [54] Huang, R., *Turbine Technol.* 43, pp: 9–13, 2001.
- [55] Evans, R.W., and Wilshire, B. “Creep of Metals and Alloys”, The Institute of Metals, London, 1985.
- [56] Evans, R. W. and Wilshire, B., *Introduction to Creep*, The Institute of Materials, London 1993.
- [57] Burt, H. and Wilshire, B., *Metall. Mater. Trans. A* 35A, pp. 1691–1701, 2004.
- [58] Burt, H. and Wilshire, B., *Metall. Mater. Trans. A* 36A (2005), pp. 1219–1227, 2005.
- [59] Zhao, Bin., et.al., ”Experiment and simulation of creep damage for duralumin alloy” 2A12, *Materials Science and Engineering A* 513-514, 91-96, 2009.
- [60] Ling, X., Zheng. Y. Y. and You, Y. J., *Int. J. Pressure Vessels Piping* 84 (2007), pp:304-309, 2007.

## **Chapter 4: Experimental Details**

### **4.1 Introduction**

In this chapter the experimental procedure conducted in this thesis study is presented. In progress of this study, initial effort was spent to characterize the material to be tested. In section 4.2.1, a brief discussion about the test material is presented with related characterization results.

After material characterization was completed, a uni-axial tensile test was conducted. A considerable attention was focused on preparation of the required experimental setup for 1D uni-axial creep-fatigue (CF) test. Temperature is known as one of the most effective stress parameter for both creep and CF damage [1]. In order to ensure a reliable test sample temperature measurement, a particular thermocouple clip was designed.

Eventually, a CF test plan was drafted according to the creep-life prediction formulas from Larson-Miller [2] and Wilshire [3]. The details of the test specifics associated with each CF tests are provided at the end this section. A rationale for selection of CF parameters is presented, and results obtained in the end of each CF tests were provided.

### **4.2 Experimental Details**

A uni-axial MTS 810 test system machine, which is available in MEMIL (Modern Engineering Materials Instructional Laboratory) in H. Kim Engineering Building at UMD, was used to perform uni-axial tensile tests. The test specimen was a round-bar dog-bone based on ASTM E8/E8M-11 (see, Figure 4.1 and Figure 4.2)

[4]. The ASTM standards used to determine the test specimen and test procedure are listed in Table 4.1.

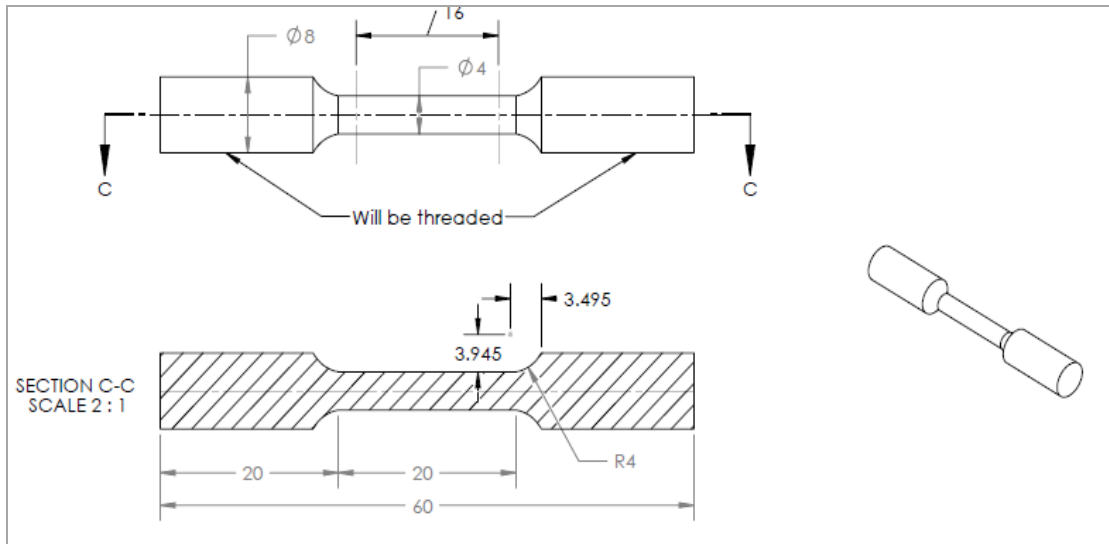


**Figure 4.1: Dimensions by ASTM E8/E8M-11**

**Table 4.1: Standards used for specimen design and parameters of experimental tests**

Design/Test	Standard	Definition
Dog-Bone Specimen	E8/E8M-11 [4]	Standard Test Methods for Tension Testing of Metallic Materials
Tension Test	E8/E8M-11 [4]	Standard Test Methods for Tension Testing of Metallic Materials
CF	E2714-09e1 [5]	Standard Test Method for CF Testing

Since the designed samples were smaller than the typical dimensions used in the MTS 810, 316 Stainless Steel fixtures were designed as mechanical support. The top ends of the test samples were threaded in order to allow mounting of the testing samples into these 316 Stainless Steel fixtures. (see Figures 4.2 and 4.3). Copper coils were wrapped around these 316 Stainless Steel fixtures to water-cool and to prevent the heat transfer from the test sample to hydraulic wedge grips of MTS 810 machine

during CF tests. Additionally, heat resistant mica sheets were placed on homemade furnace to limit heat transfer to the wedge grips.

CF tests were performed on a 20 kip Instron test machine in the Reliability Engineering lab in J.M. Patterson Building. To monitor the temperature of the test samples, OMEGA K-type Chromega Alomega SH-1-24-K-12 and OMEGA TT-K24-SLE thermocouples were used (see, Figure 4.4). Temperature fluctuations during the CF tests affected the results in the test data. Therefore, a particular thermocouple clip was needed to design to make sure that exact temperature measurements of the test sample during CF tests were recorded. A 304 Stainless Steel thermocouple clip was designed according to the dimensions in Appendix A-I.

The homemade furnace available in the Reliability and Mechanics lab was previously designed by Faridani [6], and used in the study of Ref. [6]. This creep furnace has a high temperature capacity up to 1200°C and an accuracy of  $\pm 5^{\circ}\text{C}$  (see, Figure 4.4 and 4.5).



(a)

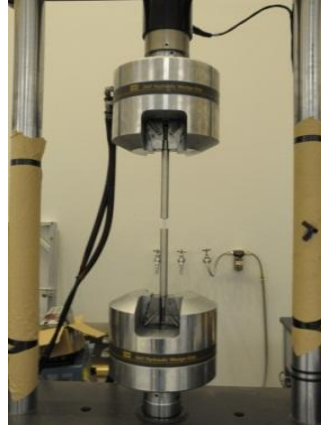


(b)

**Figure 4.2: (a) Rounded dog-bone sample and (b) rounded dog-bone sample placed in particularly designed 316 Stainless Steel grips**

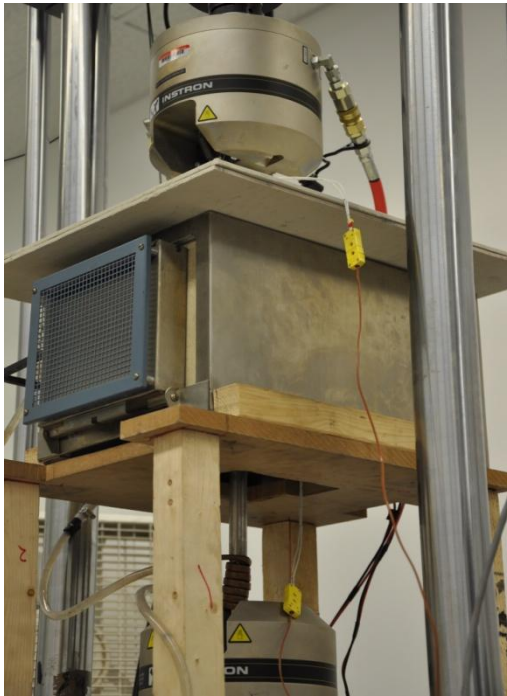


(a)



(b)

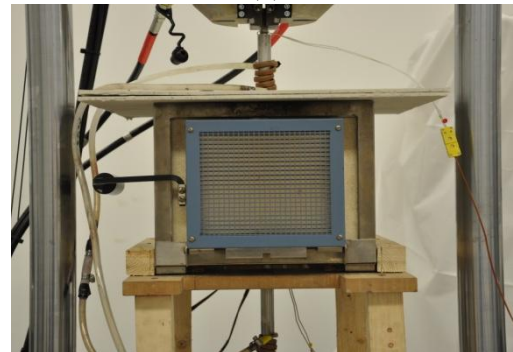
**Figure 4.3: (a) Designed 316 Stainless Steel fixtures for rounded dog-bone samples; (b) A view from tension testing of a rounded dog-bone sample which is fixed on 647 Hydraulic Grips together with the particularly designed 316 Stainless Steels**



(a)



(c)



(b)

**Figure 4.4: Creep furnace setup with (a) thermocouples, and (b) copper coil coolers; (c) 316 Stainless Steel thermocouple clip attached to test specimen inside the creep furnace**

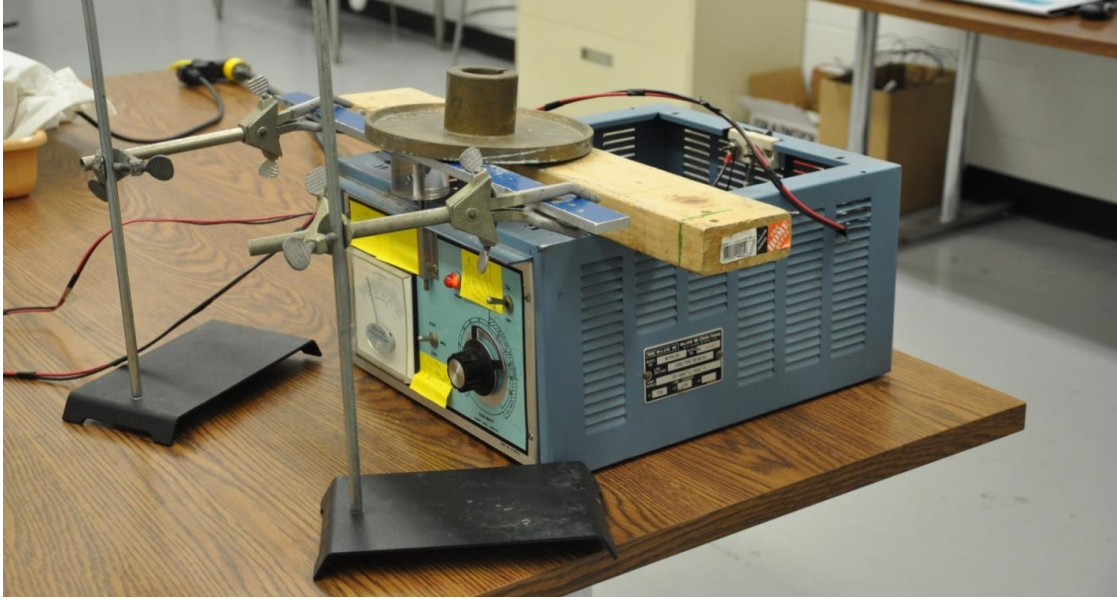


**Figure 4.5: Power supply unit of home-made creep furnace used to control the furnace temperature**

#### **4.2.1 Material**

Energy-dispersive X-ray spectroscopy (EDS) for compositional analysis was performed on the test material steel alloy using Hitachi SEM-70 in NISP Lab at UMD. Consequently, a uni-axial tensile test was performed using the MTS 810 in the MEMIL lab at UMD.

Next, both tested and untested samples were characterized using Scanning Electron Microscopy (SEM: *Hitachi, SU-70*) and Atomic Force Microscopy (AFM: *Veeco, D-3000*). In order to prepare the untested 7x7mm metal piece of steel alloy material for SEM analysis, it was first encapsulated in epoxy mixture (see, Figure 4.7 and Appendix B-I). After the encapsulation, the metal piece was polished using silicon carbide electro coated water proof abrasive papers of CC-23 P600, P1000 and P1500 respectively under water lubricant to provide a mirror-like quality on the metal

piece (see Figures 4.6 and 4.7). The encapsulated metal was analyzed using FEG-SEM (Hitachi, SU-70). The results of the EDS analysis are presented in Table 4.2.

AFM and SEM pictures of the raw metal surface are provided in Figure 4.8. Figure 4.9 shows elements dispersion on fractured surface of the tested material after tension test. This figure also helps us to understand influential elements on the test material.



**Figure 4.6: Automated polishing to provide a mirror-like quality on encapsulated metal pieces**

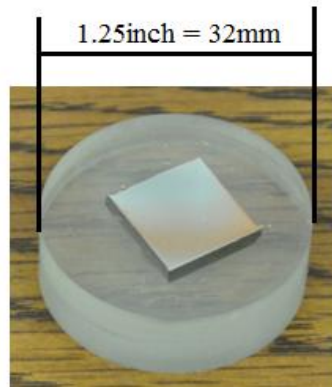


**Figure 4.7: Encapsulated 7 x 7 mm metal piece for EDS analysis after polishing**

**Table 4.2: EDS chemical composition results (wt.%)**

C	Al	P	S	Ti	Cr	Mn	Fe	Co	Ni	Cu	Nb
0.66	0.10	0.01	0.14	0.35	16.77	1.83	70.83	0.09	7.44	1.21	0.57

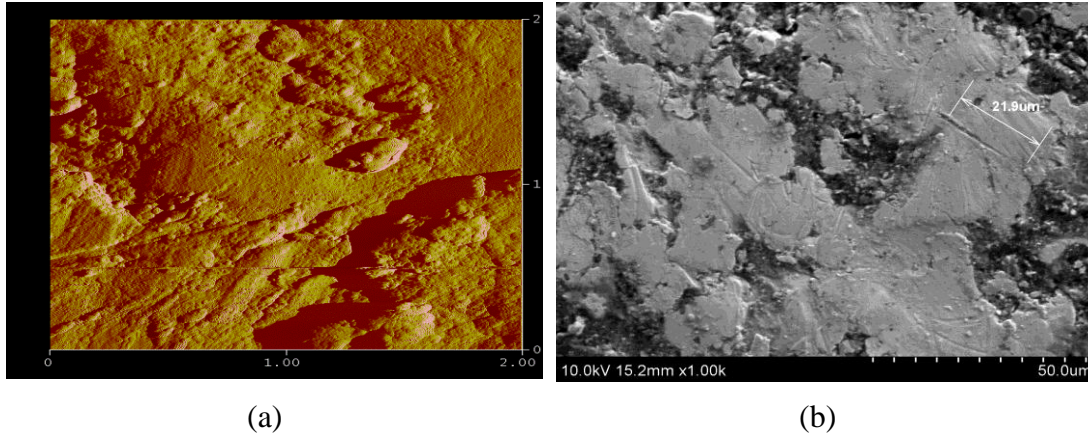


**Figure 4.8: (a) AFM picture of raw material surface in nanometer scale, (b) SEM picture (1000x) of raw material surface in micrometer scale**

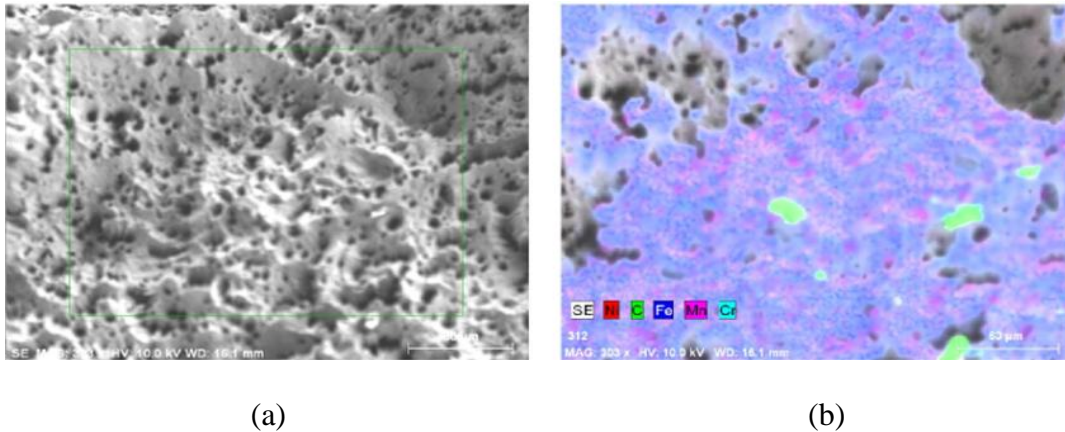


**Figure 4.9: (a) Fractured tensile specimen, (b) Dispersion of the elements on the fractured sample surface under SEM microscope**

In order to study the general microstructure of steel alloy samples, samples were etched first using an etchant based on ASTM E407-07 [7]. The chemical composition preferred was 10mL  $\text{HNO}_3$ , 20-50mL  $\text{HCl}$  and 30mL water with respect to the chemical composition results obtained from SEM analysis. The encapsulated metal was immersed into this etchant solution for times varying from 5min to 15min to observe the surface topography and general structure (see, Figure 4.10). It was observed that the applied etchant solution on the polished material did not provide a sufficient view for general structure investigation.

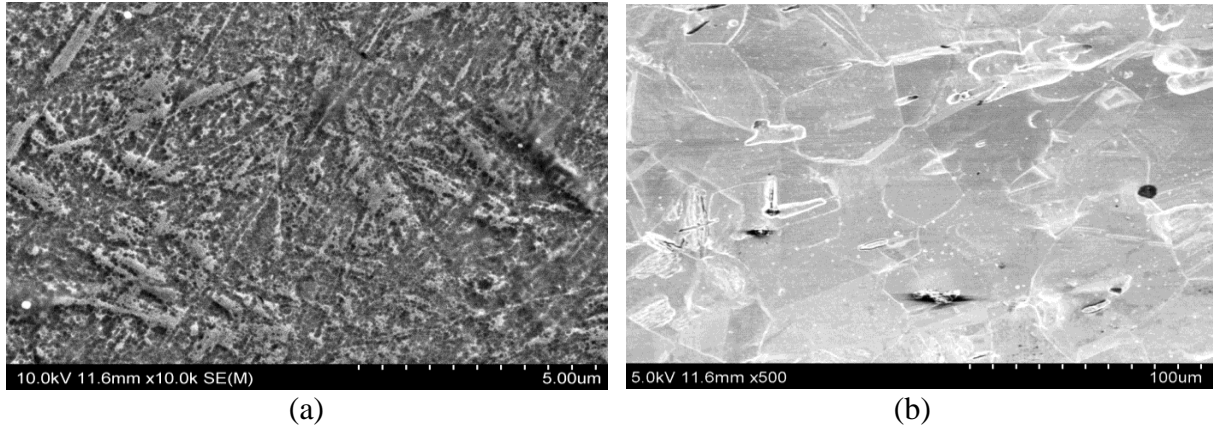


**Figure 4.10: (a) SEM picture for surface topography of 5min immersed metal, and (b) SEM picture of 15min immersed metal**

#### **4.2.2 Tensile Test**

A uni-axial tensile test based on ASTM E8/E8M-11 [4] was performed (see, Figure 4.13). Regarding elongations greater than 5%, suggested range is indicated as 0.05 and 0.5 [mm/mm/min] by the ASTM E8/E8M-11 standard [4]. Hence, 16 mm gage length of the test sample enabled 0.8 [mm/min] displacement rate. Test inputs for the MTS 810 software are shown in Figure 4.11. Room temperature tension test result for the steel alloy is presented in Figure 4.12. Yield strength was defined as 261.3 MPa, and tensile strength was defined as 691.5 MPa. The sample surface featuring a ductile cup and cone fracture is shown in Figure 4.13-b and Figure 4.14-a.

SEM pictures of the fracture surface at 35x and ruptured surface pores of metal dog-bone sample at 1000x are shown in Figure 4.14-a and b. It is also observed that most of the pores were located in the center of the ruptured sample surface.

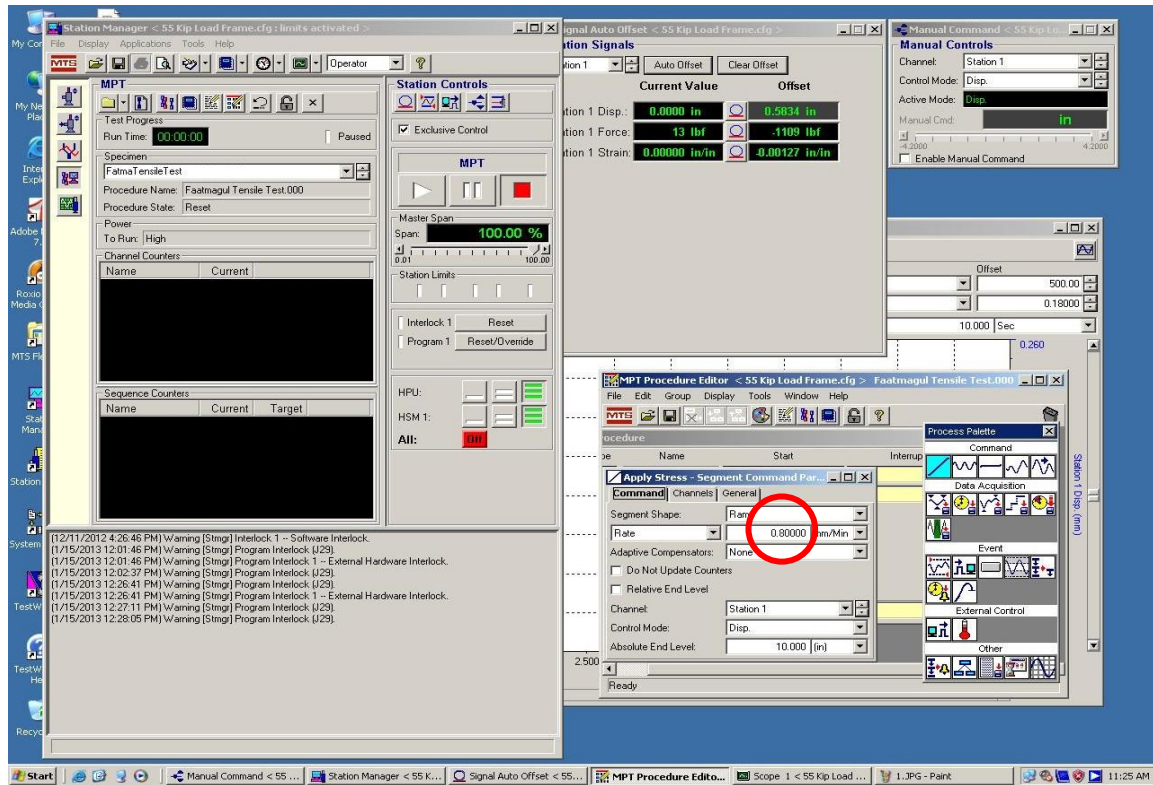


**Figure 4.11: MTS 810 test machine software and tension test inputs**

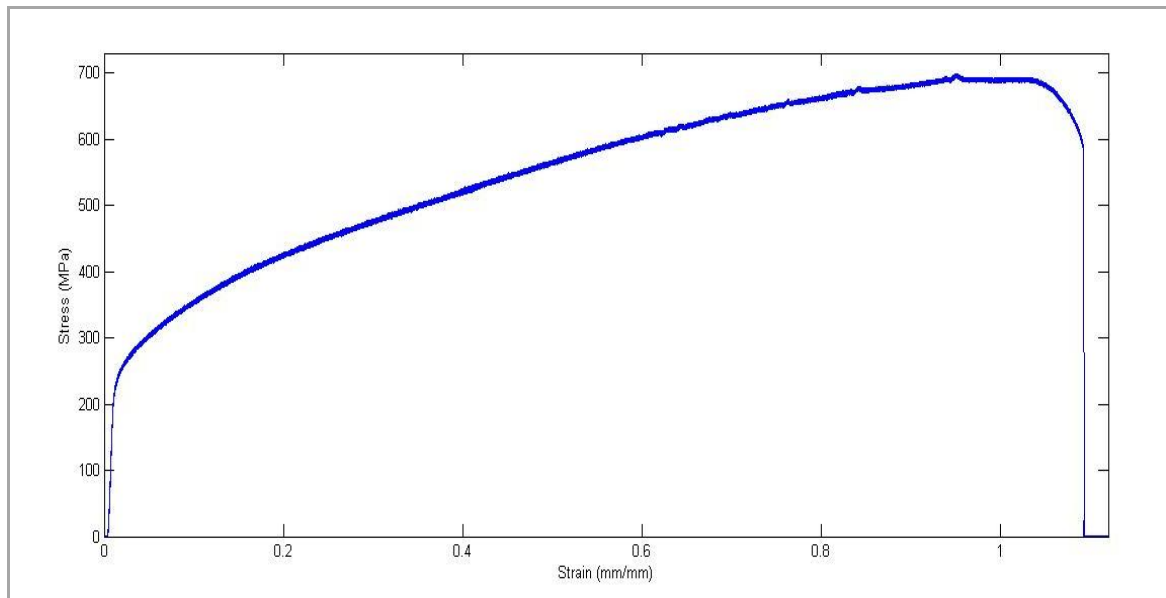


**Figure 4.12: Tension test result in room temperature for the steel alloy**

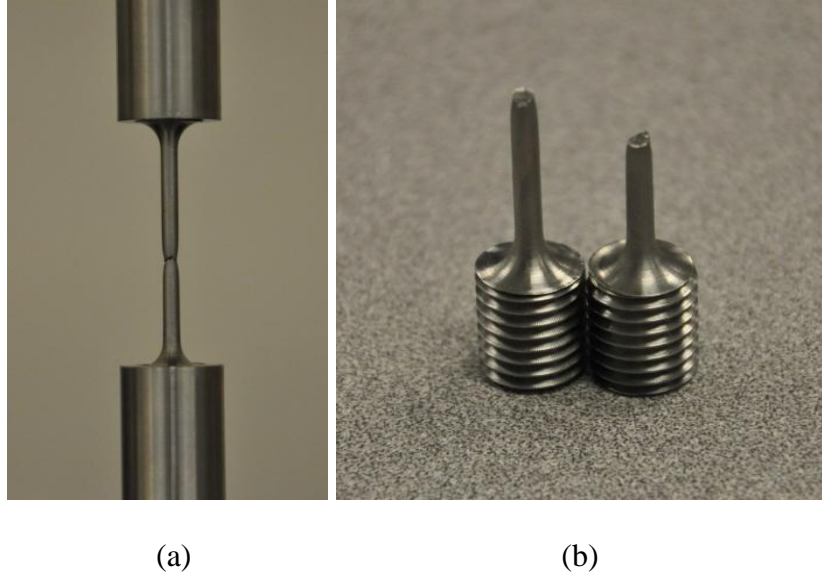


**Figure 4.13: (a) Ruptured dog-bone sample and (b) ductile cup and cone form of ruptured cross section of the steel alloy**

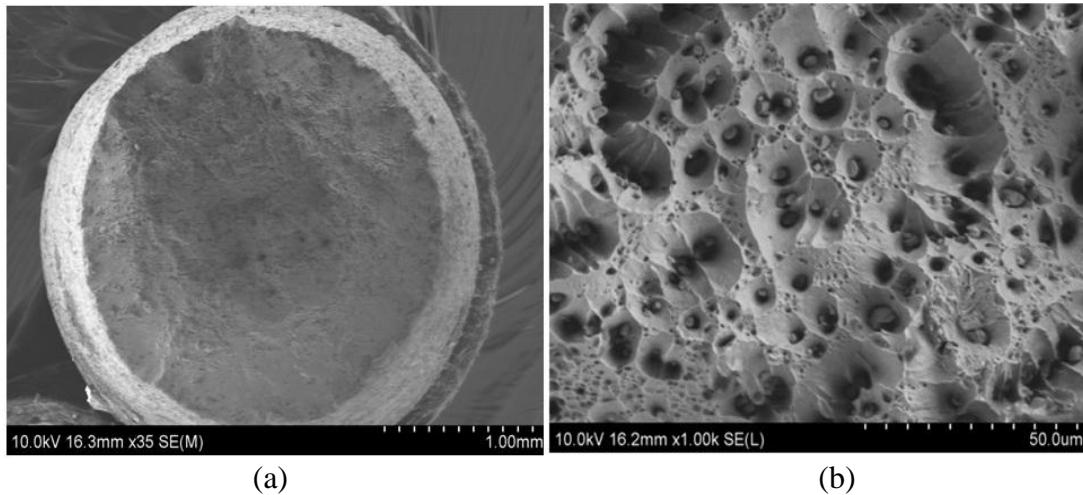


**Figure 4.14: SEM pictures of the fracture surface of the uni-axial tensile test sample (a) at 35x and (b) at 1000x showing the presence of surface pores**

#### **4.2.3 1D Uniaxial CF Test**

Depending on the component type and the purpose of the analysis, a defect-free or defect assessment procedure (or both) is undertaken to assess fitness for service at high temperatures [9]. Defect-free assessment procedures are commonly used for design purposes whereas defect assessment procedures are used for

inspection management and remaining life evaluations [8]. Data sets may be a result of (a) concurrent or (b) sequential CF loading campaigns [8]. The focus of this thesis study is on the data requirements for defect assessment of high temperature components which can be determined from CF tests. The data used in this study was the result of concurrent CF loading.

In this study, CF deformation was evaluated as non-separated regarding the study of Holmstrom et al. [9]. Holmstrom et al. [9] proposed a robust model for CF expended life assessment with a minimal set of fitting constants, and without the need to separate CF or expended life fractions. The CF damage is evaluated simply with  $D_{CF} = \sum(t_h / t_{CF})$  where  $\sum t_h$  is the corresponding time in hold.

According to ASTM E2714-09e1 [5], the preferred cycle shape in this study was a cycle with a hold at peak of the control parameter in tension (see, Figure 4.15-a). During the tests performed in this work, no compressive loads were applied because of the small cross-sectional diameter (4mm) of the samples. ASTM standard E606/E606M-12 for Standard Test Method for Strain-Controlled Fatigue Testing [10] recommends the cross-section dimension to be at least 6.35 mm (0.25 in.). Therefore, to prevent any potential buckling failure during CF test, compressive stresses were not applied on the test sample. The applied cycle shape which was modified from ASTM standard E2714-09e1[5] is demonstrated in Figure 4.15-b.

Isothermal CF tests were under strain control with tensile hold periods. Tests were performed at a stress ratio  $R = 0$  and a fixed temperature at  $400^{\circ}\text{C}$  ( $673.15^{\circ}\text{K}$ ). Additionally, before any CF tests were performed, calibration of the entire temperature measurement and control system were performed and it was found that

temperatures stayed within  $\pm 5^{\circ}\text{C}$  of the setpoint. In Figure 4.16, a view from creep-fatigue test set-up in Reliability and Mechanics lab was demonstrated.

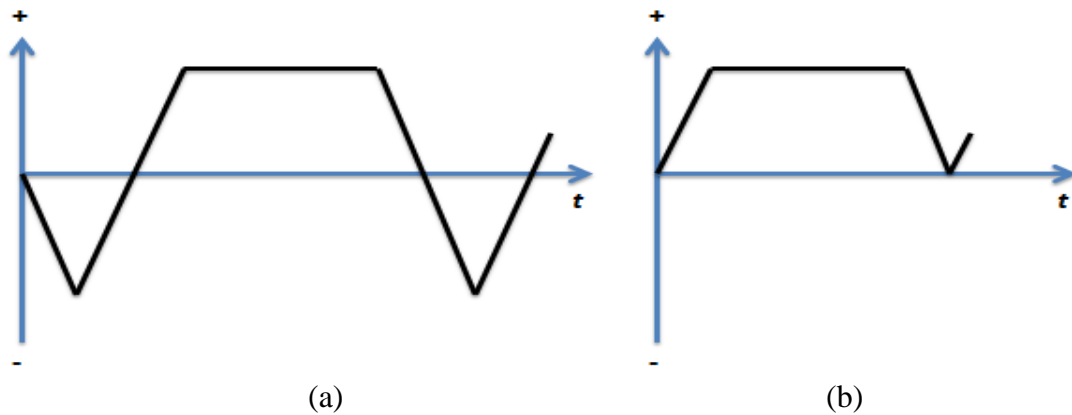


**Figure 4.15: (a) ASTM E2714-09 CF cycle shape: is a cycle with a hold at peak of the control parameter in tension [5]; (b) Adjusted CF cycle shape according to the available dog-bone sample design**



**Figure 4.16: CF test setting in Reliability and Mechanics lab**

#### 4.2.3.1 Rationale for Selection of CF Parameters

In this thesis study, strain-controlled CF tests were performed on round-bar dog-bone specimens according to ASTM E2714-09e1 [5]. The CF damage model proposed by Holmstrom et al. [9] has been used as the focal point of this research. A number of experimental studies have shown that hold times can have a detrimental effect on cyclic fatigue life [1, 9]. The hold times used in this study were defined as 10min (600s), 14min (840s) and 21min (1260s) for complete testing in a suitable timeframe.

**Table 4.3: Expected time to failures based on the Larson Miller and Wilshire formulas and equivalent test stress range**

	EXPECTED Time to Failure [hours] @ 673.15 K (400 °C)	
STRESS [MPa]	LARSON MILLER (C=20)	WILSHIRE
170	7.76	7.96
175	7.24	7.43
181	6.76	6.93
186	6.31	6.47
192	5.89	6.04
197	5.50	5.63
202	5.13	5.26
208	4.79	4.91
213	4.47	4.58
219	4.17	4.28
224	3.89	3.99
229	3.64	3.72
235	3.39	3.48
240	3.17	3.24
246	2.96	3.03
251	2.76	2.83
256	2.58	2.64
262	2.40	2.46
267	2.24	2.30
273	2.09	2.14
278	1.96	2.00
283	1.82	1.87
289	1.70	1.74
294	1.59	1.63
300	1.48	1.52

Based on the stress-strain curve in Figure 4.12, the displacement amplitude was set to 0.24mm to prevent any potential premature failure in CF tests. It is suggested by Ref. [11] that at a temperature beyond 30% of the absolute melting temperature of the material, significant time-dependent damage is accumulated. Since 30% of the absolute melting temperature of steel alloys is nearly equivalent to 400°C (673.15°K), the test temperature was decided to keep fixed at this level. This test temperature level was also preferred in order to prevent any heat-related damage on the test equipment that might occur at higher temperatures. Rump up and rump down times were set to 180s which makes a strain rate at 0.005 mm/mm/min. Table 4.3 provides a summary of the predicted time to failure based on the Larson-Miller [2] or Wilshire [3] models. These results were derived from the initially performed CF test results at 10min (600s) hold time.

Defined strain amplitude takes into account the coefficient thermal expansion of the material at 400°C(673.15°K). However, the contribution which came from the thermal expansion theory was considerably small, and did not affect the results. The details of the thermal expansion of the test material at 400°C(673.15°K) are explained in following discussion.

The length increment is linearly proportional to temperature given as [12]:

$$\Delta l = l_0 \cdot \alpha \cdot \Delta t \quad (4.1)$$

$$\Delta t = (t_1 - t_0) \quad (4.2)$$

$\Delta l$ : change in length (m, inches)

$l_0$ : initial length (m, inches)

$\alpha$ : linear expansion coefficient (m/m°C, in/in°F)

$\Delta t$ : change in temperature (°C)

$t_0$ : initial temperature (°C)

$t_1$ : final temperature (°C)

Since  $l_0=0.016\text{m}$ ,  $\alpha=0.000013\text{m/m}^\circ\text{K}$  for steel [13-14] and  $t_1: 400^\circ\text{C}$  ( $673.15^\circ\text{K}$ ) as well as  $t_0: 23^\circ\text{C}(296.15^\circ\text{K})$  change in length is calculated as:

$$\Delta l = 0.016\text{m} \cdot 0.000013\text{mm} \cdot \text{K} \cdot 673.15 - 296.15 \text{ K} = 0.078416 \text{ mm} \quad (4.3)$$

Therefore metal length at temperature  $400^\circ\text{C}(673.15^\circ\text{K})$  is:

$$l_1 = l_0 + \Delta l = 16 + 0.078416 = 16.08 \text{ mm} \quad (4.4)$$

**Table 4.4: Summary of test parameters for 3 CF Tests**

	Test 1	Test 2	Test 3
<b>Ramp up time</b>	180s	180s	180s
<b>Unloading time</b>	180s	180s	180s
<b>Hold time</b>	600s	840s	1260s
<b>Temperature</b>	$400^\circ\text{C}$	$400^\circ\text{C}$	$400^\circ\text{C}$
<b>Displacement amplitude</b>	0.24mm	0.24mm	0.24mm
<b>Strain amplitude</b>	0.015 mm/mm	0.015 mm/mm	0.015 mm/mm
<b>Stress ratio (R)</b>	0	0	0
<b>Data record frequency</b>	10Hz	10Hz	10Hz

Regarding Eq. (4.4), the strain amplitude in all CF tests was defined as 0.015 mm/mm. Table 4.4 provides a summary of the test parameters to be used on the 3 individual tests for this thesis study.

Figure 4.17 represents the cyclic loading steps of the CF test which were defined on the Instron MTS test machine software. Figure 4.18-20 demonstrate the consecutive steps followed on the software of MTS machine to perform CF test under strain control with tensile hold periods.

The print-screen in Figure 4.18 demonstrates the inputs provided in first step. In this demo test, step1 in Figure 4.18 was completed in 30s, and ramped up to the specified displacement position according to the Instron MTS coordinate system. Figure 4.19 demonstrates the inputs in the second step of the cycle presented in Figure 4.17. Figure 4.20 shows the third step of the cycle presented in Figure 4.17. Rump down duration was set equal to the rump up duration. The end point was specified as the defined end point in the step 1 minus specified displacement level.

Figure 4.21 presents the instant test monitor module. In this module, triple chart display option was selected. The display graphs were defined to monitor instantly stress-time, strain-time and stress-strain hysteresis diagrams.

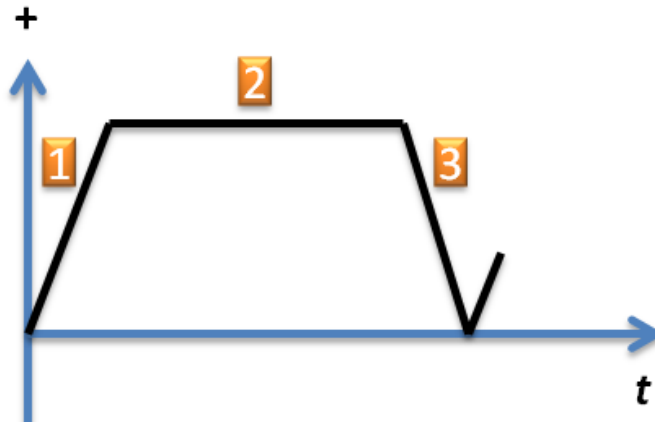


**Figure 4.17: Strain controlled CF test cycle with stress Ratio = 0, where Step1(Tension), Step 2(hold) and Step 3(release)**

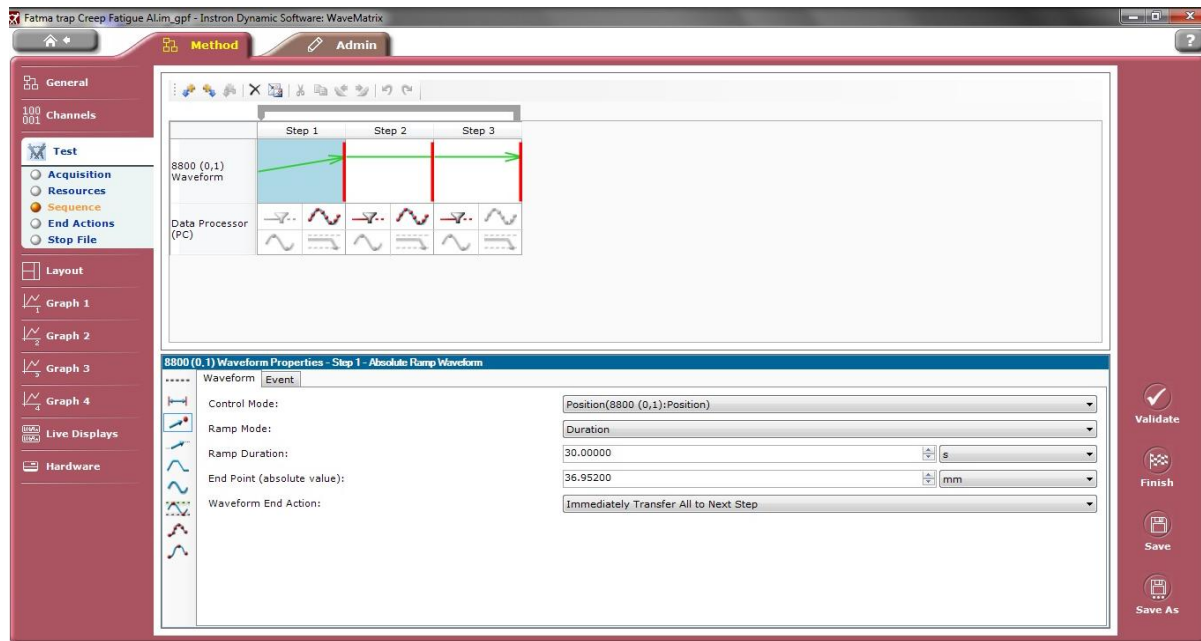


**Figure 4.18: Instron Dynamic Software WaveMatrix CF test inputs: Step 1**

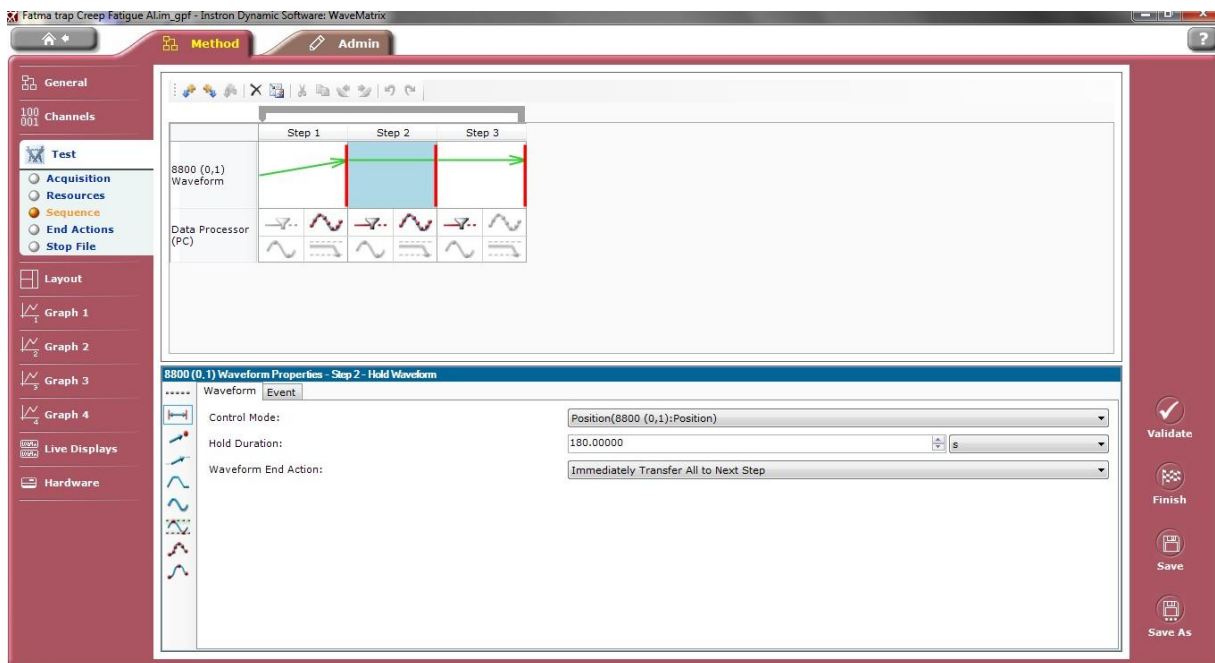


**Figure 4.19: Instron Dynamic Software WaveMatrix CF test inputs: Step 2**

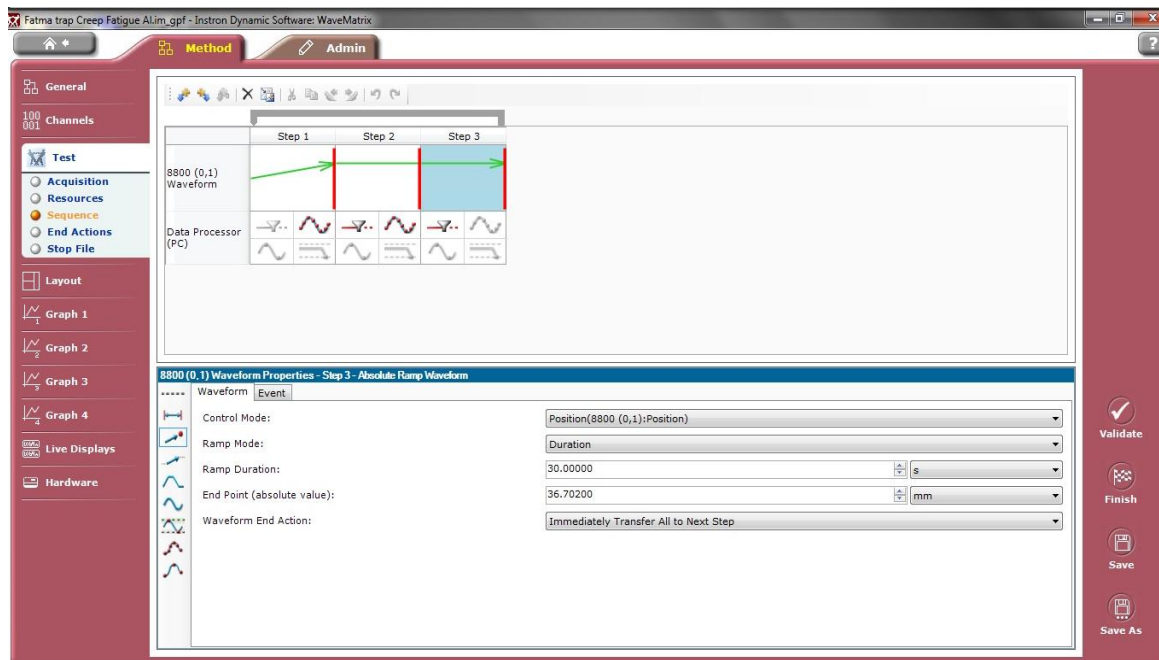


**Figure 4.20: Instron Dynamic Software WaveMatrix CF test inputs: Step 3**

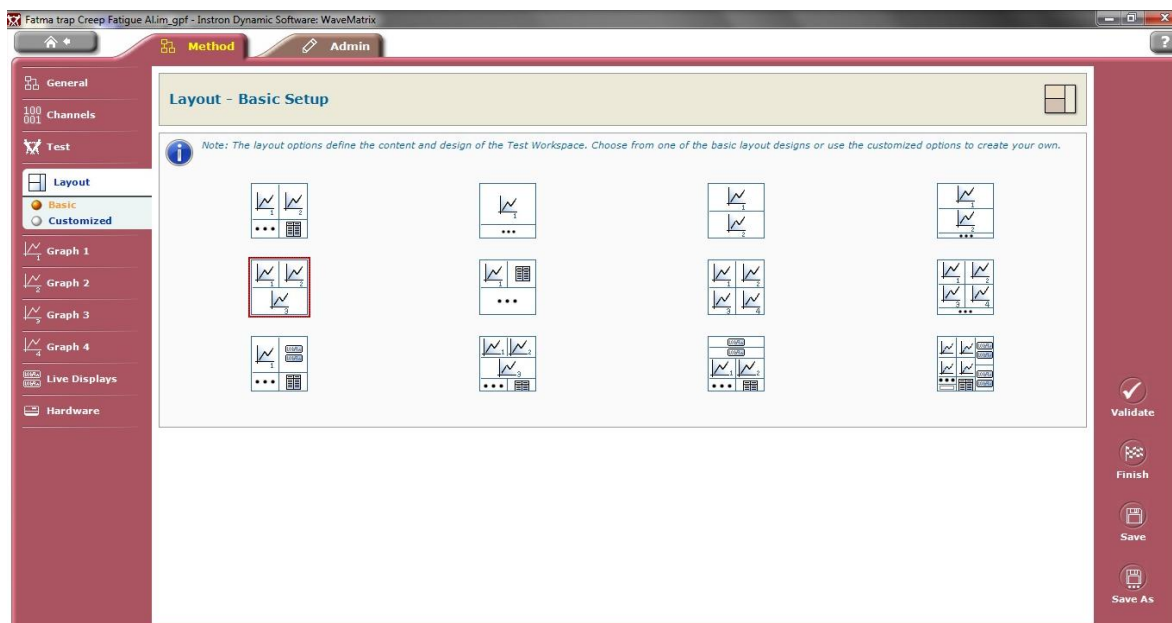


**Figure 4.21: Instron Dynamic Software WaveMatrix test monitoring options**

ASTM standard E2714-09e1 [5] defines the failure criteria for CF tests when at least a 10% reduction in the stress with respect to the maximum load is observed (as seen in Figure 4.22 where  $x = 10\%$ ). Therefore, the failure criterion in each CF test

used in this study was initially defined according to the observed stress reduction with respect to the observed maximum reference stress during the test. It was observed that nearly after 60% drop with respect to the reference  $\sigma$  (stress) level, instant  $\sigma$  on the same CF test reached to zero level.

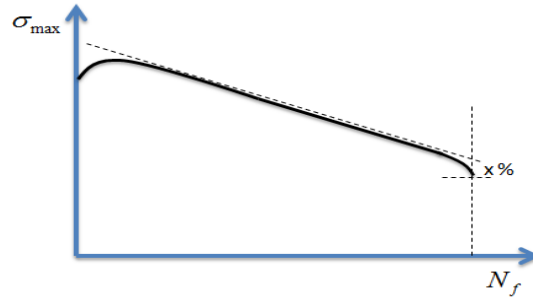


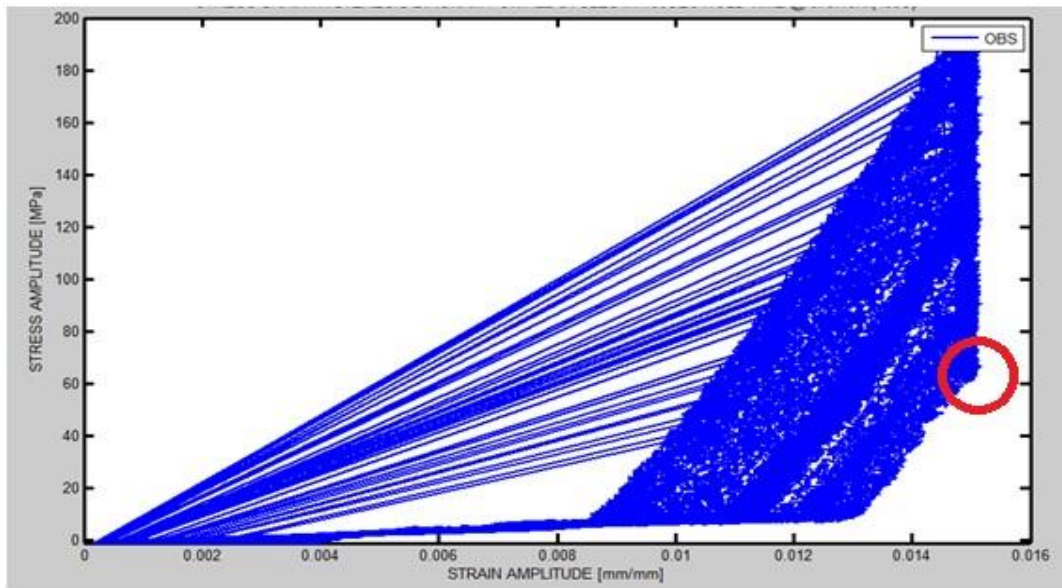
**Figure 4.22: ASTM standard E2714-09 end-of-test criterion based on reduction of peak stress for softening materials**

#### 4.2.3.2 1D Uniaxial CF Test Results

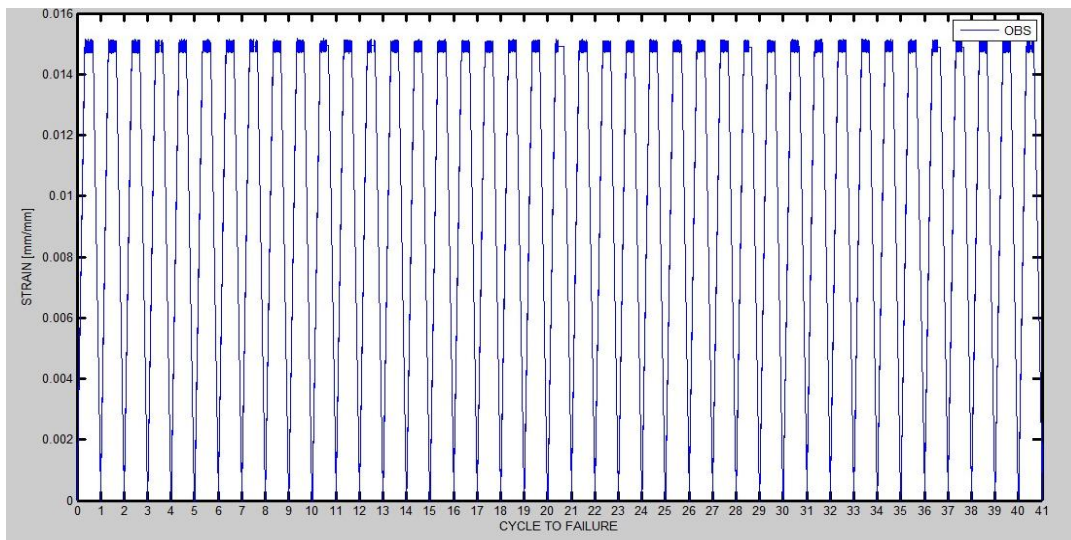
Figure 4.23 provides stress-strain hysteresis diagram for a 10min (600s) hold time strain controlled creep-fatigue test at 673.15°K(400°C). Due to the short hold time of the test, it is difficult to observe any certain reduction of stress in each hysteresis cycle at the strain control point of 0.015 mm/mm. The expected reduction of stress is shown in the red circle for a definite hysteresis cycle (see, Figure 4.23).

Figure 4.24 demonstrates strain – cycles to failure graph for 10min (600s) hold time CF test at 0.015 [mm/mm]. Strain amplitude can be seen easily in this figure.

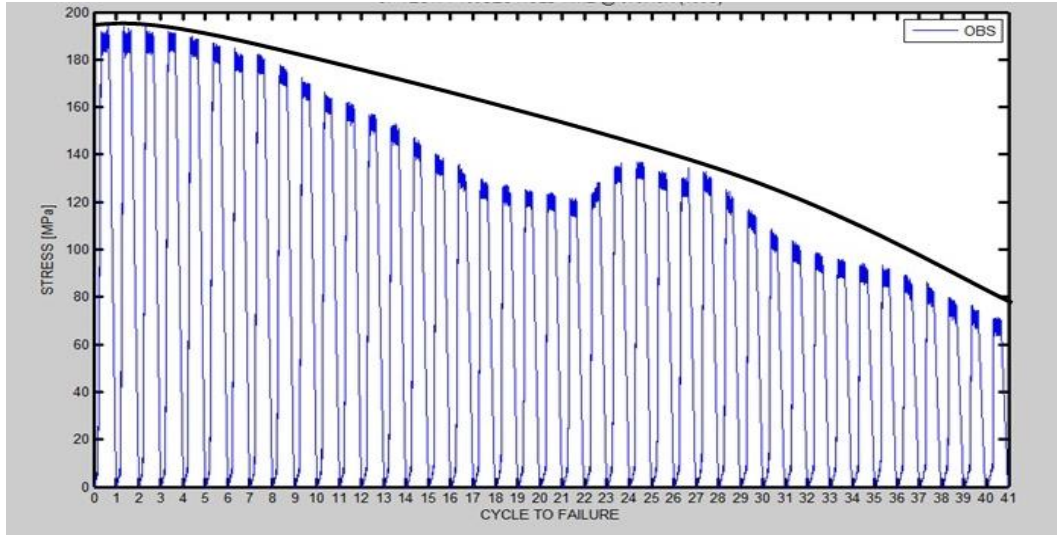
Figure 4.25 provides a stress-cycle to failure graph for the 10min (600s) hold time test at 400°C (673.15°K). After 41 cycles, a 58% drop in the stress with respect to the initial reference stress was observed. In the subsequent cycle, a sudden drop to zero stress level was observed.



**Figure 4.23: Stress-strain hysteresis diagram for all cycles in 10min (600s) hold time creep CF test at 673.15°K(400°C)**

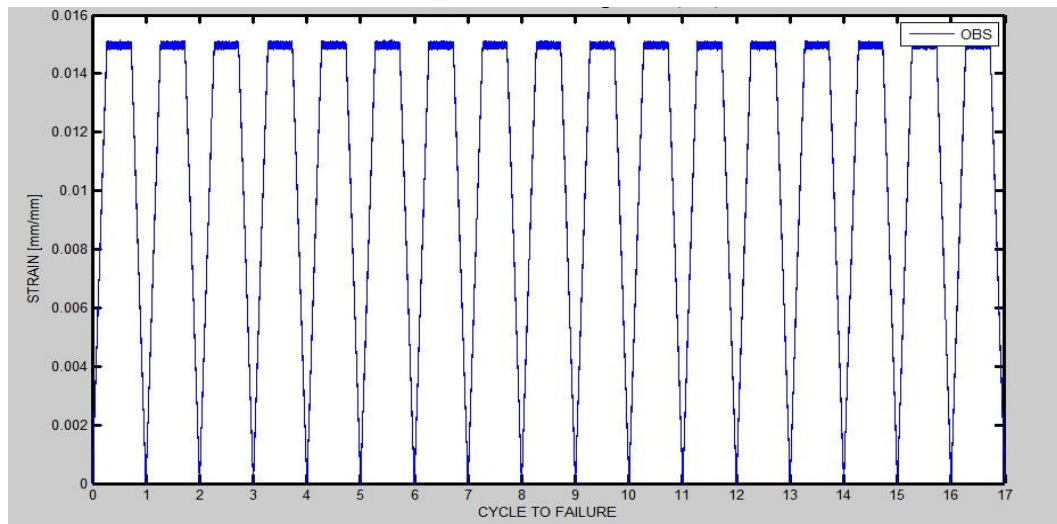


**Figure 4.24: Strain-cycle to failure diagram for all cycles in 10min(600s) hold time CF test at 673.15°K(400°C)**



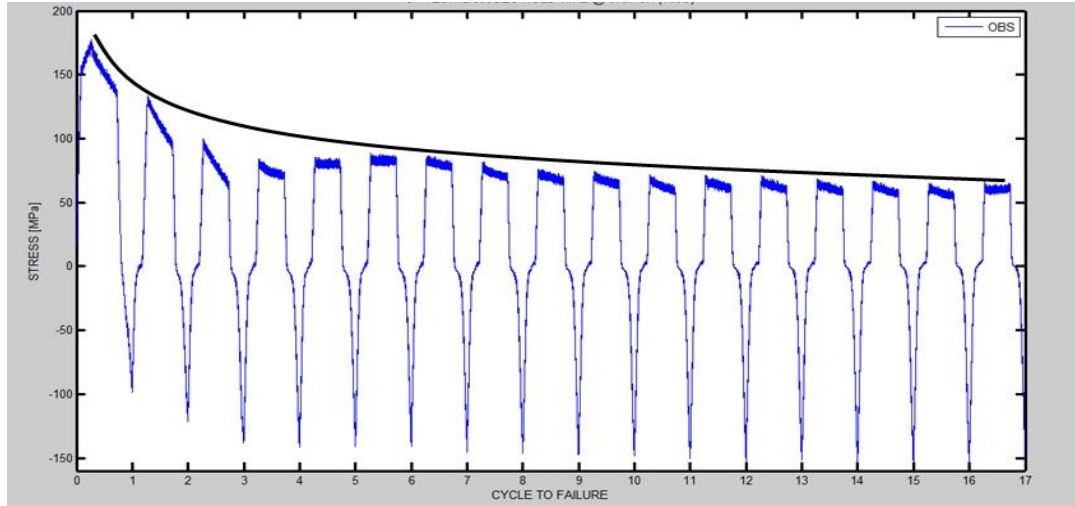
**Figure 4.25: Stress-cycle to failure diagram for all cycles in 10min (600s) hold time CF test in 673.15°K(400°C)**

In Figure 4.26, strain – cycle to failure graph of 14min (840s) hold time creep-fatigue test is provided. Strain control in 0.015 [mm/mm] was maintained throughout the all cycles in this test.



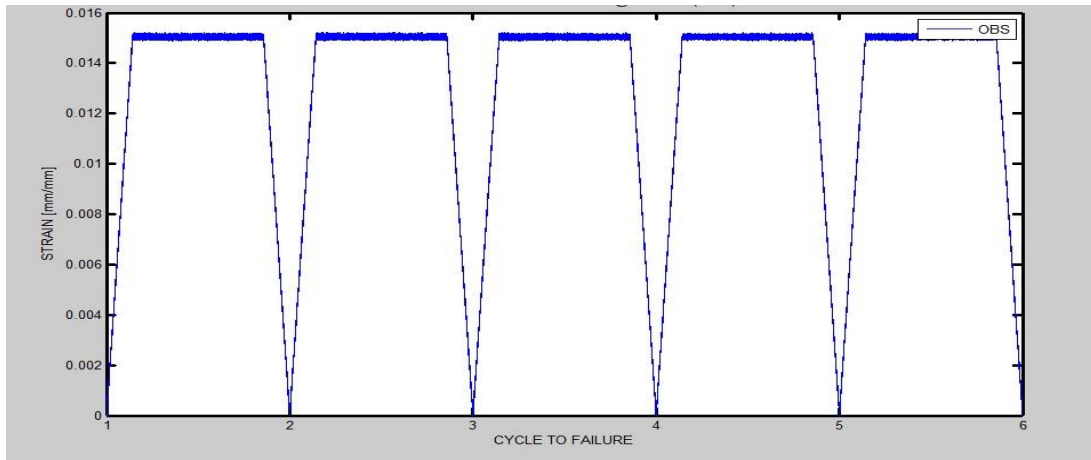
**Figure 4.26: Strain-cycle to failure diagram for all cycles in 14min (840s) hold time CF test at 673.15°K(400°C)**

Figure 4.27 provides stress – cycle to failure graph for 14min (840s) hold time test. After 17 cycles, a 65% drop with respect to the initial stress level was observed. In the subsequent cycles, a sudden drop to zero stress level was seen.



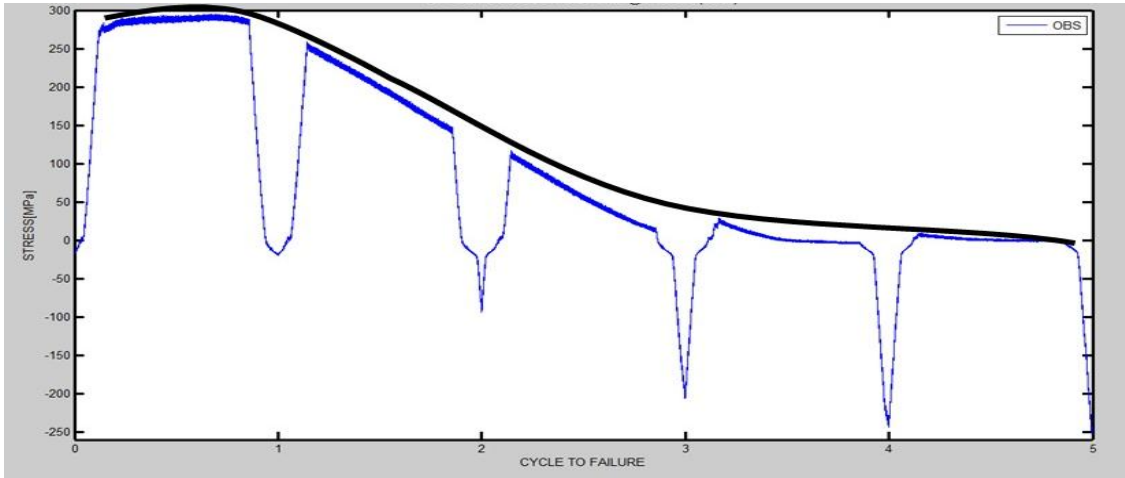
**Figure 4.27: Stress-cycle to failure diagram for all cycles in 14min (840s) hold time CF test in  $673.15^{\circ}\text{K}(400^{\circ}\text{C})$**

In Figure 4.28, strain – cycle to failure graph for the 21min (1260s) hold time creep-fatigue test is provided. Strain control in 0.015 [mm/mm] was maintained throughout the all cycles in this test.



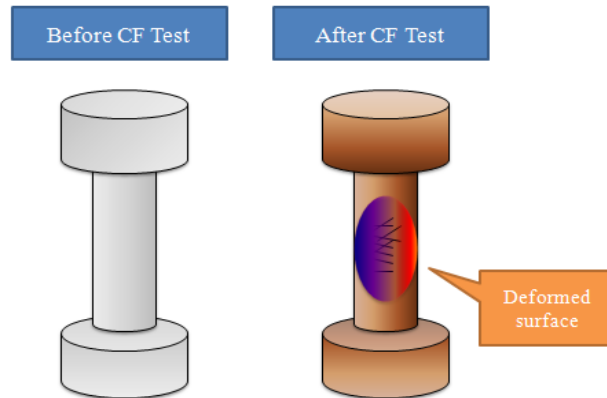
**Figure 4.28: Strain-cycle to failure diagram for all cycles in 21min (1260s) hold time creep-fatigue test in  $673.15^{\circ}\text{K}(400^{\circ}\text{C})$**

Figure 4.29 provides stress – cycle to failure graph for 21min (1260s) hold time test. After 5 cycles, 100% drop with respect to the initial stress level was observed.



**Figure 4.29: Stress-cycle to failure diagram for all cycles in 21min (1260s) hold time CF test in  $673.15^{\circ}\text{K}$  ( $400^{\circ}\text{C}$ )**

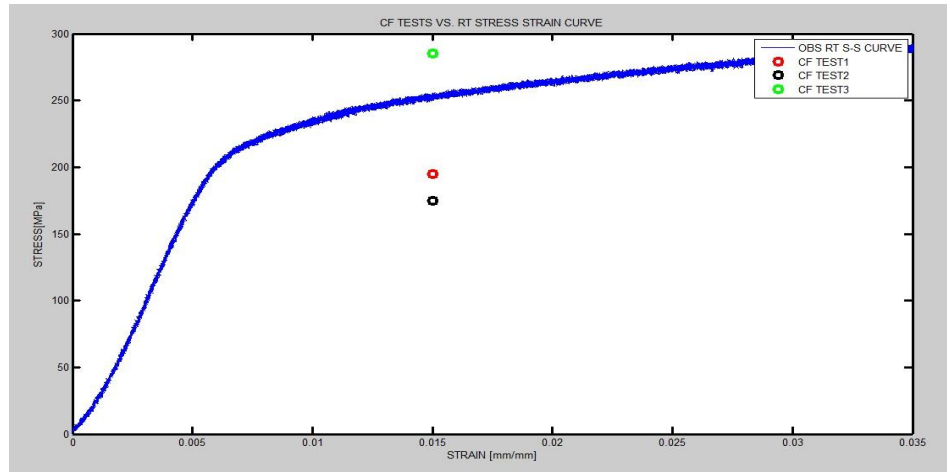
Figure 4.30 illustrates the striated surface of visually deformed test sample after CF test. The actual observations were akin to this illustration.



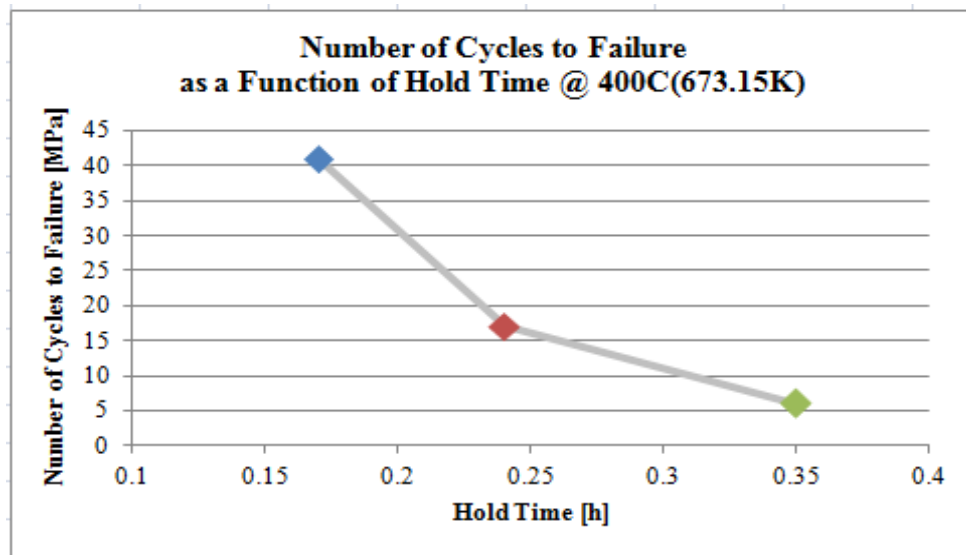
**Figure 4.30: Test sample before and after CF test showing the visual impact of CF deformation on the sample surface**

Figure 4.31 illustrates the observed stress levels in each creep- fatigue test with respect to the stress – strain curve of the material in room temperature. Figure 4.32

shows the number of cycles to failure with respect to different hold times for the different creep-fatigue tests. It was observed that as hold time increases the time to failure decreases.



**Figure 4.31: Observed stress levels in each CF test with respect to the stress-strain curve in room temperature**



**Figure 4.32: Observed number of cycles to failure with respect to the hold times in each CF test**

### 4.3 References

- [1] Brinkman, C.R., "High-temperature time-dependent behavior of several engineering structural alloys," International Metal Reviews, Vol.30, Issue:5,

pp:235-258, 1985.

- [2] Larson, F.R., Miller, E.J., "Time-temperature relationship for rupture and creep stresses," *Trans. ASME*, vol.74, p.765-775, 1952.
- [3] Wilshire, B., Scharning, P.J., Hurst, R., "A new approach to creep data assessment," *Materials Science and Engineering A*, Vol.510-511, Issue:3-6, 2009.
- [4] ASTM Standard E8/E8M-11, "Standard test methods for tension testing on metallic materials," ASTM International, West Conshohocken, PA, 2011, DOI:10.1520/E0008\_E0008M-11, [www.astm.org](http://www.astm.org).
- [5] ASTM Standard E2714-09e1, "Standard test method for creep-fatigue testing," ASTM International, West Conshohocken, PA, 2009, DOI: 10.1520/E2714-09EOI, [www.astm.org](http://www.astm.org)
- [6] Faridani, M.N, and Modarres, M., "A probabilistic model of creep failure mechanism for structural reliability assessment with applications," 2012.
- [7] ASTM Standard E407-07, "Standard practice for microetching and alloys," ASTM International, West Conshohocken, PA, 2007, DOI: 10.1520/E0407-07, [www.astm.org](http://www.astm.org).
- [8] Holdsworth, S.R., "Component Assessment Data Requirements from Creep-Fatigue Tests," *Journal of ASTM International*, 2011, [www.astm.org](http://www.astm.org).
- [9] Holmstrom, S., Auerkari, P., "A robust model for creep-fatigue life assessment," *Material Science and Engineering A*, vol.559, pp: 333-335, 2013.
- [10] ASTM Standard E606/E606M, "Standard Test Method for Strain-Controlled Fatigue Testing," ASTM International, West Conshohocken, PA, 2012, DOI: 10.1520/E0606-04E01, [www.astm.org](http://www.astm.org) .
- [11] Mao, H., Mahadevan, S., "Reliability analysis of creep-fatigue failure," *International Journal of Fatigue*, Vol.22, pp:789-797, 2000.
- [12] Jaske, C.E., Mindlin, H and Perrin, J.S., "Combined low-cycle fatigue and stress relaxation of alloy 800 and type 304 stainless steel at elevated temperatures," *Fatigue at elevated temperature*, ASTM STP 520, American Society for Testing and Materials, pp:365-376, 1973.
- [13] Sun, G., Chen, Z., Liu, Z., "Analytical and Experimental Investigation of Thermal Expansion Mechanism of Steel Cables," *Journal of Materials in Civil Engineering*, Vol.1017, July 2011.

- [14] The Engineering Toolbox, *Coefficients of Thermal Expansion*.  
[available online: [http://www.engineeringtoolbox.com/linear-expansion-coefficients-d\\_95.html](http://www.engineeringtoolbox.com/linear-expansion-coefficients-d_95.html)]

# Chapter 5: Estimation of Empirical Parameters using Bayesian Inference

## 5.1 Introduction

In the framework of the Bayesian approach, the parameters of interest are treated as random variables (r.v.s.), the true values of which are unknown. Thus a distribution can be assigned to represent the parameter; the mean (or, for some cases, the median) of the distribution can be used as an estimate of the parameter of interest. The probability density function (pdf) of a parameter in Bayesian terms can be obtained from a prior and a posterior pdf. In practice, however, the prior pdf is used to represent prior knowledge, including subjective judgment regarding the characteristics of the parameter and its distribution. When the prior knowledge is combined with other relevant information (often statistics obtained from tests and observations), a posterior distribution is obtained, which better represents the parameter of interest (see, Figure 5.1) [1].

A generic algorithm for Bayesian inference is provided as follows.

- Step1: Formulate the model as a collection of probability distributions conditional on different values for model parameter(s).
- Step2: Organize your beliefs about parameter(s) into a (prior) probability distribution.
- Step3: Collect the data and insert them into the family of distributions given in Step1.
- Step4: Use Bayes' theorem to calculate your new beliefs about parameter(s).

Tools such as WinBUGS allow us to draw samples from the established posterior distribution (using observed data, and choosing suitable prior). WinBUGS (BUGS stands for **B**ayesian **I**nference **U**sing **G**ibbs **S**ampling [2]) is an open source

Bayesian analysis software tool which uses Markov Chain Monte Carlo (MCMC) methods to fit statistical models. It can be used in statistical problems as simple as estimating means and variances or as complicated as fitting multilevel models. The posterior distribution from Bayes theorem, especially in the case of model parameter estimates in accelerated life testing analysis is often a complicated quantity to evaluate when the number of parameters is large [3]. In order to advance in WinBUGS software, *Bayesian Modeling Using WinBUGS* [3] is an excellent source.

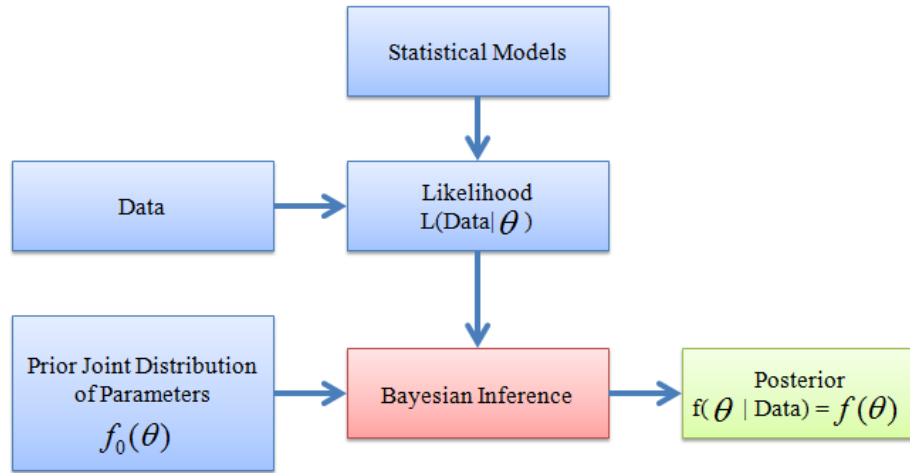


**Figure 5.1: Bayesian Inference Framework [1]**

MCMC creates a markov chain whose stationary distribution is the same as target distribution. If a lot of samples from the chain are taken, then the correct distribution is provided. However, the decision of ‘correct distribution is reached’ can be challenging. The actual question here remains as how well the samples approximate the target distribution. One solution suggested for this problem is removing the first few values from the consecutive iterations. This removed section from the sampled data is called as the burn-in. Therefore, in this study first 500 points from the sampled data were removed from the parameter predictions in the proposed

robust creep-fatigue life models. It was understood that when the posterior has reached the stationary distribution, it has converged. In order to provide a good convergence, all the chains were run for an extended period. It was observed that running the chain for a longer period provided a good mixing.

As a second concern to provide the better estimate of the model parameters, every 10 points from the all iterations were taken. This process is called as thinning. It was observed that taking iterations at an even interval reduces the autocorrelation between iterations. This can be seen easily in following section, explaining estimation of empirical model parameters for Soviet [4,11], Larson-Miller [5,6,11], Orr-Sherby Dorn [7,11], Manson Haferd [8,11] and Wilshire Models [9-11]. In order to get a good convergence of the target distribution, a large number of iterations was required. In this study, data points more than 10,000 were evaluated.

To understand how well the estimation can be assessed, comparing the mean of the samples and the true posterior mean may be required. This is called as markov chain error (MC error) in WinBUGS node statistics table. It is appropriate if this MC error is less than 5% of the true error [3].

In order to control if chains have converged, the simplest way is to check WinBUGS history report. The history reports of the all predictions for model parameters are provided in Appedix D I-V. They mostly show the pattern which provides a good convergence.

Thereupon, running longer chain, thinning and trying different parameterizations of the models to provide the best predictions have been very helpful in healthy progress of this research. As an additional control mechanism to

propose valid model parameters, model error  $e$  and R2B (Bayesian Pearson coefficient of determination) were included in WinBUGS model codes. This can be seen in Appendix C I-V. In each update, it was monitored if R2B remained between 0 and 1, and if model error  $e$  was positive. When R2B was an invalid value, model error  $e$  was invalid simultaneously. Afterwards, all the posterior parameters were checked in MS Excel Goal Seek dialog box, OriginPro9.0, Matlab R2012 and Minitab 16 to see if they were still providing an acceptable master curve for creep-fatigue (CF) expended life of the test metal which was used in this study.

## 5.2 Estimation of Empirical Model Parameters Using Bayesian Inference

In this section, probabilistic models were developed for the Soviet [4,11], Larson-Miller [5,6,11], Orr-Sherby Dorn [7,11], Manson-Haferd [8,11], and Wishire [9-11] Models by using Bayesian inference framework. To present the variability in likelihood function of creep-fatigue life, a normal distribution was assumed. In Figure 5.2, a normal distribution probability plot of failed CF data is presented. Since there is not a large scatter in the test data, this assumption for likelihood function is suitable.

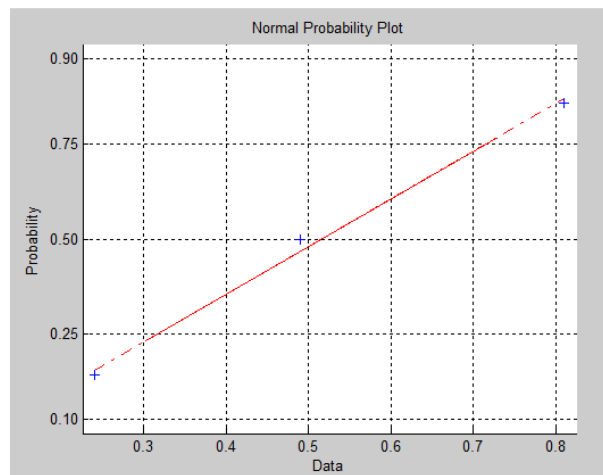


**Figure 5.2: Normal distribution probability plot of failed CF data**

In this thesis study, the number of valid test data was only three. The available analysis tools and probabilistic Bayesian Inference framework have contributed a lot in this study to question further the effectiveness of the published robust creep-fatigue life models. This is also attributed to the strength of Bayesian inference.

In determination of prior distributions initially, the available data from CF tests [12] was referred to. However, a considerable spread from the estimated master curves was diagnosed. As a next step, the available test data only was evaluated by Nonlinear Least Squares method, using a trust region algorithm. The estimates provided from this method allowed an estimation of the most proper initial distribution parameters for each proposed model. Best fits were obtained after applying Bayesian Inference framework in WinBUGS software. The R2B results of each robust CF models are provided in Figure 5.3. The provided results in the following sub-sections 5.2.1-5 were presented according to the order in Figure 5.3 from the highest to the lowest R2B.

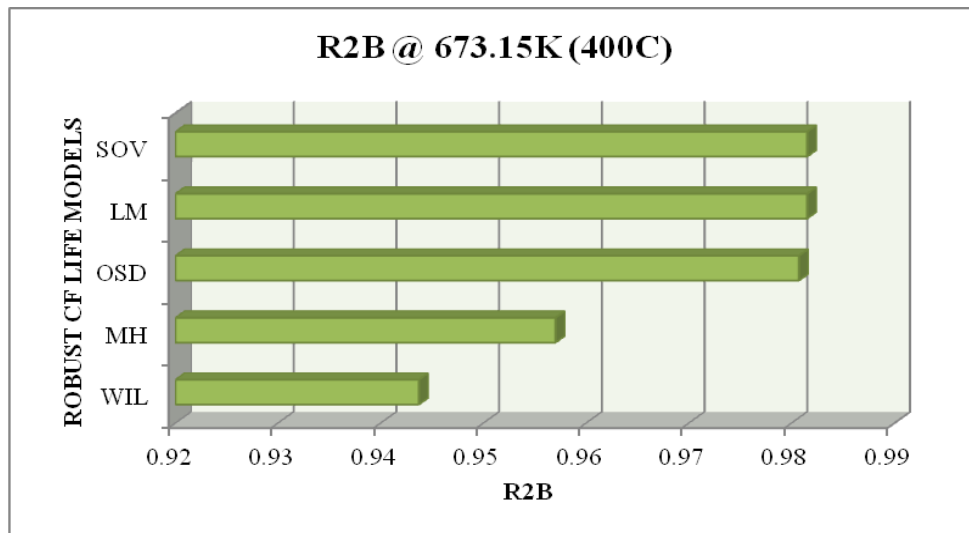


**Figure 5.3: WinBUGS Bayesian Inference framework R2B results for each robust creep-fatigue models**

### 5.2.1 Soviet Model

Soviet Model [4,11] is presented in Eq.(5.1). This form of the model was used in consequent Bayesian Inference framework steps. It was observed that  $\beta_2$  and  $\beta_3$  had the least effect in curvature of the model. Therefore, those parameters were kept as fixed constants. This also helped in assessing the performance of the Soviet Model [4,11] despite of the limited test data.

$$\log(t_{CF}) = \beta_0 + \beta_1 \cdot \log[T] + \beta_2 \cdot \log[\sigma_{max}] + \frac{\beta_3}{T} + \beta_4 \cdot \frac{\sigma_{max}}{T} \quad (5.1)$$

Assuming a normal distribution to represent the variability of CF expended life, the likelihood function of the CF data, and the corresponding different percentiles of this distribution was expressed as:

$$f(\log(t_{CF})) = N(\mu_i, s_i) \quad (5.2)$$

$$\mu_i = N\left(\beta_0 + \beta_1 \cdot \log[T] + \beta_2 \cdot \log[\sigma_{max}] + \frac{\beta_3}{T} + \beta_4 \cdot \frac{\sigma_{max}}{T}\right) \quad (5.3)$$

where  $\mu_i$  and  $s_i$  are the normal-mean and normal-standard deviation of the CF expended life distribution. After substituting Eq.(5.3) into Eq.(5.2), conditional distribution function of the logarithmic CF expended life “ $\log(t_{CF})$ ” given stress and temperature condition was obtained.

$$\begin{aligned} & f(\log(t_{CF})|\sigma_{max_i}, T_i) \\ &= \frac{1}{s \cdot \sqrt{2\pi}} \cdot \exp\left(\frac{-1}{2s^2} \left[ \log(t_{CF}) - \left( \beta_0 + \beta_1 \cdot \log[T] + \beta_2 \cdot \log[\sigma_{max}] + \frac{\beta_3}{T} + \beta_4 \cdot \frac{\sigma_{max}}{T} \right) \right]^2\right) \end{aligned} \quad (5.4)$$

Therefore, likelihood function was given by Eq.(5.5).

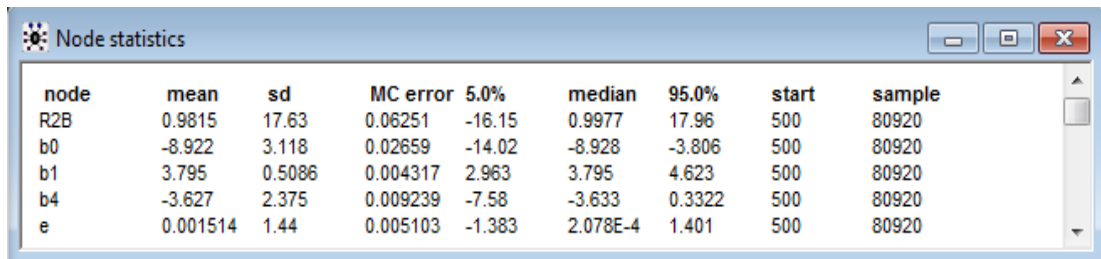
$$L(t_{CF_i}) = \prod_{i=1}^N f(\log(t_{CF})|\sigma_{max_i}, T_i) \quad (5.5)$$

In addition to Eq.(5.5), posterior distribution of parameters  $\beta_0$ ,  $\beta_1$ ,  $\beta_4$  and  $s$  which is standard deviation of the likelihood function were derived by using Bayes' estimation according to:

$$f(\beta_0, \beta_1, \beta_4, s | \log(t_{CF})) = \frac{f_0(\beta_0, \beta_1, \beta_4, s) \cdot L(\beta_0, \beta_1, \beta_4, s | \log(t_{CF}))}{\int_s \int_{\beta_4} \int_{\beta_1} \int_{\beta_0} f_0(\beta_0, \beta_1, \beta_4, s) \cdot L(\beta_0, \beta_1, \beta_4, s | \log(t_{CF})) d\beta_0 d\beta_1 d\beta_4 ds} \quad (5.6)$$

where  $f_0(\beta_0, \beta_1, \beta_4, s)$  is the subjective prior distribution . Prior distributions are updated using the experimental data from experiments.

There is no closed form solution available for posteriors in Eq.(5.6). Therefore, Bayesian posteriors were estimated using the sophisticated sampling approach Markov Chain Monte Carlo (MCMC) method using Metropolis-Hasting algorithm. In this method the posterior function is recreated by generating enough samples rather than by direct integration. Then a sample drawn from a generating distribution is modified through a series of conditional probability calculations until becomes a sample of the target posterior. Codes written in WinBUGS for Bayesian Inference of parameters from Soviet Models [4,11] were provided in Appendix C-I. In Figure 5.4, WinBUGS node statistics for Soviet Model [4,11] are presented.



node	mean	sd	MC error	5.0%	median	95.0%	start	sample
R2B	0.9815	17.63	0.06251	-16.15	0.9977	17.96	500	80920
b0	-8.922	3.118	0.02659	-14.02	-8.928	-3.806	500	80920
b1	3.795	0.5086	0.004317	2.963	3.795	4.623	500	80920
b4	-3.627	2.375	0.009239	-7.58	-3.633	0.3322	500	80920
e	0.001514	1.44	0.005103	-1.383	2.078E-4	1.401	500	80920

**Figure 5.4: WinBUGS node statistics for Soviet Model**

Posterior distributions of the Bayesian Inference in Soviet Model are:

$$\begin{aligned} \beta_0 &\sim N(-8.922, 3.118) \\ \beta_1 &\sim N(3.795, 0.5086) \\ \beta_4 &\sim N(-3.627, 2.375) \end{aligned}$$

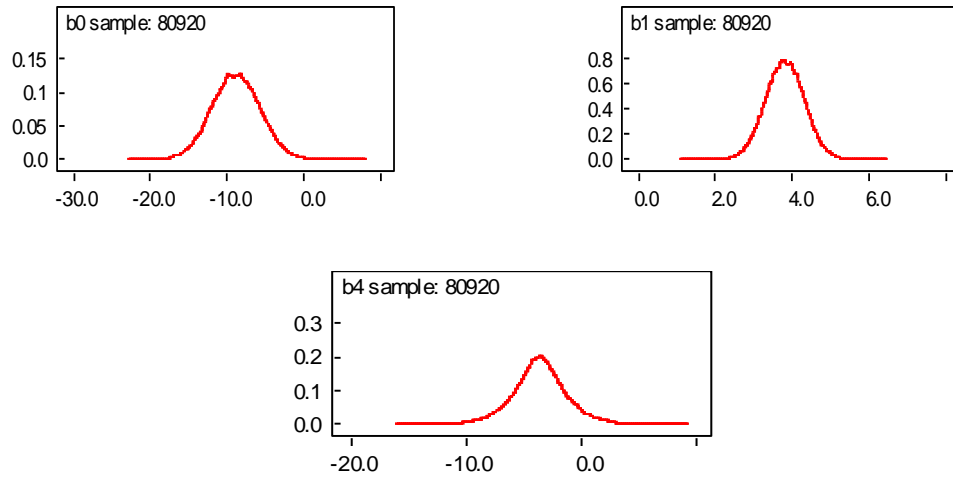


**Figure 5.5: WinBUGS sample densities for parameters  $b_0$ ,  $b_1$  and  $b_4$  in Soviet Model**

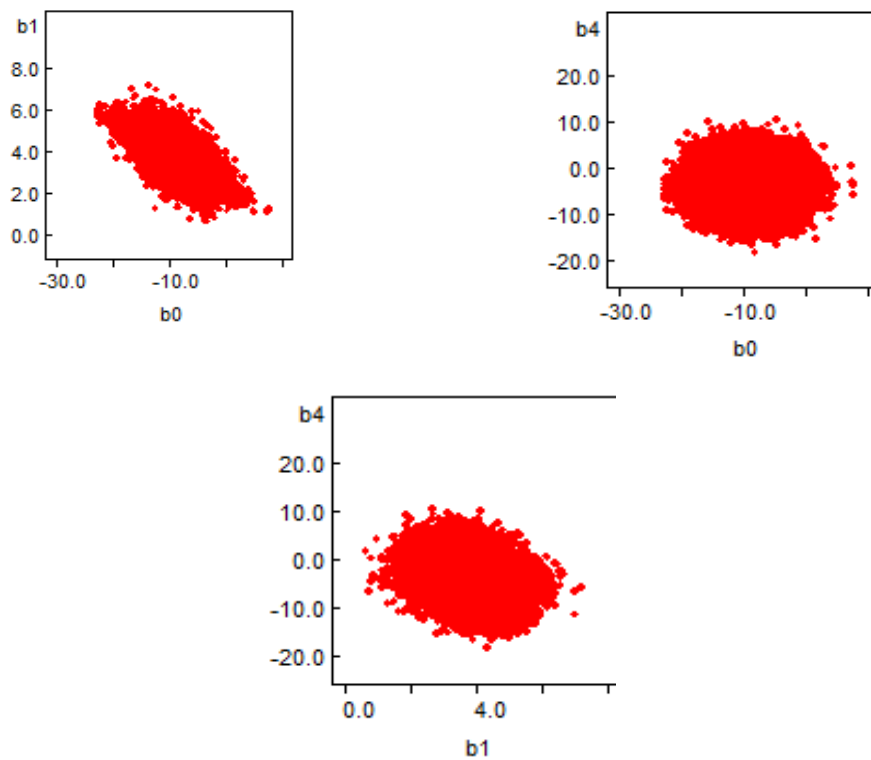


**Figure 5.6: WinBUGS correlation tool result between parameters  $b_0$ ,  $b_1$  and  $b_4$  in Soviet Model**

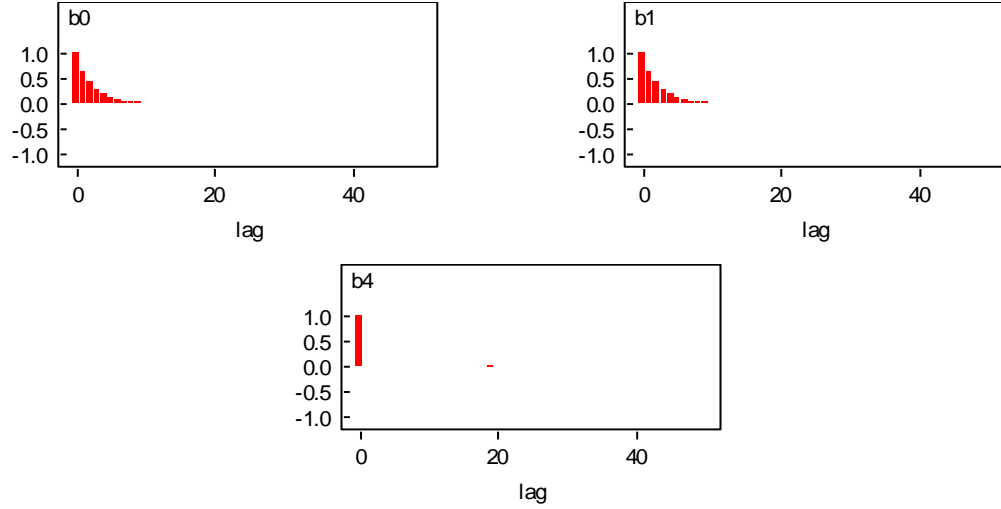


**Figure 5.7: WinBUGS autocorrelation tool results for parameters b0,b1 and b4 in Soviet Model**

Probability densities of posterior parameters are also provided in Figure 5.5.

Figure 5.6 shows correlations between parameters  $\beta_0, \beta_1$ , and  $\beta_4$ . There are not any apparent relationships between the parameter of which posterior distributions were estimated.

In Figure 5.7, autocorrelation tool results for  $\beta_0, \beta_1$  and  $\beta_4$  are provided. In this figure, it is seen that there is not a significant autocorrelation for any of the parameters of which posterior distributions are predicted. Therefore, performance of the sampler was considerably well. Sampling history of each parameter evaluated in this model was provided in Appendix D-I.

### 5.2.2 Larson Miller Model

Larson Miller Model [5,11] is presented in Eq.(5.7). This form of the model was used in consequent Bayesian Inference framework steps.  $\beta_3$  parameter in this model is equal to  $-C$ .  $C$  is the constant in Larson Miller parameter equation (see, Eq.(5.8)) [6]. In this study,  $C$  constant was fixed at 20 [6].

$$\log(t_r) = \left\{ \sum_{k=0}^n \beta_k (\log[\sigma_{\max}])^k \right\} / T + \beta_3 \quad n=2, k=0,1,2 \quad (5.7)$$

$$LM = T(\log t_r + C) \quad (5.8)$$

Assuming a normal distribution to represent the variability of CF expended life, the likelihood function of the CF data, and the corresponding different percentiles of this distribution were expressed as:

$$f(\log(t_{CF})) = N(\mu_i, s_i) \quad (5.9)$$

$$\mu_i = N \left( -C + \frac{1}{T} \left( \beta_0 + \beta_1 \log(\sigma_{\max}) + \beta_2 \log^2(\sigma_{\max}) \right) \right) \quad (5.10)$$

where  $\mu_i$  and  $s_i$  are the normal-mean and normal-standard deviation of the CF expended life distribution. After substituting Eq.(5.10) into Eq.(5.9), conditional distribution function of the logarithmic CF life “ $\log(t_{CF})$ ” given stress and temperature condition was obtained.

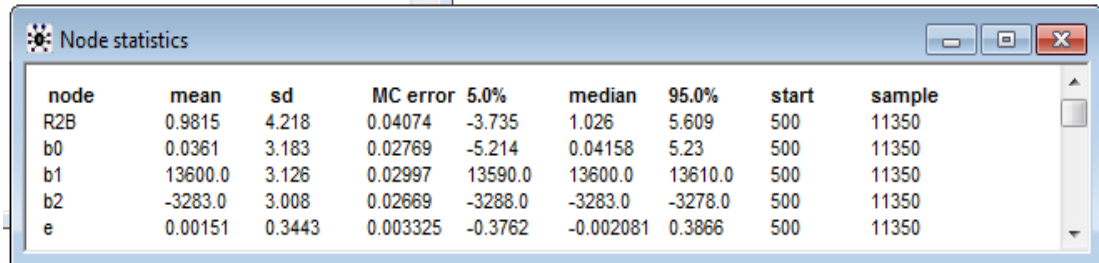
$$f(\log(t_{CF}) | \sigma_{\max_i}, T_i) = \frac{1}{s \cdot \sqrt{2\pi}} \cdot \exp \left( \frac{-1}{2s^2} \left[ \log(t_{CF}) - \left( -C + \frac{1}{T} \left( \beta_0 + \beta_1 \log(\sigma_{\max}) + \beta_2 \log^2(\sigma_{\max}) \right) \right) \right]^2 \right) \quad (5.11)$$

Therefore, likelihood function was given by Eq.(5.5). In addition to Eq.(5.5), posterior distribution of parameters  $\beta_0, \beta_1, \beta_2$  and  $s$  which is standard deviation of the likelihood function were derived by using Bayes' estimation according to:

$$f(\beta_0, \beta_1, \beta_2, s | \log(t_{CF})) = \frac{f_0(\beta_0, \beta_1, \beta_2, s) \cdot L(\beta_0, \beta_1, \beta_2, s | \log(t_{CF}))}{\int_s \int_{\beta_2} \int_{\beta_1} \int_{\beta_0} f_0(\beta_0, \beta_1, \beta_2, s) \cdot L(\beta_0, \beta_1, \beta_2, s | \log(t_{CF})) d\beta_0 d\beta_1 d\beta_2 ds} \quad (5.12)$$

where  $f_0(\beta_0, \beta_1, \beta_2, s)$  is the subjective prior distribution. Prior distributions are updated using the experimental data from experiments.

Codes written in WinBUGS for Bayesian Inference of parameters from Larson Miller Model [5,6,11] were provided in Appendix C-II. In Figure 5.8, WinBUGS node statistics for Larson Miller Model [5,6,11] are presented.



node	mean	sd	MC error	5.0%	median	95.0%	start	sample
R2B	0.9815	4.218	0.04074	-3.735	1.026	5.609	500	11350
b0	0.0361	3.183	0.02769	-5.214	0.04158	5.23	500	11350
b1	13600.0	3.126	0.02997	13590.0	13600.0	13610.0	500	11350
b2	-3283.0	3.008	0.02669	-3288.0	-3283.0	-3278.0	500	11350
e	0.00151	0.3443	0.003325	-0.3762	-0.002081	0.3866	500	11350

**Figure 5.8: WinBUGS node statistics for Larson-Miller Model**

Posterior distributions of the Bayesian Inference in Larson Miller Model [5,6,11] are:

$$\begin{aligned}\beta_0 &\sim N(0.0361, 3.183) \\ \beta_1 &\sim N(13600, 3.126) \\ \beta_2 &\sim N(-3283, 3.008)\end{aligned}$$

Probability densities of posterior parameters are also provided in Figure 5.9.

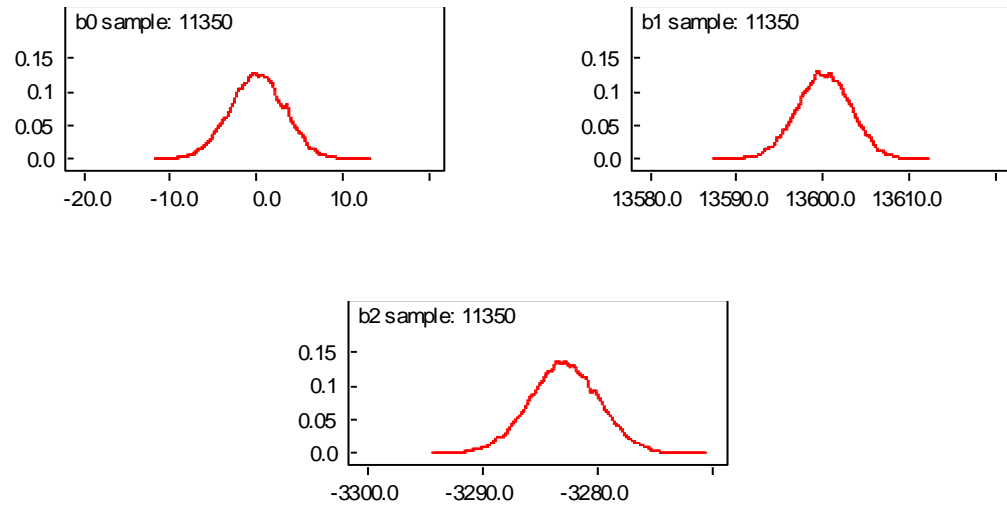


**Figure 5.9: WinBUGS sample densities for b0,b1 and b2 in Larson-Miller Model**

Figure 5.10 shows correlations between parameters  $\beta_0, \beta_1$ , and  $\beta_2$ . There are not any relationships between the parameter of which posterior distributions were estimated. In Figure 5.11, autocorrelation tool results for  $\beta_0, \beta_1$  and  $\beta_2$  are provided. Those results are helpful to understand the performance of the sampler.

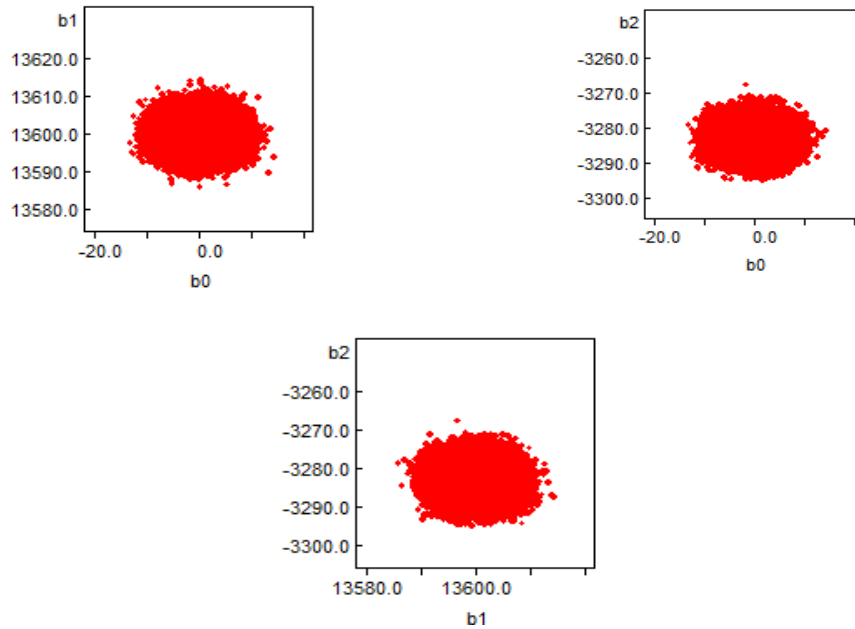


**Figure 5.10: WinBUGS correlation tool results between parameters b0,b1 and b2 in Larson-Miller Model**

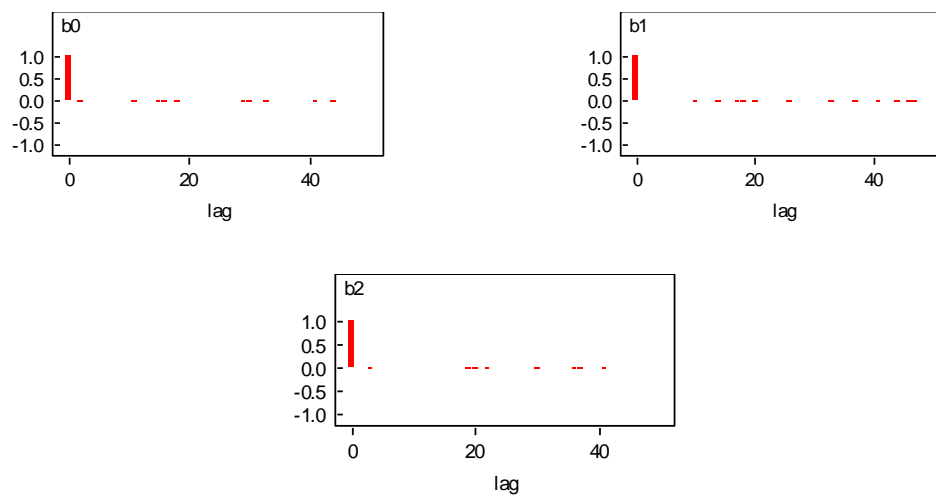


**Figure 5.11: WinBUGS autocorrelation results for parameters b0, b1 and b2 in Larson-Miller Model**

In Figure 5.11, it is seen that there is not an autocorrelation for any of the parameters of which posterior distributions are predicted. Therefore, performance of the sampler was considerably well. Sampling history of each parameter evaluated in this model was provided in Appendix D-II. Those history reports also present a good sampling performance.

### 5.2.3 Orr-Sherby Dorn Model

Orr-Sherby Dorn Model [7,11] is presented in Eq.(5.14). This form of the model was used in consequent Bayesian inference framework steps.  $\beta_3$  parameter in this model is equal to  $\frac{Q_c^*}{R}$  [7].  $Q_c^*$  is the apparent activation energy calculated for each of the CF tests in this study. The average of the  $Q_c^*$  for three consecutive strain controlled CF tests was found to be 263,917 J/mol. After dividing this value by gas constant R (8.314 J/mol<sup>°K</sup>),  $\beta_3$  parameter was defined as 31,744, and kept fixed at this point.

$$\log(t_{CF}) = \left\{ \sum_{k=0}^n \beta_k (\log[\sigma_{max}]^k) \right\} + \beta_3/T \quad n = 2, k = 0,1,2 \quad (5.13)$$

Assuming a normal distribution to represent the variability of CF expended life, the likelihood function of the CF data, and the corresponding different percentiles of this distribution was expressed as:

$$f(\log(t_{CF})) = N(\mu_i, s_i) \quad (5.14)$$

$$\mu_i = N\left(\beta_0 + \beta_1 \log(\sigma_{max}) + \beta_2 \log^2(\sigma_{max}) + \frac{\beta_3}{T}\right) \quad (5.15)$$

where  $\mu_i$  and  $s_i$  are the normal-mean and normal-standard deviation of the CF life distribution. After substituting Eq.(5.15) into Eq.(5.14), conditional distribution

function of the logarithmic CF expended life “ $\log(t_{CF})$ ” given stress and temperature condition was obtained.

$$f(\log(t_{CF})|\sigma_{\max_i}, T_i) = \frac{1}{s \cdot \sqrt{2\pi}} \cdot \exp\left(\frac{-1}{2s^2} \left[ \log(t_{CF}) - \left( \beta_0 + \beta_1 \log(\sigma_{\max}) + \beta_2 \log^2(\sigma_{\max}) + \frac{\beta_3}{T} \right) \right]^2\right) \quad (5.16)$$

Therefore, likelihood function was given by Eq.(5.5). Posterior distribution of parameters  $\beta_0$ ,  $\beta_1$ ,  $\beta_2$  and  $s$  which is standard deviation of the likelihood function were derived by using Bayes’ estimation according to:

$$f(\beta_0, \beta_1, \beta_2, s | \log(t_{CF})) = \frac{f_0(\beta_0, \beta_1, \beta_2, s) \cdot L(\beta_0, \beta_1, \beta_2, s | \log(t_{CF}))}{\int_s \int_{\beta_2} \int_{\beta_1} \int_{\beta_0} f_0(\beta_0, \beta_1, \beta_2, s) \cdot L(\beta_0, \beta_1, \beta_2, s | \log(t_{CF})) d\beta_0 d\beta_1 d\beta_2 ds} \quad (5.17)$$

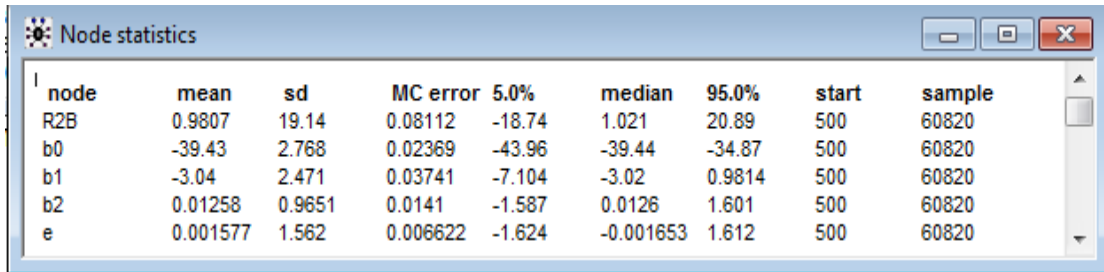
where  $f_0(\beta_0, \beta_1, \beta_2, s)$  is the subjective prior distribution. Prior distributions are updated using the experimental data from experiments. Codes written in WinBUGS for Bayesian inference of parameters from Orr-Sherby Dorn Model [7,11] were provided in Appendix C-III. In Figure 5.12, WinBUGS node statistics for Orr-Sherby Dorn Model [7,11] are presented.

Posterior distributions of the Bayesian Inference in Orr-Sherby Dorn [7,11] Model are:

$$\begin{aligned} \beta_0 &\sim N(-39.43, 2.768) \\ \beta_1 &\sim N(-3.04, 2.471) \\ \beta_2 &\sim N(0.01258, 0.9651) \end{aligned}$$

Probability densities of posterior parameters are also provided in Figure 5.13.

In Figure 5.14 shows correlations between parameters  $\beta_0, \beta_1$ , and  $\beta_2$ . There are not any apparent relationships between the parameters b0-b1 and b0-b2 of which posterior distributions were estimated. However, b1 and b2 was observed slightly to be negative correlated.



node	mean	sd	MC error	5.0%	median	95.0%	start	sample
R2B	0.9807	19.14	0.08112	-18.74	1.021	20.89	500	60820
b0	-39.43	2.768	0.02369	-43.96	-39.44	-34.87	500	60820
b1	-3.04	2.471	0.03741	-7.104	-3.02	0.9814	500	60820
b2	0.01258	0.9651	0.0141	-1.587	0.0126	1.601	500	60820
e	0.001577	1.562	0.006622	-1.624	-0.001653	1.612	500	60820

**Figure 5.12: WinBUGS node statistics for Orr-Sherby Dorn Model**

In Figure 5.15, autocorrelation tool results for  $\beta_0, \beta_1$  and  $\beta_2$  are provided. Those results are helpful to understand the performance of the sampler. In Figure 5.15, it is seen that there is a little autocorrelation in the parameters of which posterior distributions are predicted. However, this followed a decreasing trend in consequent chains. Running longer chain and thinning have been helpful. Therefore, performance of the sampler was well.

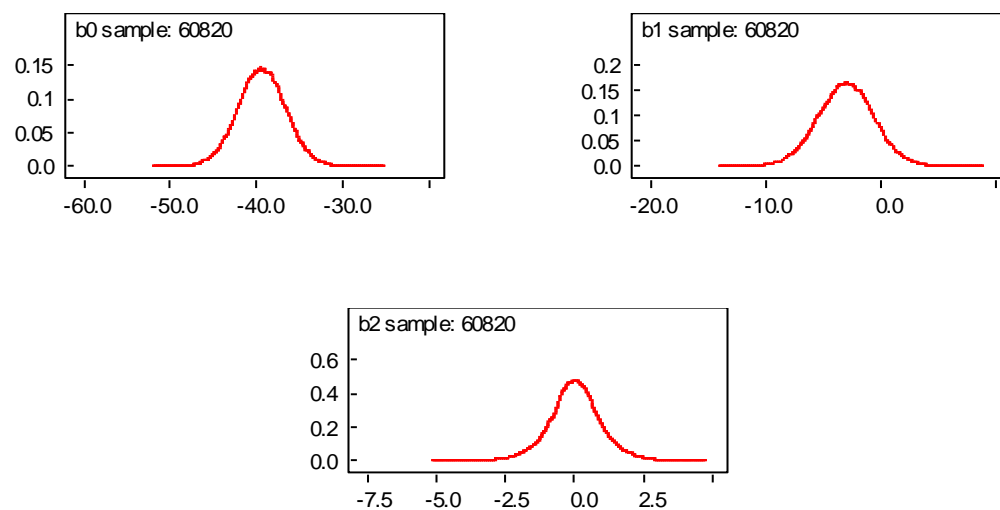


**Figure 5.13: WinBUGS sample densities for  $b_0, b_1$  and  $b_2$  in Orr-Sherby Dorn Model**

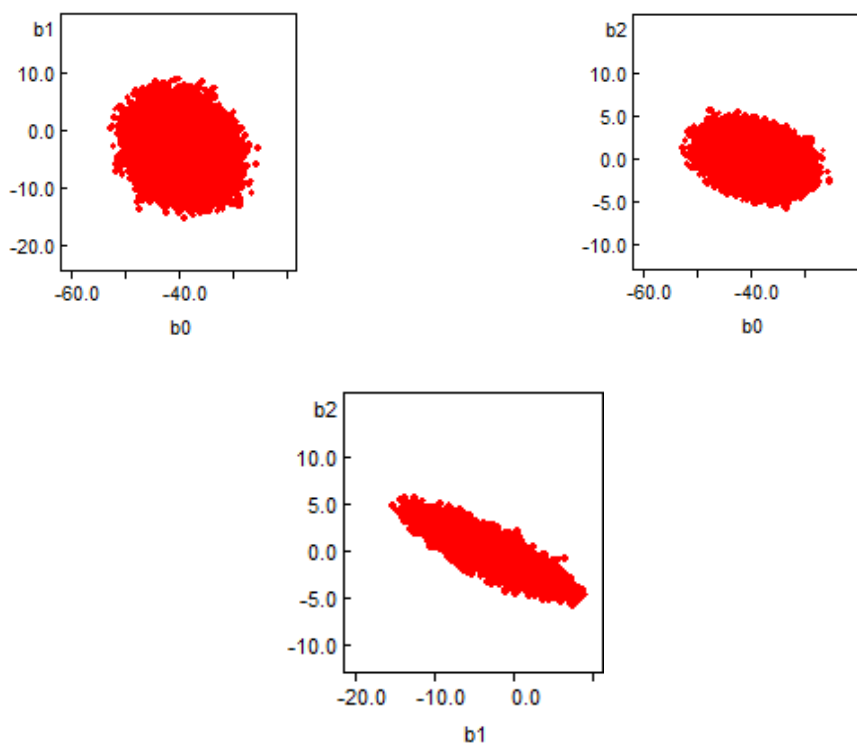


**Figure 5.14: WinBUGS correlation tool results between parameters  $b_0, b_1$  and  $b_2$  in Orr-Sherby Dorn Model**

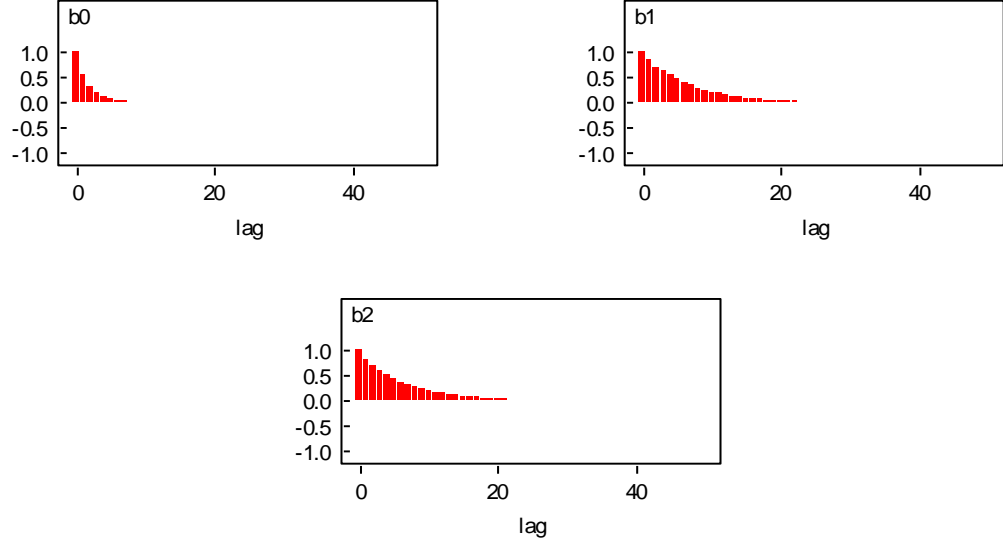


**Figure 5.15: WinBUGS autocorrelation results for parameters b0,b1 and b2 in Orr-Sherby Dorn Model**

Sampling history of each parameter evaluated in this model was provided in Appendix D-III. Those history reports also present a good sampling performance.

#### 5.2.4 Manson-Haferd Model

Manson-Haferd Model [8,11] is presented in Eq.(5.18). This form of the model was used in consequent Bayesian inference framework steps.  $T_0$  parameter in this model was kept fixed at 666.5. Additionally,  $\beta_3$  was kept fixed at -29.9. Since the limited data were available in this study, fixing the value of the least contributing parameters helped further investigation of this model. Therefore,  $T_0$  and  $\beta_3$  were treated as the model constants with respect to the published data for steels in the literature.

$$\log(t_r) = \left\{ \sum_{k=0}^n \beta_k (\log[\sigma_0]^k) \right\} (T - T_0) + \beta_3 \quad n=2, k=0,1,2 \quad (5.18)$$

Assuming a normal distribution to represent the variability of CF expended life, the likelihood function of the CF data, and the corresponding different percentiles of this distribution was expressed as:

$$f(\log(t_{CF})) = N(\mu_i, s_i) \quad (5.19)$$

$$\mu_i = N\left(\left(\beta_0 + \beta_1 \log(\sigma_{max}) + \beta_2 \log^2(\sigma_{max})\right)(T - T_0) + \beta_3\right) \quad (5.20)$$

where  $\mu_i$  and  $s_i$  are the normal-mean and normal-standard deviation of the CF expended life distribution. After substituting Eq.(5.20) into Eq.(5.19), conditional distribution function of the logarithmic CF life “ $\log(t_{CF})$ ” given stress and temperature condition was obtained.

$$\begin{aligned} & f(\log(t_{CF}) | \sigma_{max_i}, T_i) \\ &= \frac{1}{s \cdot \sqrt{2\pi}} \cdot \exp\left(\frac{-1}{2s^2} \left[ \log(t_{CF}) - \left( \left( \beta_0 + \beta_1 \log(\sigma_{max}) + \beta_2 \log^2(\sigma_{max}) \right) (T - T_0) + \beta_3 \right) \right]^2 \right) \end{aligned} \quad (5.21)$$

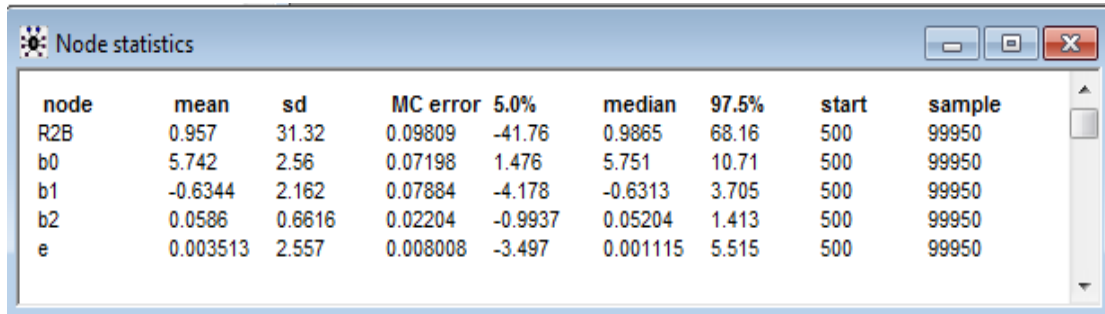
Therefore, likelihood function was given by Eq.(5.5). Posterior distribution of parameters  $\beta_0$ ,  $\beta_1$ ,  $\beta_2$  and  $s$  which is standard deviation of the likelihood function were derived by using Bayes’ estimation according to:

$$f(\beta_0, \beta_1, \beta_2, s | \log(t_{CF})) = \frac{f_0(\beta_0, \beta_1, \beta_2, s) \cdot L(\beta_0, \beta_1, \beta_2, s | \log(t_{CF}))}{\int_s \int_{\beta_2} \int_{\beta_1} \int_{\beta_0} f_0(\beta_0, \beta_1, \beta_2, s) \cdot L(\beta_0, \beta_1, \beta_2, s | \log(t_{CF})) d\beta_0 d\beta_1 d\beta_2 ds} \quad (5.22)$$

where  $f_0(\beta_0, \beta_1, \beta_2, s)$  is the subjective prior distribution. Prior distributions are updated using the experimental data from experiments. Codes written in WinBUGS for Bayesian Inference of parameters from Manson Haferd Model [8,11] were provided in Appendix C-IV. In Figure 5.16, WinBUGS node statistics for Manson Haferd Model [8,11] are presented.

Posterior distributions of the Bayesian Inference in Manson Haferd Model [8,11] are:

$$\begin{aligned}\beta_0 &\sim N(5.742, 2.56) \\ \beta_1 &\sim N(-0.6344, 2.162) \\ \beta_2 &\sim N(0.0586, 0.6616)\end{aligned}$$



node	mean	sd	MC error	5.0%	median	97.5%	start	sample
R2B	0.957	31.32	0.09809	-41.76	0.9865	68.16	500	99950
b0	5.742	2.56	0.07198	1.476	5.751	10.71	500	99950
b1	-0.6344	2.162	0.07884	-4.178	-0.6313	3.705	500	99950
b2	0.0586	0.6616	0.02204	-0.9937	0.05204	1.413	500	99950
e	0.003513	2.557	0.008008	-3.497	0.001115	5.515	500	99950

**Figure 5.16: WinBUGS node statistics for Manson-Haferd Model**

Probability densities of posterior parameters are also provided in Figure 5.17. Figure 5.18 shows correlations between parameters  $\beta_0, \beta_1$ , and  $\beta_2$ . There are not apparent relationships between the parameters b0-b1 and b0-b2 of which posterior distributions were estimated. However, b1 and b2 was observed slightly to be negative correlated.

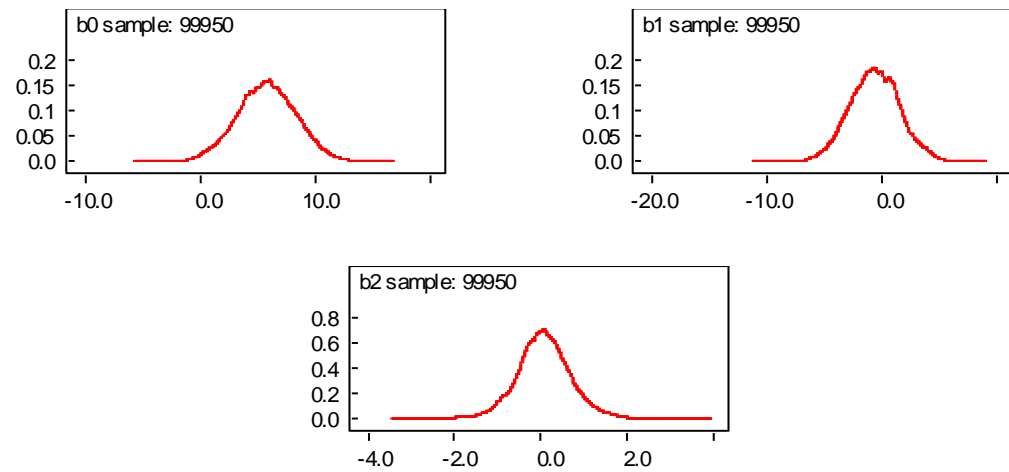


**Figure 5.17: WinBUGS sample densities for  $b_0, b_1$  and  $b_2$  in Manson-Haferd Model**

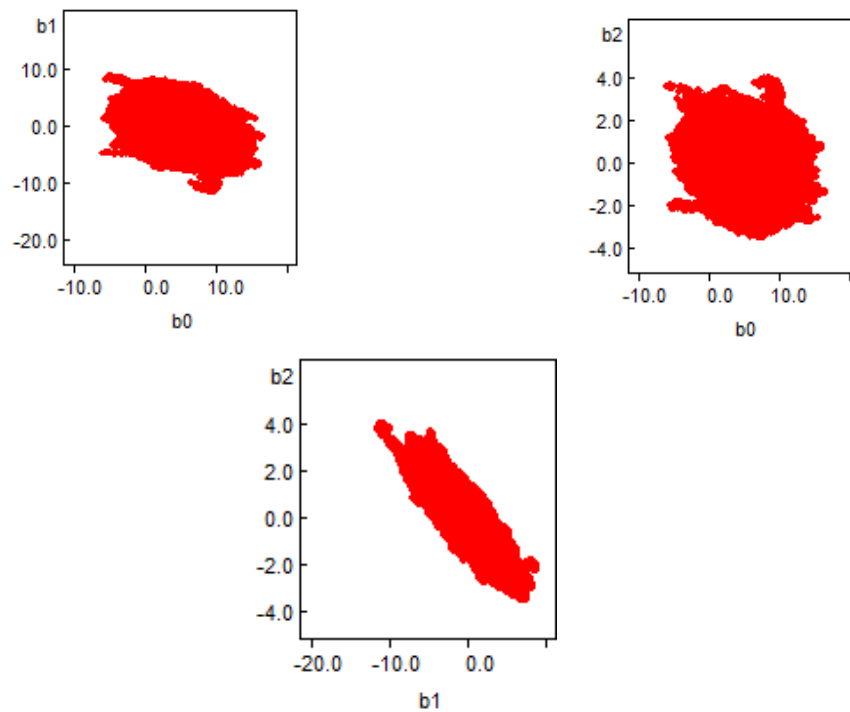


**Figure 5.18: WinBUGS correlation tool results between parameters  $b_0, b_1$  and  $b_2$  in Manson-Haferd Model**

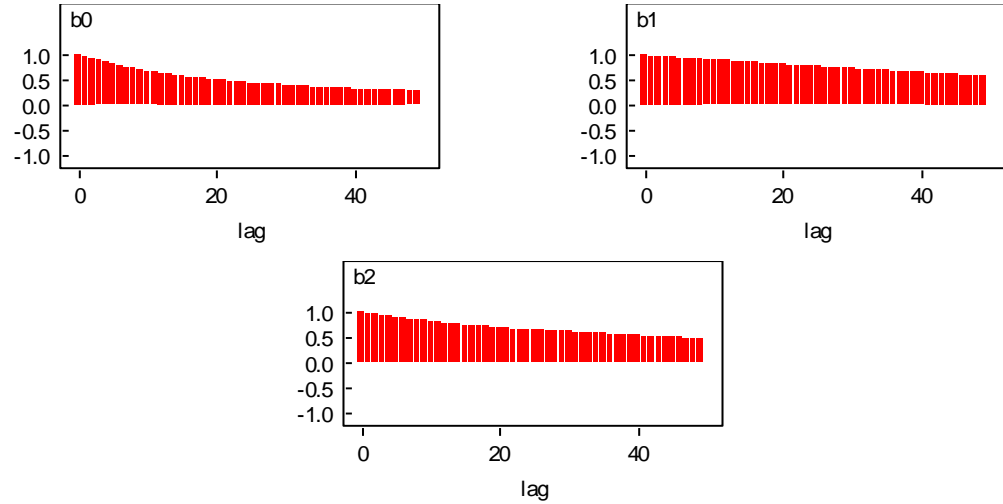


**Figure 5.19: WinBUGS autocorrelation results between parameters b0, b1 and b2 in Manson-Haferd Model**

In Figure 5.19, autocorrelation tool results for  $\beta_0$ ,  $\beta_1$  and  $\beta_2$  are provided. Those results are helpful to understand the performance of the sampler. In this figure, it is seen that there is a little autocorrelation in the parameters of which posterior distributions are predicted. However, this followed a decreasing trend in consequent chains. Running longer chain and thinning have been helpful. Therefore, performance of the sampler was acceptable. Sampling history of each parameter evaluated in this model was provided in Appendix D-IV. Those history reports also present a good sampling performance. Therefore, it was understood that the distributions which were reached in the end of the sampling were acceptable.

### 5.2.5 Wilshire Model

Wilshire Model [9-11] is presented in Eq.(5.23). This form of the model was used in consequent Bayesian Inference framework steps.  $Q_c^*$  is the apparent activation energy calculated for each of the creep-fatigue tests in this study. The average of the  $Q_c^*$  for three consecutive strain controlled creep-fatigue tests was found to be 263,917

J/mol. After dividing this value by gas constant  $R$  ( $8.314 \text{ J/mol}^\circ\text{K}$ ),  $\frac{Q_c^*}{R \cdot T}$  parameter was defined as  $\frac{31.744}{T}$ , and kept fixed at this point.

$$\log(t_{CF}) = \left( \frac{\ln\left(\frac{\sigma}{\sigma_{UTS}}\right)}{-k} \right)^{1/u} \cdot \frac{1}{\exp\left(\frac{-Q_c^*}{R \cdot T}\right)} \quad (5.23)$$

Table 5.1 presents the data used in evaluation of this model. Chen et al. [13] previously proposed stress strain curves for stainless steel at elevated temperatures. From this resource, it was understood that the ultimate tensile strength (UTS) of EN 1.4462 and EN 1.4301 at  $400^\circ\text{C}$  temperature was approximately 0.7 of the ultimate tensile strength which was defined at room temperature. The normalized stress values were defined according to this ratio.

**Table 5.1: Data used for prediction of Wilshire Model for the test material**

$\ln \left[ -\ln \left( \frac{\tau}{\tau_{TS}} \right) \right]$	$\ln[t_{CF}]$	$\frac{Q_c^*}{RT}$
-0.456	0.83	47.157
-0.495	0.59	47.157
-0.284	0.24	47.157

Assuming a normal distribution to represent the variability of CF expended life time the likelihood function of the creep-fatigue lifetime, and the corresponding different percentiles of this distribution is expressed as:

$$f(\log(t_{CF})) = N(\mu_i, s_i) \quad (5.24)$$

$$\mu_i = N \left( \left( \ln \left( \frac{\sigma}{\sigma_{UTS}} \right) / -k \right)^{1/u} \cdot (1/\exp(-Q_c^*/R \cdot T)) \right) \quad (5.25)$$

where  $\mu_i$  and  $s_i$  are the normal-mean and normal-standard deviation of the creep-fatigue life distribution. After substituting Eq.(5.25) into Eq.(5.24), conditional

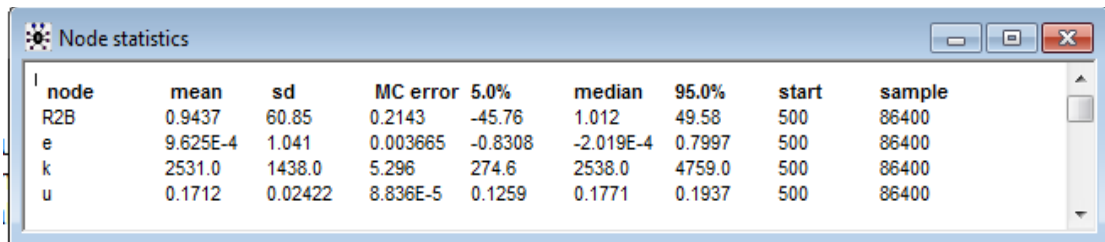
distribution function of the creep-fatigue life distribution given normalized stress condition and test temperature becomes:

$$f\left(\log(t_{CF}) \mid \left(\frac{\sigma}{\sigma_{UTS}}\right)_i, T_i\right) = \frac{1}{t_{CF_i} \sqrt{2\pi}} \cdot \exp\left(\frac{-1}{2s^2} \left[ \log(t_{CF_i}) - \left(\ln\left(\frac{\sigma}{\sigma_{UTS}}\right)_i / -k\right)^{1/u} \cdot (1/\exp(-Q_c^*/R \cdot T_i)) \right]^2\right) \quad (5.26)$$

Therefore, likelihood function is given by Eq.(5.5). In addition to Eq.(5.5), posterior distribution of parameters  $k, u$  can be derived by using Bayes' estimation according to:

$$f(k, u, s | \log(t_{CF_i})) = \frac{f_0(k, u, s) \cdot L(k, u, s | \log(t_{CF_i}))}{\int_s \int_u \int_k f_0(k, u, s) \cdot L(k, u, s | \log(t_{CF_i})) dk du ds} \quad (5.27)$$

where  $f_0(k, u, s)$  is the subjective prior distribution. Prior distributions are updated using the experimental data from experiments. Codes written in WinBUGS for Bayesian Inference of parameters from Wilshire Model [9-11] were provided in Appendix C-V. In Figure 5.20, WinBUGS node statistics for Wilshire Model [9-11] are presented.



node	mean	sd	MC error	5.0%	median	95.0%	start	sample
R2B	0.9437	60.85	0.2143	-45.76	1.012	49.58	500	86400
e	9.625E-4	1.041	0.003665	-0.8308	-2.019E-4	0.7997	500	86400
k	2531.0	1438.0	5.296	274.6	2538.0	4759.0	500	86400
u	0.1712	0.02422	8.836E-5	0.1259	0.1771	0.1937	500	86400

**Figure 5.20: WinBUGS node statistics for Wilshire Model**

Posterior distributions of the Bayesian Inference in Wilshire Model [9-11] are:

$$k \sim \text{UNIF}(0, 5000)$$

$$u \sim N(0.1712, 0.02422)$$

Probability densities of posterior parameters are also provided in Figure 5.21. Figure 5.22 shows correlations between parameters  $k$  and  $u$ . There are not apparent relationships between the parameters  $k$  and  $u$  of which posterior distributions were estimated.

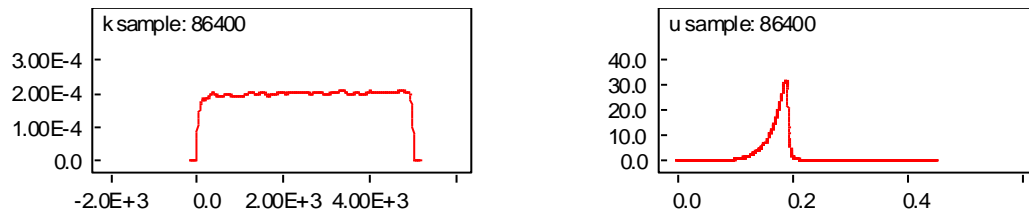


**Figure 5.21: WinBUGS sample densities for  $k$  and  $u$  in Wilshire Model**

In Figure 5.23, autocorrelation tool results for  $k$  and  $u$  are provided. Those results are helpful to understand the performance of the sampler. In this figure, it is seen that there is not any apparent autocorrelation in the parameters of which posterior distributions are predicted. Therefore, performance of the sampler was good. Sampling history of each parameter evaluated in this model was provided in Appendix D-V. Those history reports also present a good sampling performance.

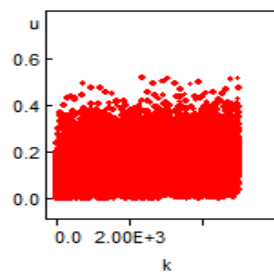


**Figure 5.22: WinBUGS correlation tool result between parameters  $k$  and  $u$  in Wilshire Model**

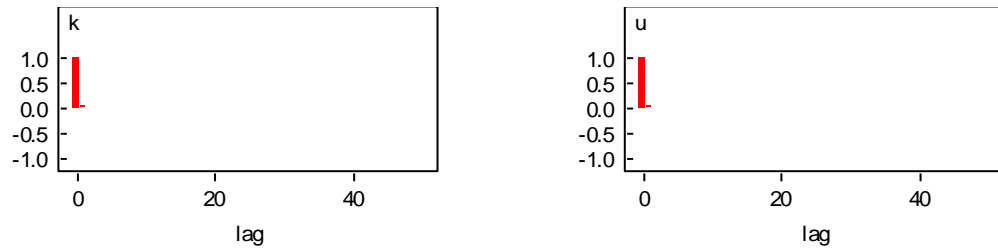


**Figure 5.23: WinBUGS autocorrelation results for parameters k and u in Wilshire Model.**

### 5.3 References

- [1] Modarres, M., Kaminskiy, M, Krivtsov, V., *Reliability Engineering and Risk Analysis, A Practical Guide*, CRC Press, 2<sup>nd</sup> Edition, 2010.
- [2] Ntzoufras, I., *Bayesian Modelling Using WinBUGS*, In. Giudici, P., Givens, G.H. and Mallick, B.K. (Eds.), John Wiley & Sons, Inc., Canada, 2009.
- [3] Wendell, F., *A Handbook on Accelerated Testing*, In Fulfillment of the Scholarly Paper Requirement for the Degree of Master of Science in Reliability Engineering, Modarres, M. (Adv.), Department of Mechanical Engineering, University of Maryland, College Park.
- [4] Trunin, I.I., Golobova, N.G., Loginov, E.A., "New method of extrapolation of creep test and long time strength results," *In: Proceedings of the Fourth International Symposium on Heat-Resistant Metallic Materials*, Mala Fatra, CSSR, p:168,1971.
- [5] Larson, F.R., Miller, J., "A time-temperature relationship for rupture and creep stress," *Trans. ASME*, Vol.74, p:765, 1952.
- [6] Eno, D.R., and Young, G.A., "A unified view of engineering creep parameters," *Proceedings of PVP2008, ASME Pressure Vessels and Piping Division Conference*, July 21-31, Chicago, Illinois, 2008.
- [7] Orr, R.L., Sherby, O.D., Dorn, J.E., "Correlation of rupture data for metals at elevated temperatures," *Trans. ASM*, Vol:46, p:113, 1954.
- [8] Manson, S.S., Haferd, A.M., "A linear time-temperature relation for extrapolation of creep and stress rupture data," *NASA TN*, 2890, 1953.
- [9] Wilshire, B., Scharning, P.J., Hurst, R., "A new approach to creep data assessment," *Materials Science and Engineering A*, Vol:3, Issue:6, pp:510-511, 2009.

- [10] Holmstrom, S., "Engineering Tools for Robust Creep Modeling, " PhD Dissertation, *VTT Publications 728*, The Faculty of Engineering and Architecture, The Aalto University School of Science and Technology, Espoo, Finland, 2010.
- [11] Holdsworth, S.R. and Davies, R.B., "A recent advance in the assessment of creep rupture data," *Nuclear Engineering and Design*, Vol.190, pp:287-296, 1999.
- [12] Takashi, Y., Shibamoto, H., Inoue, K., "Long-term creep rupture behavior of smoothed and notched bar specimens of low-carbon nitrogen-controlled 316 stainless steel (316 FR) and their evaluation," *Nuclear Engineering and Design*, Vol.238, pp:310-321, 2008.
- [13] Chen, J. and Young, B., "Stress-strain curves for stainless steel at elevated temperatures," *Engineering Structures*, Vol.28, pp: 229-239, 2006.

## Chapter 6: Assessment of Creep-Fatigue and Creep in Cyclic Relaxation

### 6.1 Introduction

The robust creep-fatigue (CF) model idea initiated by Holmstrom [6] is further evaluated in this chapter under the section separated for creep-fatigue life curves. Creep rupture models previously applied in common creep deformation problems presented good performance with CF life data for the steel alloy. The  $\Phi$  model [6] derived from Wilshire model was approved to work with minimum data in this study. Nevertheless, it was observed that Bayesian inference also could propose feasible predictions despite of the insufficient data problem as long as proper prior distributions were initially determined for the predicted model parameters. Therefore, creep rupture models evaluated on CF data presented high goodness of fit values in this study. Section 6.2 presents the details of this prediction feasibility investigation.

Section 6.3 confirms that the activation energies obtained for the three CF test with different hold times for 10, 14 and 21 min are compatible with the published values given for steel materials.

Section 6.4 is divided into four sub-sections. In Section 6.4.1, creep in cyclic relaxation response under CF conditions is evaluated. The main difference with respect to well-known monotonic creep is that the total strain is constant in tensile hold test on the stress changes with time, whereas the stress is constant in monotonic creep. It may be possible to interpret the stress dependence of the rate change throughout the hold time. It was previously shown that the creep mechanism was identical with that of steady-state in monotonic creep after a substantial hold time.

However, in this steady-state monotonic creep time dependency is neglected regarding the three consecutive regions on a regular creep deformation. Therefore, the applicability of the some highly feasible time dependent creep models (Norton Bailey [10], Nuhi's Empirical [8] and Modified Theta [12]) were investigated on the creep curves derived from the cyclic relaxation response under CF condition. In Section 6.4.2, probability of exceedance estimation at strain 0.006 [mm/mm] is provided. In the following Section 6.4.3, the simple definition of CF damage proposed by Holmstrom [6] for  $\Phi$  model was applied on the Soviet model. Finally, a remaining useful life estimation based on the deterministic framework is presented with respect to a service aged secondary superheater in service conditions.

## **6.2 CF Expended Life Curves**

The probabilistic parameters proposed in Chapter 5 were used in this section to project CF at the specified test temperature 673.25°K (400°C). The master curves are presented in the order according to the R2B results presented in Chapter 5: Soviet, Larson-Miller, Orr-Sherby Dorn, Manson Haferd and Wilshire Model. The goodness of fit for the each of those life prediction models was evaluated in the end of this section. The results obtained were confirming the R2B results proposed in Chapter 5. Therefore, the creep life models performed well adaption on the life assessment of CF life for the steel alloy used in this study.

### **6.2.1 Soviet Model**

Soviet Model [1] was evaluated in Chapter 5 in terms of the derivation of probabilistic model parameters. Model form is presented in Eq.(6.1). It was observed

that  $\beta_2$  and  $\beta_3$  had the least effect in curvature of the model. Therefore, those parameters were kept as fixed constants. Table 6.1 presents mean and coefficient of variation results of normally distributed model parameters. Figure 6.1 and Figure 6.2 show the CF life curve and 3D life graph of the model prediction at 673.15°K(400°C).

$$\log(t_{CF}) = \beta_0 + \beta_1 \cdot \log[T] + \beta_2 \cdot \log[\sigma_{max}] + \frac{\beta_3}{T} + \beta_4 \cdot \frac{\sigma_{max}}{T} \quad (6.1)$$

**Table 6.1: Soviet Model Bayesian parameters and their coefficient of variation**

Bayesian	$\beta_0$	$\beta_1$	$\beta_4$
Parameter	-8.922	3.795	-3.627
Coefficient of variation	0.349	0.134	0.655

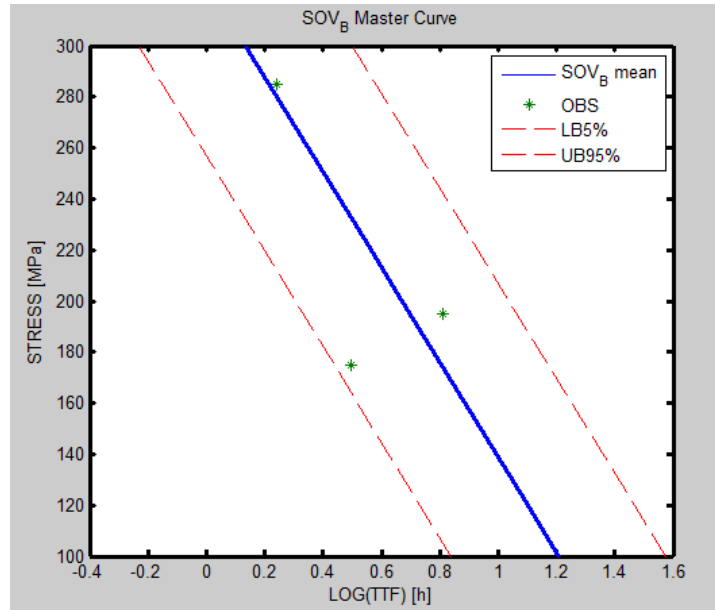


**Figure 6.1: Soviet Model creep – fatigue expended life curve for steel alloy at 673.15°K (400°C)**

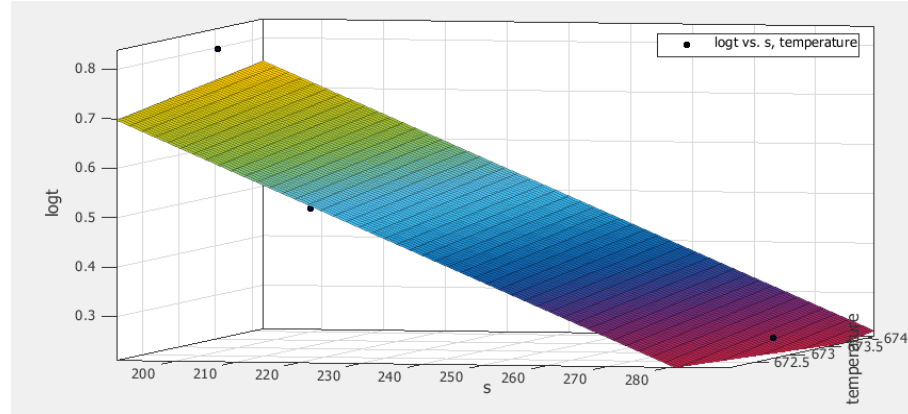


**Figure 6.2: Soviet Model creep – fatigue 3D life graph for the steel alloy at 673.15°K (400°C)**

### 6.2.2 Larson-Miller Model

Larson-Miller Model [2] was evaluated in Chapter 5 in terms of the derivation of probabilistic model parameters. Model form is presented in Eq.(6.2).  $\beta_3$  parameter in this model is equal to  $-C$ .  $C$  is the constant in Larson-Miller parameter equation (see, Eq.(6.3)) [2]. In this study  $C$  constant was fixed at 20. Table 6.2 presents mean and coefficient of variation results of normally distributed model parameters. Figure 6.3 and Figure 6.4 show the CF life curve and 3D life graph of the model prediction at 673.15°K(400°C).

$$\log(t_r) = \left\{ \sum_{k=0}^n \beta_k (\log[\sigma_{\max}])^k \right\} / T + \beta_3 \quad n=2, k=0,1,2 \quad (6.2)$$

$$LM = T(\log t_r + C) \quad (6.3)$$

**Table 6.2: Larson-Miller Model Bayesian parameters and their coefficient of variation**

Bayesian	$\beta_0$	$\beta_1$	$\beta_2$
Parameter	0.0361	13600	-3283
Coefficient of variation	88.172	2.298E-4	9.16E-4

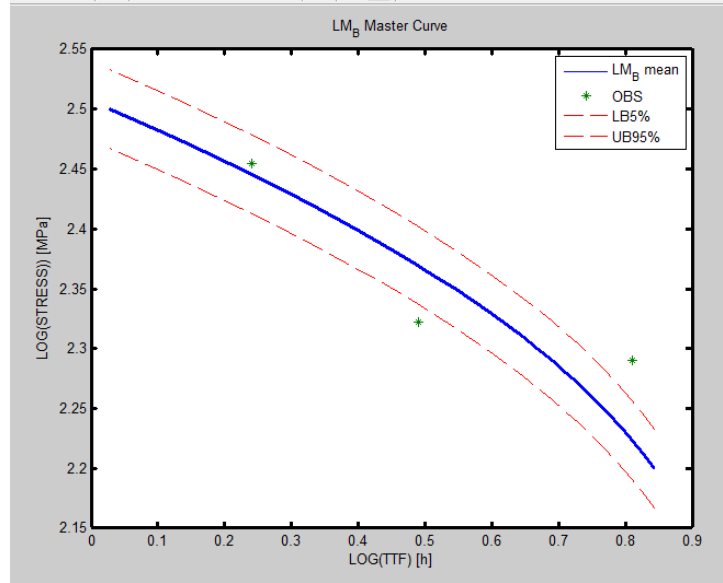


**Figure 6.3: Larson-Miller Model creep – fatigue expended life curve for the steel alloy at 673.15°K (400°C)**

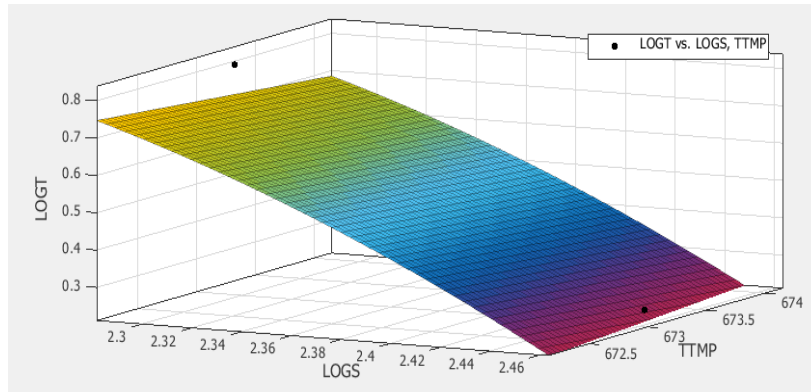


**Figure 6.4: Larson-Miller Model creep – fatigue 3D life graph for the steel alloy at 673.15°K (400°C)**

### 6.2.3 Orr-Sherby Dorn

Orr-Sherby Dorn Model [3] was evaluated in Chapter 5 in terms of the derivation of probabilistic model parameters. Model form is presented in Eq.(6.4).  $\beta_3$  parameter in this model is equal to  $\frac{Q_c^*}{R}$ .  $Q_c^*$  is the apparent activation energy calculated for each of the CF tests in this study. The average of the  $Q_c^*$  for three consecutive

strain controlled CF tests was 263,917 J/mol in this study. After dividing this value by gas constant R (8.314 J/mol<sup>°K</sup>),  $\beta_3$  parameter was defined as 31,744 and kept fixed at this point. Table 6.3 presents mean and coefficient of variation results of normally distributed model parameters. Figure 6.5 and Figure 6.6 show the CF life curve and 3D life graph of the model prediction at 673.15°K(400°C).

$$\log(t_{CF}) = \left\{ \sum_{k=0}^n \beta_k (\log[\sigma_{max}]^k) \right\} + \beta_3/T \quad n = 2, k = 0,1,2 \quad (6.4)$$

**Table 6.3: Orr-Sherby Dorn Bayesian parameters and their coefficient of variation**

Bayesian	$\beta_0$	$\beta_1$	$\beta_2$
Parameter	-39.43	-3.04	0.01258
Coefficient of variation	0.0702	0.8125	76.717

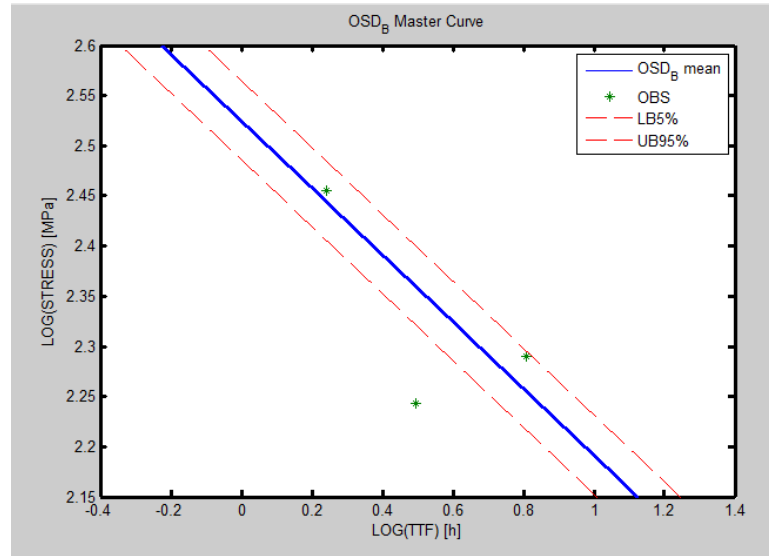


**Figure 6.5: Orr-Sherby Dorn Model creep – fatigue expended life curve for the steel alloy at 673.15°K (400°C)**

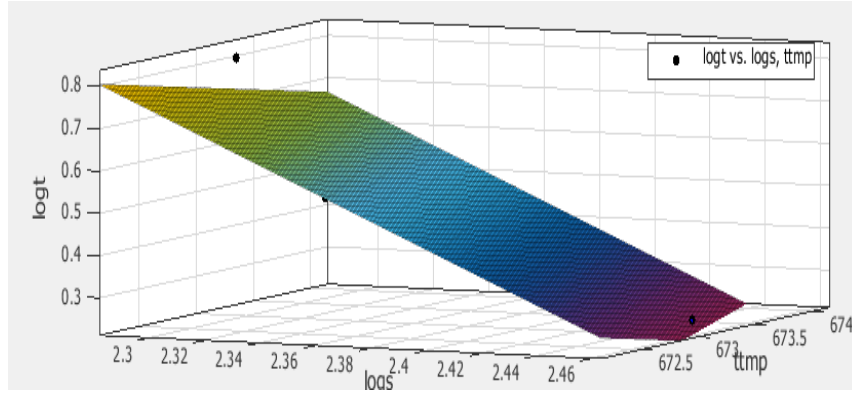


**Figure 6.6: Orr-Sherby Dorn Model creep – fatigue 3D expended life graph for the steel alloy at 673.15°K (400°C)**

#### 6.2.4 Manson Haferd Model

Manson Haferd Model [4] was evaluated in Chapter 5 in terms of the derivation of probabilistic model parameters. Model form is presented in Eq.(6.5).  $T_0$  parameter of this model was kept fixed at 666.5. Additionally,  $\beta_3$  was kept fixed at -29.9. Since the limited data were available in this study fixing the least contributing parameters helped further investigation of this model. Table 6.4 presents mean and coefficient of variation results of normally distributed model parameters. Figure 6.7 and Figure 6.8 show the CF life curve and 3D life graph of the model prediction at 673.15°K(400°C).

$$\log(t_r) = \left\{ \sum_{k=0}^n \beta_k (\log[\sigma_0]^k) \right\} (T - T_0) + \beta_3 \quad n=2, k=0,1,2 \quad (6.5)$$

**Table 6.4: Manson Haferd Model Bayesian parameters and their coefficient of variation**

Bayesian	$\beta_0$	$\beta_1$	$\beta_2$
Parameter	5.742	-0.6344	0.0585
Coefficient of variation	0.4458	3.4079	11.309

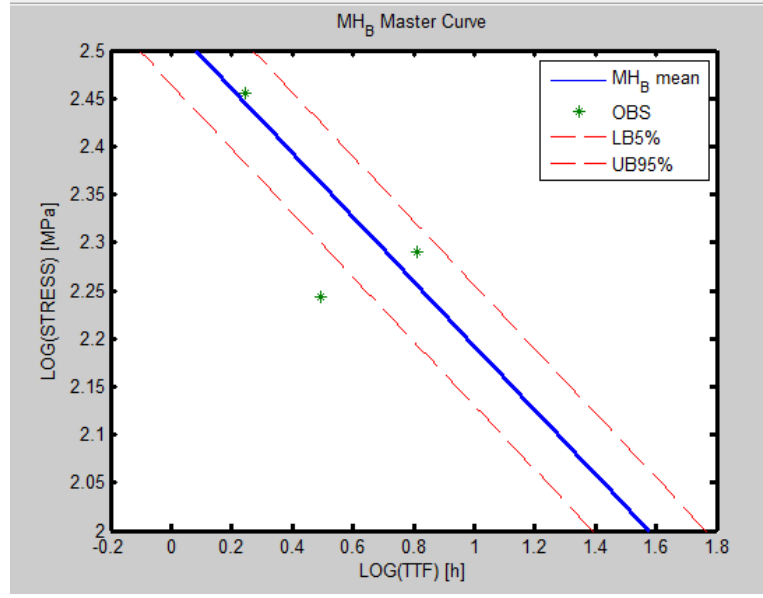


**Figure 6.7: Manson Haferd Model creep – fatigue expended life curve for the steel alloy at 673.15°K (400°C)**

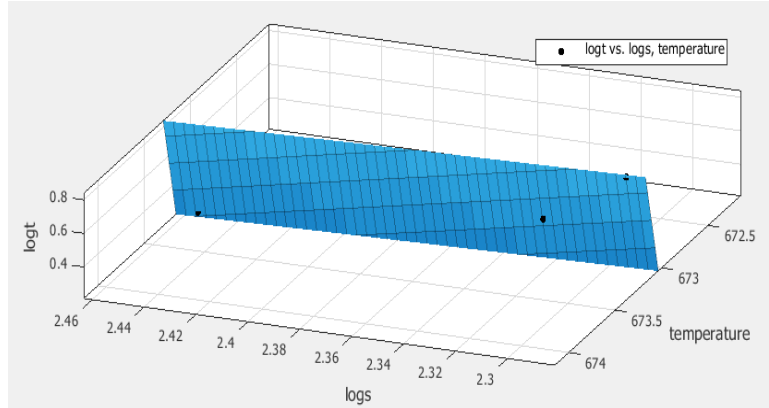


**Figure 6.8: Manson Haferd Model creep – fatigue 3D expended life graph for the steel alloy at 673.15°K (400°C)**

### 6.2.5 Wilshire Model ( $\Phi$ Model)

Wishire Model [5] was evaluated in Chapter 5 in terms of the derivation of probabilistic model parameters. Model form is presented in Eq.(5.26).  $Q_c^*$  is the apparent activation energy calculated for each of the CF tests in this study. The average of the  $Q_c^*$  for three consecutive strain controlled CF tests was found to be

263,917J/mol. After dividing this value by gas constant  $R$  (8.314 J/mol<sup>°K</sup>),  $\frac{Q_c}{R \cdot T}$  parameter was defined as  $\frac{31,744}{T}$ , and kept fixed at this point. Table 6.5 presents mean and coefficient of variation results of normally distributed model parameters. Figure 6.9 and Figure 6.10 show the CF life curve and 3D life graph of the model prediction at 673.15°K(400°C).

$$\log(t_{CF}) = \left( \frac{\ln\left(\frac{\sigma}{\sigma_{UTS}}\right)}{-k} \right)^{1/u} \cdot \frac{1}{\exp\left(\frac{-Q_c}{R \cdot T}\right)} \quad (6.6)$$

**Table 6.5: Wilshire Bayesian parameters and their coefficient of variation**

Bayesian	k	u
Parameter	2531	0.1712
Coefficient of variation	0.568	0.14147

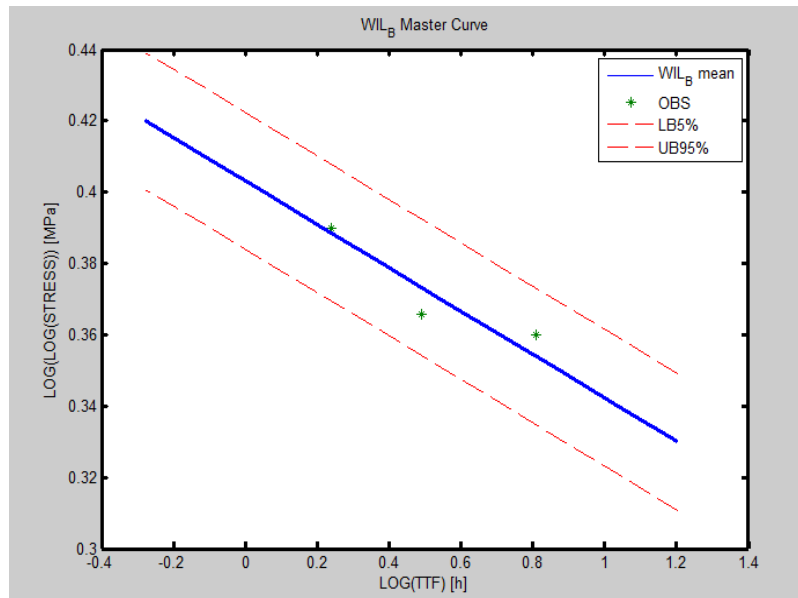


**Figure 6.9: Wilshire Model creep – fatigue expended life curve for the steel alloy at 673.15°K (400°C)**

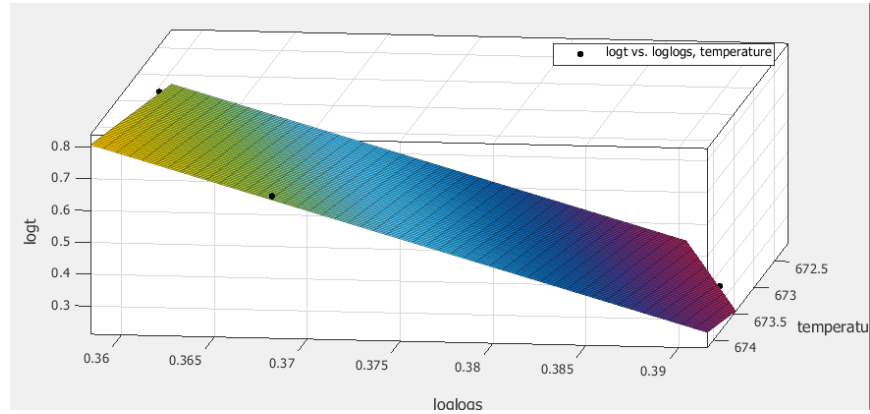


**Figure 6.10: Wilshire Model creep – fatigue 3D expended life graph for the steel alloy at 673.15°K (400°C)**

### 6.2.6 Comparison of CF Life Models

Figure 6.11 presents the comparison of CF life (creep rupture) models for the steel alloy. In Figure 6.11, the stress for the assessed material is shown as a function of temperature-compensated life ( $t_r$  for creep or  $t_{CF}$  for CF). Homström et al. [6] notes also that predicted time to creep rupture ( $t_r$ ) and time to CF failure ( $t_{CF}$ ) fall on the same material-specific curves.

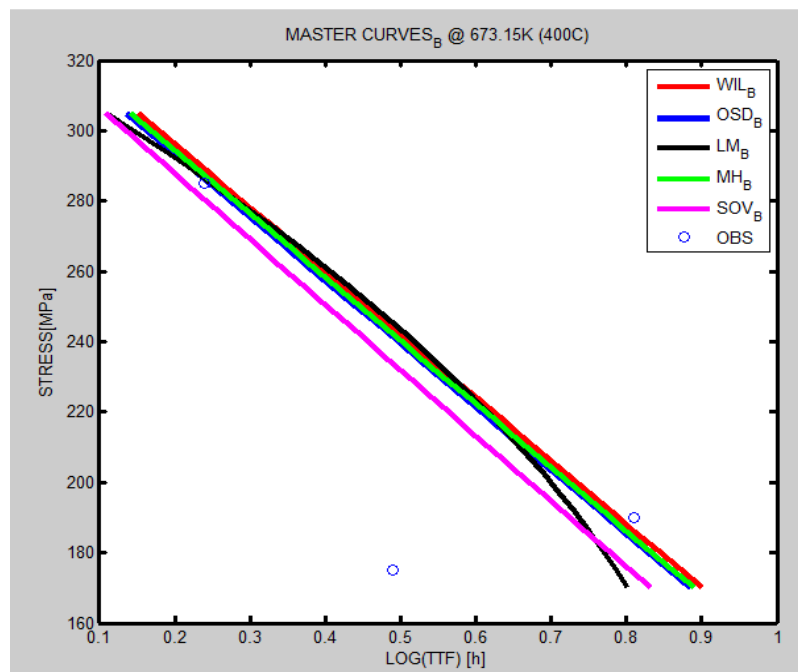


**Figure 6.11: Time to CF failure comparison for the steel alloy**

The goodness of fit can be expressed as the scatter factor Z [6-7]. The scatter factor Z formula is given in Eq.(6.7):

$$Z = 10^{2.5 \cdot \sqrt{\frac{(\sum(\log(t_{CF}) - \log(\sum t_h)))^2}{n-1}}} \quad (6.7)$$

where n is the number of data points. In this study, the agreement between predicted and observed CF life is very good as for all of the model predictions  $Z \leq 4.93$ . Assuming normal distribution for CF life, the observed  $\log(N_{CF})$  would lie in almost 99% of the observed times within predicted  $\log(N_{CF}) \pm \log(Z)$ . A comparison of the predicted vs. observed CF life in terms of cycles to failure is shown in Figure 6.12.

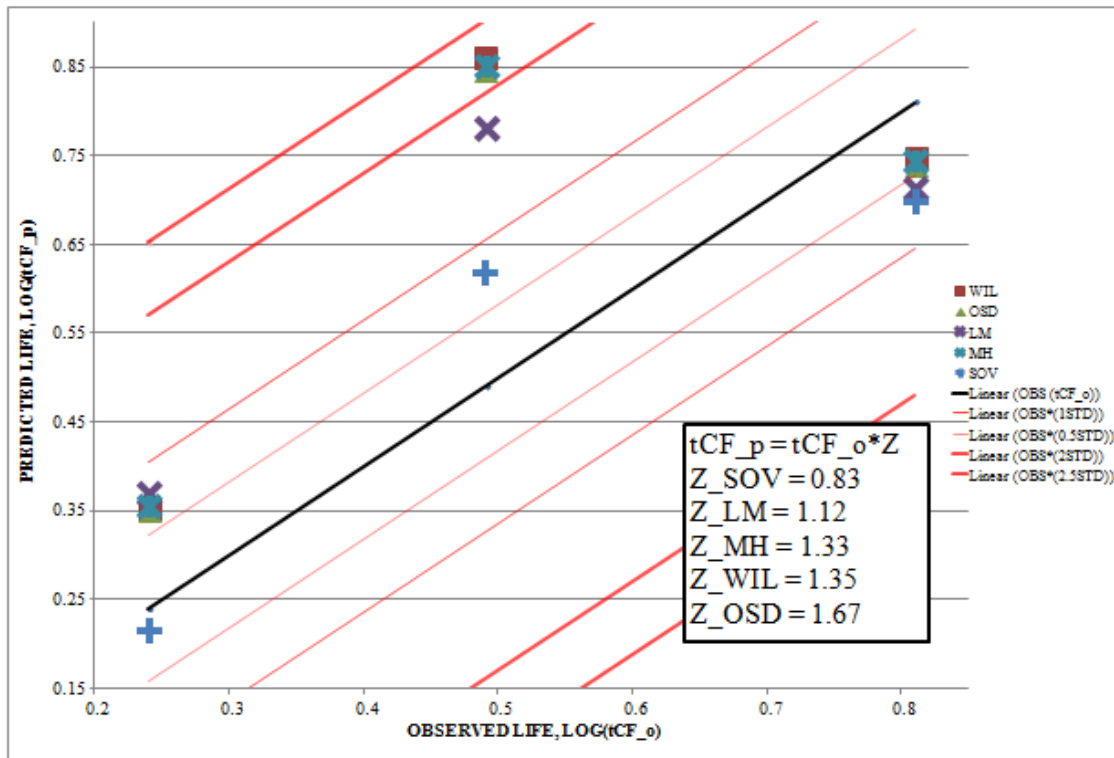


Figure 6.12: Predicted vs. observed CF expended life for the steel alloy

### 6.3 Assessment of Creep Activation Energy of Test Material

Larson-Miller parameter [2] helps to estimate the creep activation energy of materials. It can be derived from Dorn relation [3].

$$\dot{\epsilon}_s = A \cdot \sigma^n \cdot \exp\left(-\frac{\Delta H}{RT}\right) \quad (6.8)$$

where A, n are constants, R is the gas constant, T is the absolute temperature in Kelvin,  $\sigma$  is the external applied stress,  $\Delta H$  is the activation enthalpy of creep process, and  $\dot{\epsilon}_s$  is the secondary strain rate. Faridani [8] explains the formula derivation for creep activation energy with respect to the Larson Miller parameter relation as follows.

$$t_r = \text{constant} \cdot \sigma^{-n} \cdot \exp\left(\frac{\Delta H}{RT}\right) \quad (6.9)$$

Taking logarithms from both sides, results in:

$$\log(t_r) = \log(\text{constant}) - n \cdot \log(\sigma) + \frac{\Delta H}{2.3R} \cdot \frac{1}{T} \quad (6.10)$$

or

$$T \cdot \log(t_r) = T \cdot [\log(\text{constant}) - n \cdot \log(\sigma)] + \frac{\Delta H}{2.3R} = T \cdot [\log C^*] + \frac{\Delta H}{2.3R} \quad (6.11)$$

Then by a given stress  $\sigma$  (constant value):

$$T \cdot [\log(t_r) - \log C^*] = \frac{\Delta H}{2.3R} \quad (6.12)$$

The Larson-Miller parameter is give by:

$$P_{LM} = \frac{\Delta H}{2.3R} = T \cdot [\log(t_r) + C] \quad 10 < C < 20 \quad (6.13)$$

Activation energy (Q) of the test material is calculated by taking C=20 for static creep and  $t_{CF}$  values observed in consecutive CF tests at

$T = 673.15^{\circ}\text{K} = 400^{\circ}\text{C}$ . Table 6.6 presents the activation energies which were calculated for each CF tests with 10, 14 and 21 min hold time at the fixed test temperature  $673.15^{\circ}\text{K}(400^{\circ}\text{C})$ .

**Table 6.6: Activation energies for different hold-times at  $673.15^{\circ}\text{K}(400^{\circ}\text{C})$**

Test No	Temperature ( $^{\circ}\text{K}$ )	Hold Time (min)	Q (J/mole)
1	673.15	10	267,883
2	673.15	14	263,322
3	673.15	21	260,546

Q values presented above are in good agreement with the published values given for steel materials (245-399 kJ/mol) [9].

#### 6.4 Assessment of Creep under CF Condition

This section is divided into four sub-sections. In the first sub-section, creep in cyclic relaxation response under CF conditions is evaluated. The main difference is that the total strain is constant in tensile hold test on the stress is changed with time, whereas the stress is constant in monotonic creep. It may be possible to interpret the stress dependence of the rate change throughout the hold time. It was previously shown that the creep mechanism was identical with that of steady-state in monotonic creep after enough hold time. However, in this steady-state monotonic creep time dependency is neglected regarding the three consecutive regions on a regular creep deformation. Therefore, the applicability of the some highly feasible time dependent creep models (Norton Bailey [1929-1935, 2003], Nuhi's Empirical [8] and Modified Theta [12]) was investigated on the creep curves derived from the cyclic relaxation response under CF condition. In the second sub-section, probability of exceedance estimation at strain 0.006 [mm/mm] is provided. In the following third sub-section,

the simple definition of CF damage proposed by Holmstrom [6] for  $\Phi$  model was applied on Soviet model. Finally, a remaining useful life estimation based on the deterministic framework is presented with respect to a service aged secondary superheater in service conditions.

#### **6.4.1 Creep in Cyclic Relaxation Response under Creep Fatigue Conditions**

In this section, the creep behaviors of stress relaxation in steel alloy during hold time cycled at high temperature ( $673.15^{\circ}\text{K}$ ) have been analyzed. Finally, the prediction performance of the well-known constitutive equations for creep deformation of stress relaxation in the test metal was compared, and degradation versus time graph was drawn to see the trend of creep deformation in cyclic relaxation response.

It has been a benefit that a large amount of creep information can be obtained from the short term of a relaxation test [9]. Since relaxation during most of the tests occurred in cyclically hardened materials, it would have been more appropriate to relate creep damage to stress-rupture curves for material that had been cyclically hardened [9]. For many types of cyclic operation at elevated temperature, the loading history can be approximated by a strain cycle followed by a hold period at constant strain with stress relaxation as illustrated in Figure 3.8 [9]. Determination the form of the relaxation curve is explained in Chapter 3.

Analyzing the value of the activation volume for the initial transient relaxation behavior in which the stress is relaxed drastically, it has been suggested that the rate controlling the dislocation mechanism is either cross slip, or overcoming Peierls-Nabarro stress. Thus the temperature dependence of creep rate was identified during

stress relaxation. It was shown that the creep mechanism is identical with that of steady state in monotonic creep after a long enough hold time, which is the dislocation climb controlled by self diffusion [11]. So if dislocation creep is considered, the strong dependence of creep rate on the applied stress is observed. The main difference is that the total strain is constant in tensile hold test and the stress is changed with time, whereas the stress is constant in monotonic creep. Therefore, it may be possible to interpret the stress dependence of the rate change throughout the hold time [11].

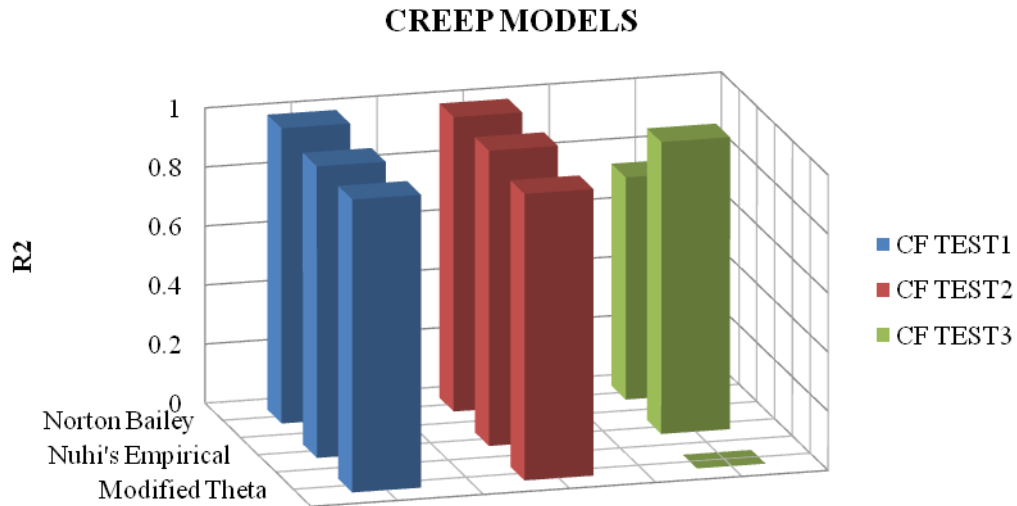


**Figure 6.13:  $R^2$  results for Norton Bailey, Nuhi's Empirical and Modified Theta Models**

Figure 6.13 shows  $R^2$  results for Norton Bailey [1929-1935, 2003], Nuhi's Empirical [8] and Modified Theta Models [12] respectively in each CF test with 10, 14 and 21 min hold times. Since only isothermal relaxation and creep response are treated in this section, the two of the equations evaluated do not include the temperature variable  $T$ . In general applications, temperature should be included.

Since the goal of this section is to initially investigate the feasibility of predicting creep curves from relaxation test results, the closed form of well known creep expressions for the relaxation curve were evaluated. According to the results in Figure 6.13, Nuhi's Empirical Model which was proposed in Ref.[8] presented the best fit throughout the all CF tests. Figure 6.14 shows the creep curves in cyclic relaxation response under CF conditions for 10min (CF Test#1), 14min (CF Test#2) and 21min (CF Test#3) hold times at  $673.155^{\circ}\text{K}(400^{\circ}\text{C})$  according to the Nuhi's Empirical model. The threshold level of 0.006 was defined according to the average useful life results for the three CF tests conducted. It was predicted that nearly after this level the tertiary part of creep curve began.

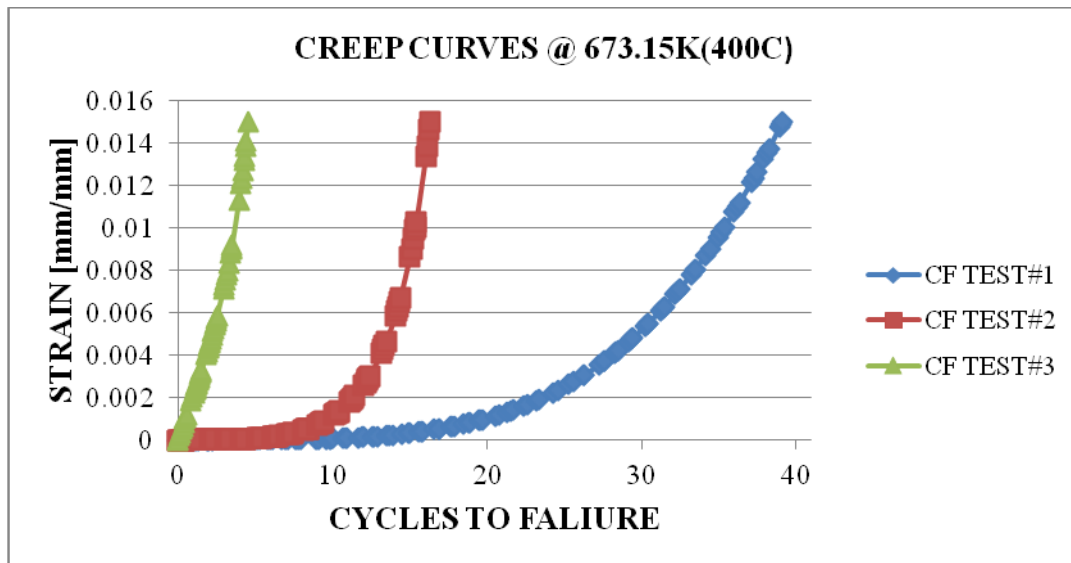


**Figure 6.14: Creep curves in cyclic relaxation response under CF conditions for 10min (CF Test#1), 14min (CF Test#2) and 21min (CF Test#3) hold times at  $673.155^{\circ}\text{K}(400^{\circ}\text{C})$**

#### **6.4.2 Probability of Exceedance Estimation at Strain 0.006 [mm/mm]**

Severe structural deformation of material begins at the end point of the secondary region or the beginning point of the tertiary region. At this level, most of

the cavities begin to agglomerate and forms a crack. In this section, exceedance probability of 0.006 [mm/mm] strain level was calculated for different hold times. A MATLAB code was written to calculate the probability of exceedance at iterative time points for the strain levels beyond the threshold strain of 0.006 [mm/mm] for the steel alloy (see, Figure 6.16).

Table 6.7 presents the probability of exceedance for 0.006 [mm/mm] at different times observed in CF test # 3. From this table it is understood that the test specimen was exposed to a considerable amount of creep damage at 13278.22s (3.415 h).

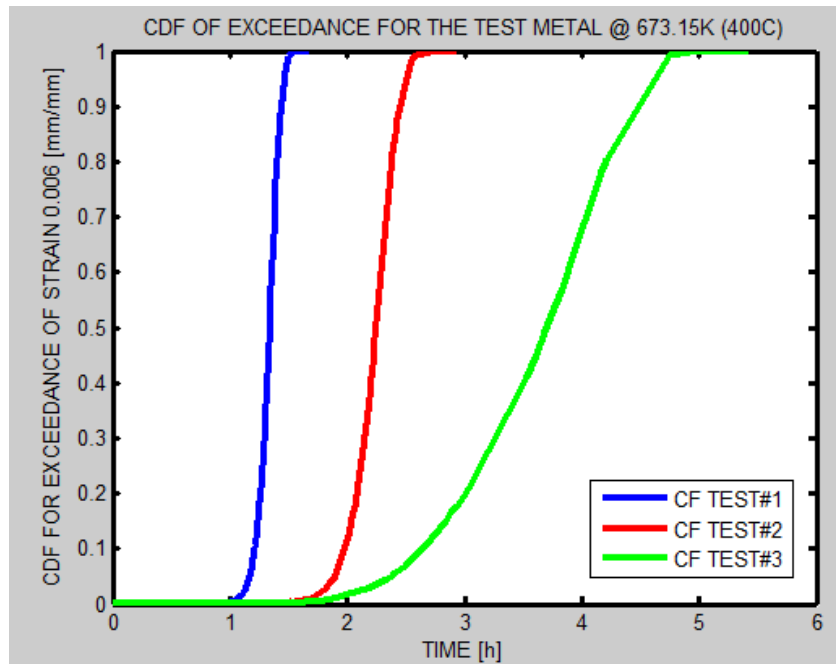


**Figure 6.15: Normal cdf at strain 0.006 [mm/mm] for creep in cyclic relaxation response under CF conditions for 10min (CF Test#1), 14min (CF Test#2) and 21min (CF Test#3) hold times at 673.155°K(400°C)**

**Table 6.7: Probability of exceedance at strain 0.006 [mm/mm] for different times at CF test # 3 (21min hold time)**

CF TEST#3	
Time [s]	$P_E$
13565	0.54
13278	0.49
12995	0.45
12712	0.41
10907	0.21

#### 6.4.3 Damage Assessment in CF

Holmstrom [6] proposes a simple definition of CF damage. In this definition there is no need to separate creep or fatigue damage or life fractions. This simple definition also allows for more straightforward damage assessment for both design and later life assessment than the common methods using summed life (or strain) fractions. This simple definition for simultaneous CF damage is given in Eq.(6.13).

**Table 6.8: Cumulative creep damage in each CF cycle for 21min hold time CF Test#3**

CF Test # 3	Cycles				
	1	2	3	4	5
$D_{CF}$	0.22	0.44	0.65	0.87	1.09

Table 6.8 presents the cumulative creep damage in each simultaneous CF cycle for the last 21min hold test according to this equation.  $t_{CF}$  values was calculated for the maximum stresses observed in each expended cycle of CF test. As the life equation, Soviet Model was chosen since it gave the highest fit for the observed CF

data. All the cumulative hold times were normalized according to the Soviet Model  $t_{CF}$  result for the maximum stress level observed during the test.

$$D_{CF} = \frac{N}{N_{CF}} = \sum \frac{t_h}{t_{CF}} \quad (6.14)$$

#### 6.4.4 Remaining Useful Life in Deterministic Framework

Banerjee et al. [13] previously investigated applicability of a physics based prognostics approach for solder joints using microstructural damage models. In their work, a PCB consisting of a heat generating chip with Ball-Grid Array (BGA) solder joints was considered for avionics application. They calculated remaining useful life (RUL) from the damage for creep and fatigue loads (D) and total mission duration time ( $t_M$ ) as given in Eq.(6.17).

$$RUL = \frac{t_M \times (1 - D)}{D} \quad (6.15)$$

The test data in this study was evaluated with respect to the service-aged superheater used in Ref. [14] to apply the deterministic remaining useful life formula that was derived in Ref. [13]. The service-aged superheater header has the service properties listed in Table 6.9.

Figure 6.16 shows the acceleration factor trend with respect to the use level stress 17.3 MPa. The acceleration factor versus stress plot displays the acceleration factor as a function of stress based on the specified use stress level. The acceleration factor is a ratio of the use stress level divided by the accelerated stress levels which were the maximum stress levels observed during the each CF tests.

**Table 6.9: Basic details of the service-aged secondary superheater [14]**

<b>Material</b>	2.25Cr-1Mo (JIS STPA24)
<b>Operation temperature</b>	569°C
<b>Operation pressure</b>	17.3MPa
<b>Operated hour</b>	163,000hr
<b>Dimension</b>	508mm in OD x 272mm in ID

After the extrapolating damage trend, which was observed in the creep fatigue tests conducted, to the proposed service stress level 17.3MPa, the damage was predicted as 0.63 regarding the service conditions defined in Ref. [14]. The RUL was predicted as 95,730 h. Therefore, the inspection time should be chosen nearly at this operation time which was predicted by the Eq.(6.15).

Accurate prediction of RUL would enable a user to gauge the health of an existing unit and optimally plan maintenance schedules as well as help in designing the unit to withstand the loads for the intended application.

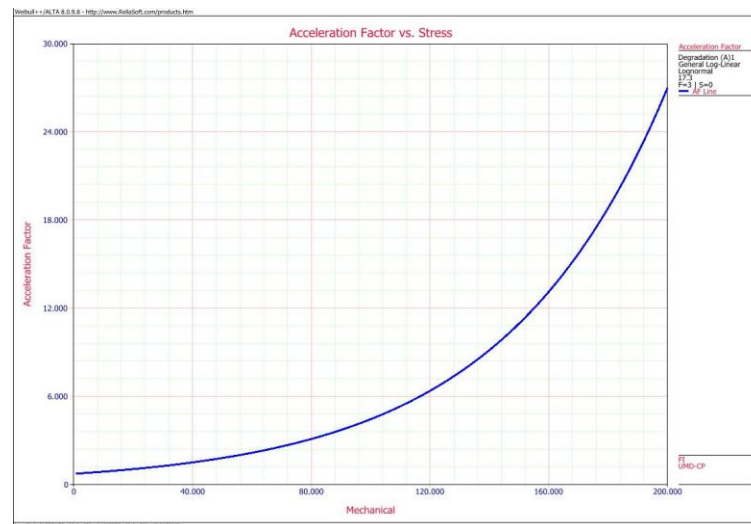


**Figure 6.16: Acceleration factor graph with respect to the specified use level stress 17.3 MPa**

## 6.5 References

- [1] Trunin, I.I., Golubova, N.G. & Loginov, E.A., "A new method of the extrapolation of creep-test and long-time strength results," Proc 4<sup>th</sup> Int Symp on Heat-Resistant Metallic Materials, Mala Fatra, CSSR, pp. 168-176, 1971.
- [2] Larson, F.R., Miller, E.J., "Time-temperature relationship for rupture and creep stresses," *Trans. ASME*, vol.74, p.765-775, 1952.
- [3] Orr, R.L., Sherby, O.D., Dorn, J.E., "Correlations of rupture data for metals at elevated temperatures," *Trans. ASM*, vol.46, pp:113-118, 1954.
- [4] Manson, S.S., Haferd, A.M., "A linear time-temperature relation for extrapolation of creep and stress rupture data," NACA TN 2890, 1953.
- [5] Wilshire, B., Scharning, P.J., Hurst, R., "A new approach to creep data assessment," *Materials Science and Engineering A*, Vol.510-511, Issue:3-6, 2009.
- [6] Holmström, S., Auerkari, P., "A robust model for creep-fatigue life assessment," *Materials Science & Engineering A*, Vol.559, pp:333-335, 2013.
- [7] Holdsworth, S.R. (Ed.), ECCC Recommendations, Vol.5, 2005.
- [8] Faridani, M.N. and Modarres, M., "Classification and probabilistic model development for creep failures of structures: study of X-70 carbon steel and 7075-T6 aluminum alloys," Thesis, In partial fulfillment of the requirements of the degree of Master of Science, Fall 2011.
- [9] Syn, C.K., Lesueur, D.R., Sherby, O.D., Taleff, E.M., "Stress-strain rate relations in ultrahigh carbon steels deformed in the ferrite range of temperature," *Materials Science Forum*, Vol.426-432, pp:853-858, 2003.
- [10] Jaske, C.E., Mindlin, H., and Perrin, J.S., "Combined Low-Cycle Fatigue and Stress Relaxation of Alloy 800 and Type 304 Stainless Steel at Elevated Temperatures," *Fatigue at Elevated Temperature, ASTM STP 520*, American Society for Testing Materials, pp:365-376, 1973.
- [11] Jeong, C.Y., Nam, S.W., "Stress dependence on stress relaxation creep rate during tensile holding under creep-fatigue interaction in 1Cr-Mo-V steel," *Journal of Material Science*, Vol.34, pp:2513-2517, 1999.
- [12] Evans, R.W., and Wilshire, B., "Creep of metals and alloys," *Institute of Metals*, 1985.

- [13] Banerjee, A., Koul, A., Kumar, A. and Goel, N., "Physics based Prognostics of Solder Joints in Avionics," *Annual Conference of the Prognostics and Health Management Society*, 2011.
- [14] Takagi, Y., Otsuki, S., "Creep-fatigue characteristics of partial repair welds and full repair welds on aged 2.25Cr-1Mo Steel," *CMMI*, Vol.3, Issue:1, 2004.

## **Chapter 7: Conclusions and Recommendations for Future Work**

Creep-fatigue (CF) expended life models were derived and validated using experimental results for an steel alloy. The robust CF expended life model was first used along with the CF of ferritic steel P91, austenitic steel, and Ni alloy by [1]. The predictions compared well with the experimental results within a scatter band close to factor of 2. This demonstrates the predictive capability of CF expended life models modified in this thesis. Uncertainties of each parameter predicted were defined using the Bayesian inference framework. Validation of simultaneous CF loading expended life models - apart from modified Wilshire model proposed by Holmstrom [1] - was accomplished in this study. The most of the previous studies have been focused mainly on the sequential CF loading expended life models. These modified models are based on the creep rupture behavior, and their input parameters are described by the hold time in tension, and maximum stress observed in each CF test. The creep behavior of cyclic relaxation response in the steel alloy under CF conditions was also analyzed.

A summary of accomplished tasks are presented below.

1. Existing creep-rupture models other than Wilshire were modified to simultaneous CF loading expended life models.
2. Isothermal CF tests under strain control, with stress ratio  $R=0$  and hold periods in tension were conducted on steel alloy samples to validate the CF expended life models modified.
3. The suggested CF expended lifetime approach by Holmstrom [1] was

confirmed in this study as an effective CF expended lifetime.

4. The modified CF expended life models were shown to predict the observed CF expended life of the tested material steel alloy sample with a scatter band close to a factor of 2.
5. CF expended life of the steel alloy was found to decrease with increase in hold time under strain control.
6. Modified CF expended life models were evaluated under Bayesian inference framework using experimental data, and posterior distributions of the predicted parameters were proposed assuming a normally distributed likelihood function.
7. Uncertainties of the predicted CF expended life model parameters were defined using Bayesian inference results.
8. Activation energies ( $Q$  values) in different hold times at  $673.15^{\circ}K$  ( $400^{\circ}C$ ) were calculated. It was observed that  $Q$  values were in good agreement with the published values for steel materials (245-399 kJ/mol).
9. The creep behavior of cyclic relaxation response in the steel alloy under CF conditions was analyzed for the overall CF expended life for each experiment. The prediction performance of the well known constitutive equations was compared based on the experimental results. Details can be further reviewed in Section 6.4. It was observed that the main difference between creep in cyclic relaxation response and monotonic creep stems from total strain and stress change with respect to time. Creep in cyclic relaxation response demonstrates a constant total strain and changing stress until the specified end

criterion for the CF test. However, monotonic creep demonstrates a constant stress and changing total strain until rupture.

10. At strain 0.6%, probability of exceedance for different times in CF test with 21 min hold time was estimated. It was understood that the test sample was exposed to a considerable amount of creep damage at 13278.22s (3.415h) at CF test with 21 min hold time.
11. Damage assessment in simultaneous CF loading was estimated according to the approach proposed by Holmstrom [1]. This approach does not need separation in CF damage or expended life. In order to predict the expected CF expended life for each peak stress observed in CF cycles, the results provided in Section 5.2 were referred to. Among the modified CF expended life models which performed acceptable prediction performance on the test material, the Soviet Model was chosen to evaluate damage assessment for CF test with 21 min hold time.
12. A remaining useful life example in deterministic framework was presented. Accurate prediction of Remaining Useful Life (RUL) would enable a user to gauge the health of an existing unit and optimally plan maintenance schedules as well as help in designing the unit to withstand the loads for the intended application.

Recommendations for future work:

1. Additional CF tests at room temperature could help observe how stable the stress relaxation response in each CF experiments performed in this study was. This could also help understand the noise pattern in CF data at elevated

temperature, and could also provide more accurate characterization of creep behavior.

2. In the course of model validation, it was understood that additional hot tension tests at the specified test temperature would help understand the exact high-temperature mechanical properties of the concerned test material. In that case, the Wilshire model could yield a higher goodness of fit since it was observed that Wilshire model provided the highest coefficient of determination value based on the CF data provided in Ref.[2]. There might also be material dependence affecting the prediction of Wilshire model. Additional hot tension tests at pre-determined test temperatures prior to starting the actual CF experiments would help device a better test plan, and also help understand the prediction performance of the proposed models with respect to the changing material properties.
3. The validity of data can be examined with respect to reproducibility between tests. More test samples are needed to perform this. It may be worthy to investigate the reproducibility of these CF tests to understand validity of the test data from this perspective.
4. CF tests can be initially modeled using finite element software packages such as ANSYS or Abaqus. The results from these simulations can be compared to actual experimental results.

## **7.1 References**

- [1] Holmström, S., Auerkari, P., “A robust model for creep-fatigue life assessment,” *Materials Science & Engineering A*, Vol.559, pp:333-335, 2013.

- [2] Takashi, Y., Shibamo, H., and Inoue, K., “Long-term creep rupture vebahieur of smoothed and nothched bar specimens of low-carbon nitrogren-controlled 316 stainless steel (316FR) and their evaluation,” *Nuclear Engineering Design*, Vol.238, 00:310-321, 2008.

## Appendix A-I: Thermocouple Clip Design Process

The simplest way to measure the temperature in a 600°C furnace is to use a thermocouple. For this experimental work, the temperature at the surface of the metal test pieces, in particular in the reduced diameter section is of particular interest. Two temperature measurements were made one at the top of the sample (far away from the reduced diameter section) and another at the surface of the reduced diameter section. There are two standard ways to attach the thermocouples to the samples glue and a metal clip, analogous to the original wooden clothes peg, the latter was chosen for this work. Small stainless steel clips (single piece, no moving parts) which had a dual feature to ensure the spherical thermocouple junction was held against the cylindrical metal sample were used. One side of peg's gap had a groove to align against the side of the cylinder, and the other side had a pocket to hold the ball on the tip of the thermocouple, so pushing the clip on automatically put the thermocouple in the right place. The thermal mass of the clip was low enough to not affect the heating of the test piece. Attached thermocouple clip and its design picture are provided in Figure A-I.1.

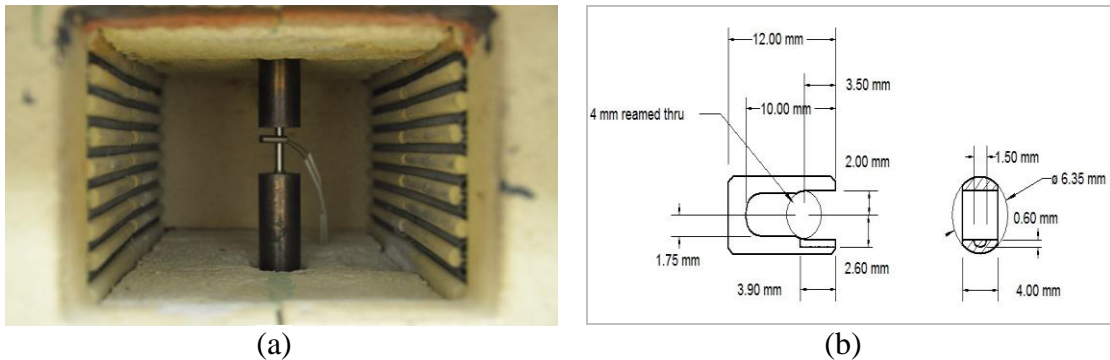


**Figure A-I.1: (a) Thermocouple clip attached to test sample, and (b) thermocouple clip design dimensions**

## Appendix B-I: Epoxy Mold Design Process

Due to lack of existing epoxy molds to fit into the polishing machine, custom epoxy molds were created using polyethylene. . The shape of the epoxy mold was cylindrical, with diameter 1.25" and height ~0.5". The tolerance of the diameter was wide ( $\pm 0.010$ ") and the height was nominal ( $\pm 0.20$ "). In order to fabricate the mold, first a 1.5" diameter polyethylene bar was bored out to depth 0.5" and diameter 1.25" leaving a thin walled bottom only 0.020" thick. Next the interior of the mold was wiped with a thin film of oil to act as a mold release. Then the sample was placed on the thin-walled bottom and epoxy potting mix (Allied Epoxy Mount Resin and Hardener) was poured on top to fill up the cup. After curing, the bottom was pushed, and since it was flexible (due to the thin wall), the cylindrical plug readily came out making it ready for the polishing machine. The standalone fabricated epoxy mold and a mounted sample epoxy are shown in Figure B-I.1.

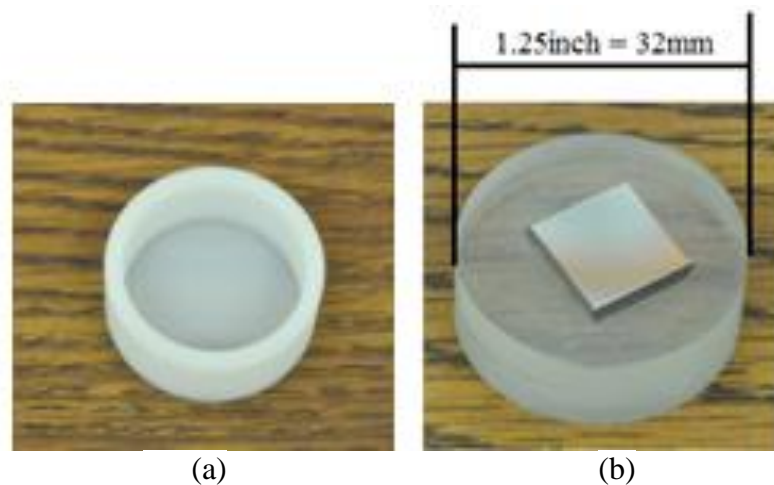


**Figure B-I.1: (a) Epoxy mold produced, (b) mounted sample using epoxy mold**

## Appendix C-I: WINBUGS Codes for Soviet Model

```
model{
  #Here the prior distributions for the model parameters b0, b1 and b4 as well as
  #the prior distribution for s, the standard deviation of normal likelihood, are
  #defined. Here, both normal and non-informative uniform distributions are
  #preferred.
  b0 ~ dnorm(-8.888,0.1)
  b1 ~ dnorm(3.789,0.1)
  b4 ~ dnorm(-3.612,0.1)

  s ~ dunif(0,10)

  #Constants are specified.
  C<- 1000
  b2 <- -8.755E-11
  b3 <- -9452

  #For likelihood function, a normal distribution is assumed, and it is written
  #out, rather than using normal distribution function (dnorm) already part of
  # the BUGS code.
  for(i in 1 : N) {
    zeros[i] <- 0
    L[i] <- exp(-0.5 * pow((x[i,2] -
(b0+(b1*log(x0[i]))+(b2*log(x[i,1]))+(b3/x0[i])+(b4*(x[i,1]/x0[i]))))/s,2))/(pow((2 *
3.141592654), 0.5) *s)
    ghr[i]<- (-1) * log(L[i]) + C
    zeros[i] ~ dpois(ghr[i])
  }

  #Here it is asked WinBUGS to use the standard deviation from the normal
  #likelihood to estimate the 'error' in the model which the data are fitted. For
  #the error, e, the normal distribution that is already provided in WinBUGS is
  #used. It is assumed that the error has a mean of 0.
  tau<-1/pow(s,2)
  e~dnorm(0,tau)

  #Here the sample variance is calculated.
  for(i in 1:N) { c.x1[i] <- x1[i] - mean(x1[]) }
  sy2 <- inprod(c.x1[], c.x1[])/(N-1)

  #Here Bayesian version R squared is calculated.
  R2B <- 1 - e/sy2}
```

## Appendix C-II: WINBUGS Codes for Larson Miller Model

```
model{
  #Here the prior distributions for the model parameters b0, b1 and b2 as well as
  #the prior distribution for s, the standard deviation of normal likelihood, are
  #defined. Here, both normal and non-informative uniform distributions are
  #preferred.
  b0 ~ dnorm(-0.00421,0.1)
  b1 ~ dnorm(1.36E+4,0.1)
  b2 ~ dnorm(-3283,0.1)

  s ~ dunif(0,10)

  #Constant is specified.
  C<- 1000

  #For likelihood function, a normal distribution is assumed, and it is written
  #out, rather than using normal distribution function (dnorm) already part of
  #the BUGS code.
  for(i in 1 : N) {
    zeros[i] <- 0
    L[i] <- exp(-0.5 * pow((x[i,2] - (-
20+(1/x0[i])*(b0+b1*x[i,1]+b2*(pow(x[i,1],2))))/s , 2))/(pow((2 * 3.141592654) ,
0.5) *s)

    ghr[i]<- (-1) * log(L[i]) + C
    zeros[i] ~ dpois(ghr[i])
  }

  #Here it is asked WinBUGS to use the standard deviation from the normal
  #likelihood to estimate the 'error' in the model which the data are fitted. For
  #the error, e, the normal distribution that is already provided in WinBUGS is
  #used. It is assumed that the error has a mean of 0.
  tau<-1/pow(s,2)
  e~dnorm(0,tau)

  #Here the sample variance is calculated.
  for(i in 1:N) {c.x1[i] <- x1[i] - mean(x1[])}
  sy2 <- inprod(c.x1[], c.x1[])/(N-1)

  #Here Bayesian version R squared is calculated.
  R2B <- 1 - e/sy2
}
```

## Appendix C-III: WINBUGS Codes for Orr Sherby Dorn Model

```

model{
  #Here the prior distributions for the model parameters b0, b1 and b2 as well as
  #the prior distribution for s, the standard deviation of normal likelihood, are
  #defined. Here, both normal and non-informative uniform distributions are
  #preferred.
  b0 ~ dnorm(-39.46,0.1)
  b1 ~ dnorm(-2.999,0.1)
  b2 ~ dnorm(-0.0003486,0.1)

  s ~ dunif(0,10)

  #Constant is specified.
  C<- 1000

  #For likelihood function, a normal distribution is assumed, and it is written
  #out, rather than using normal distribution function (dnorm) already part of
  #the BUGS code.
  for(i in 1 : N) {
    zeros[i] <- 0
    L[i] <- exp(-0.5 * pow((x[i,2] -
  ((31744/x0[i])+b0+b1*x[i,1]+b2*(pow(x[i,1],2))))/s , 2))/(pow((2 * 3.141592654) ,
  0.5) *s)

    ghr[i]<- (-1) * log(L[i]) + C
    zeros[i] ~ dpois(ghr[i])
  }

  #Here it is asked WinBUGS to use the standard deviation from the normal
  #likelihood to estimate the 'error' in the model which the data are fitted. For
  #the error, e, the normal distribution that is already provided in WinBUGS is
  #used. It is assumed that the error has a mean of 0.
  tau<-1/pow(s,2)
  e~dnorm(0,tau)

  #Here the sample variance is calculated.
  for(i in 1:N) {c.x1[i] <- x1[i] - mean(x1[])}
  sy2 <- inprod(c.x1[], c.x1[])/(N-1)

  #Here Bayesian version R squared is calculated.
  R2B <- 1 - e/sy2
}

```

## Appendix C-IV: WINBUGS Codes for Manson Haferd

### Model

```

model{
  #Here the prior distributions for the model parameters b0,b1 and b2 as well as
  #the prior distribution for s, the standard deviation of normal likelihood, are
  #defined. Here, both normal and non-informative uniform distributions are
  #preferred.
  b0 ~ dnorm(5.634,0.1)
  b1 ~ dnorm(-0.4502,0.1)
  b2 ~ dnorm(-1.027E-6,0.1)

  s ~ dunif(0,10)

  #Constant is specified.
  C<- 1000
  b5 <- -29.9
  Ta <- 666.5

  #For likelihood function, a normal distribution is assumed, and it is written
  #out, rather than using normal distribution function (dnorm) already part of
  #the BUGS code.
  for(i in 1 : N) {
    zeros[i] <- 0
    L[i] <- exp(-0.5 * pow((x[i,2] - (b5+((x0[i]-Ta)*b0)+((x0[i]-
Ta)*(b1*x[i,1]))+(x0[i]-Ta)*(b2*pow(x[i,1],2))))/s , 2))/(pow((2 * 3.141592654) ,
0.5) *s)

    ghr[i]<- (-1) * log(L[i]) + C
    zeros[i] ~ dpois(ghr[i])
  }

  #Here it is asked WinBUGS to use the standard deviation from the normal
  #likelihood to estimate the 'error' in the model which the data are fitted. For
  #the error, e, the normal distribution that is already provided in WinBUGS are
  #used. It is assumed that the error has a mean of 0.
  tau<-1/pow(s,2)
  e~dnorm(0,tau)

  #Here the sample variance is calculated.
  for(i in 1:N) { c.x1[i] <- x1[i] - mean(x1[]) }
  sy2 <- inprod(c.x1[], c.x1[])/(N-1)

  #Here Bayesian version R squared is calculated.
  R2B <- 1 - e/sy2
}

```

## Appendix C-V: WINBUGS Codes for Wilshire Model

```
model{
  #Here the prior distributions for the model parameters k and u as well as the
  #prior distribution for s, the standard deviation of normal likelihood, are
  #defined. Here, non-informative uniform distributions are preferred.
  k~ dunif(0,10000)
  u ~ dunif(0,1)
  s ~ dunif(0,10)

  #Constant is specified.
  C<- 1000

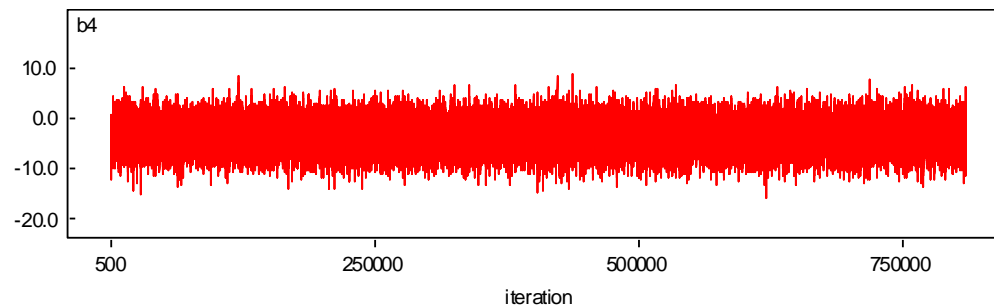
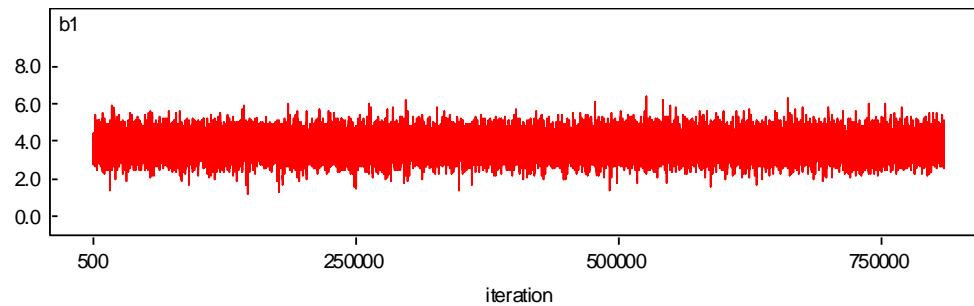
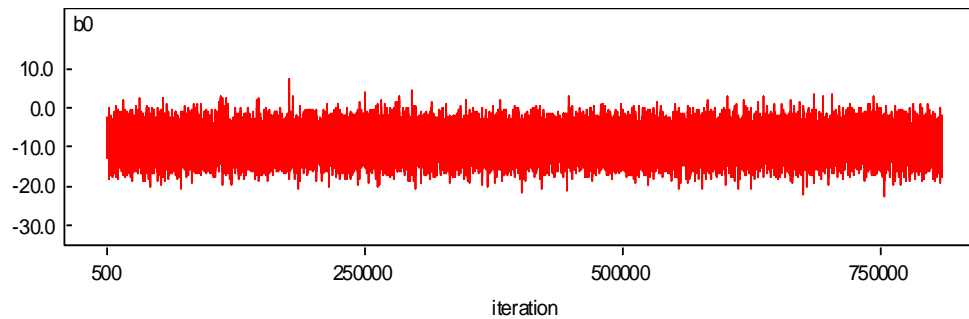
  #For likelihood function, a normal distribution is assumed, and it is written
  #out, rather than using normal distribution function (dnorm) already part of
  #the BUGS code.
  for(i in 1 : N) {
    zeros[i] <- 0
    L[i] <- exp(-0.5 * pow((x[i,2] - (pow((x[i,1]/-
k),1/u)*3.0E+20))/s , 2))/(pow((2 * 3.141592654) , 0.5) *s)
    ghr[i]<- (-1) * log(L[i]) + C
    zeros[i] ~ dpois(ghr[i])
  }

  #Here it is asked WinBUGS to use the standard deviation from the normal
  #likelihood to estimate the 'error' in the model which the data are fitted. For the
  #error, e, the normal distribution that is already provided in WinBUGS are
  #used. It is assumed that the error has a mean of 0.
  tau<-1/pow(s,2)
  e~dnorm(0,tau)

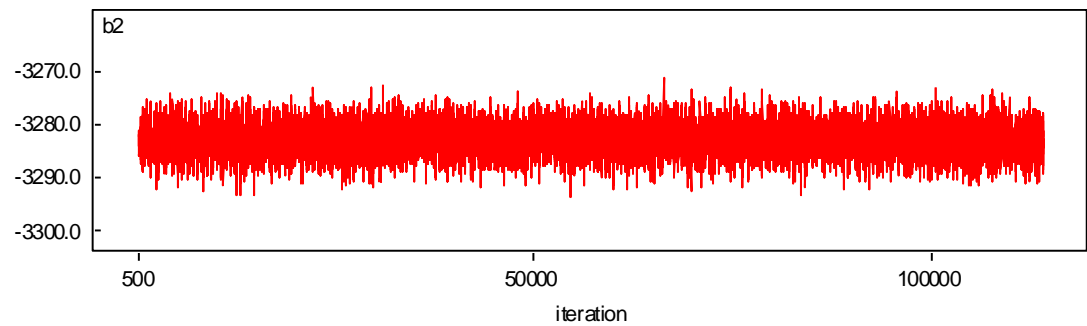
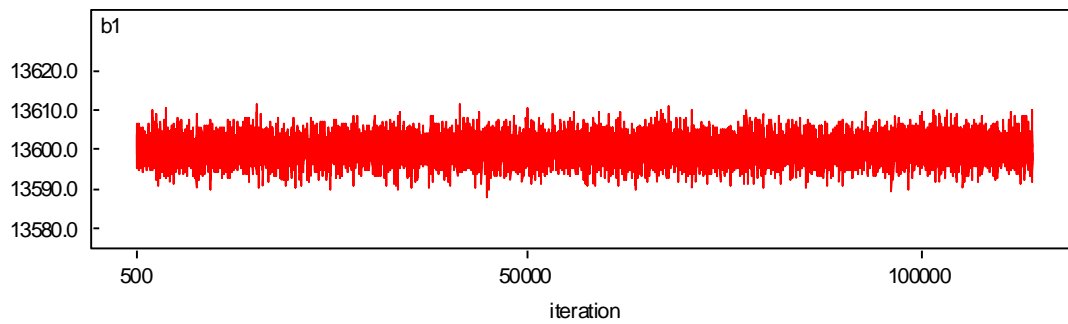
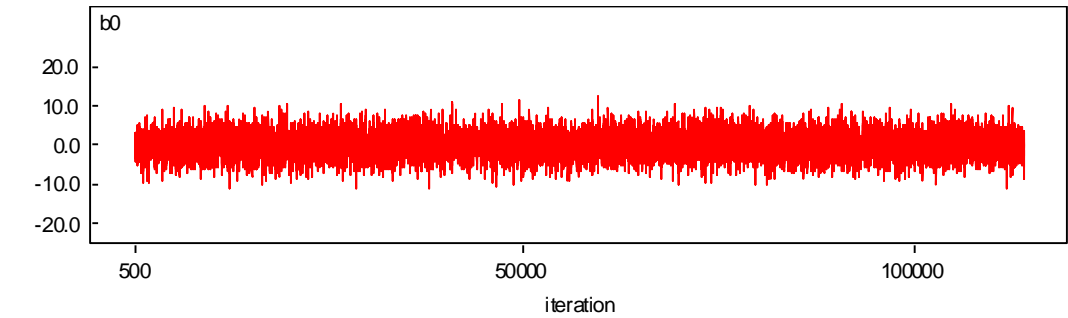
  #Here the sample variance is calculated.
  for(i in 1:N) { c.x1[i] <- x1[i] - mean(x1[])}
  sy2 <- inprod(c.x1[], c.x1[])/(N-1)

  #Here Bayesian version R squared is calculated.
  R2B <- 1 - e/sy2
}
```

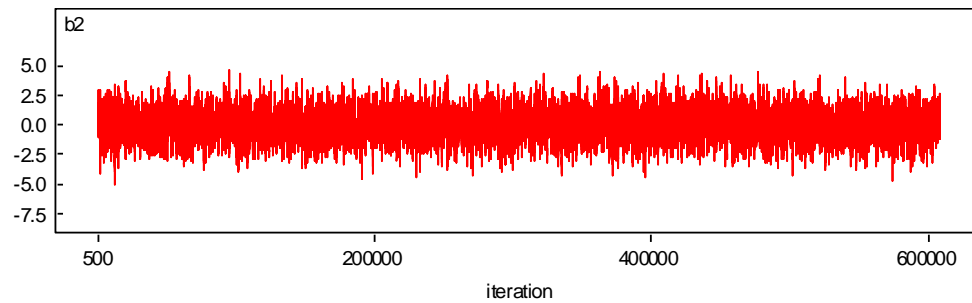
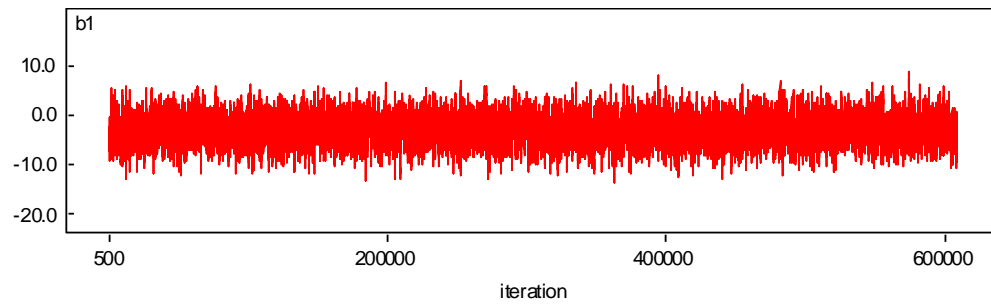
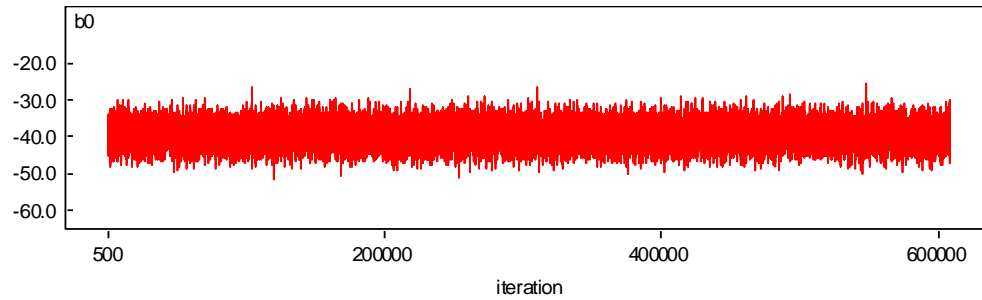
## Appendix D-I: WINBUGS Chain History for Soviet Model Parameters



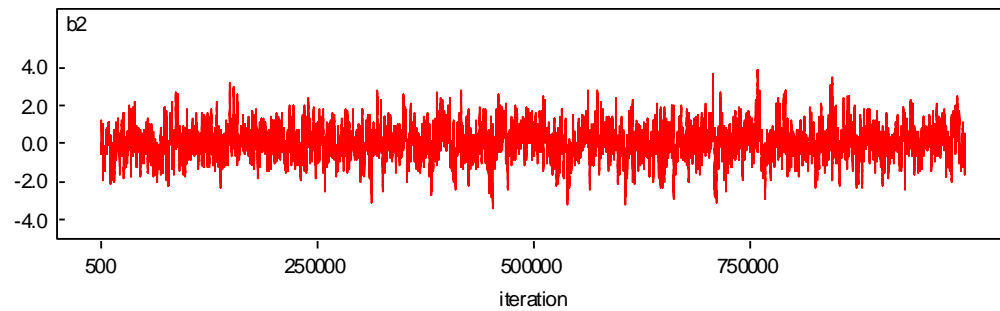
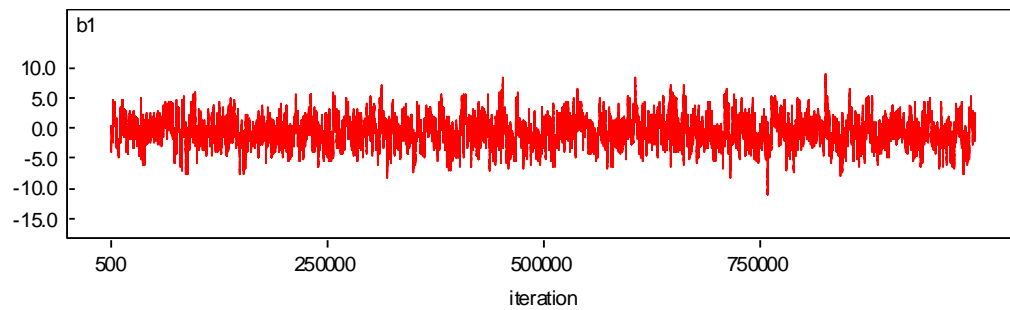
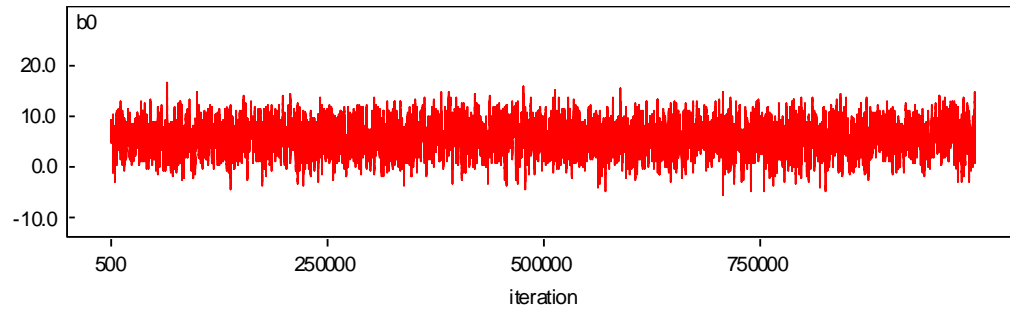
## Appendix D-II: WINBUGS Chain History for Larson Miller Model Parameters



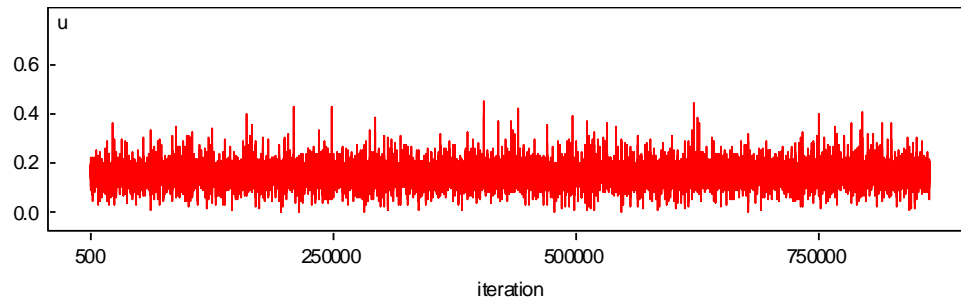
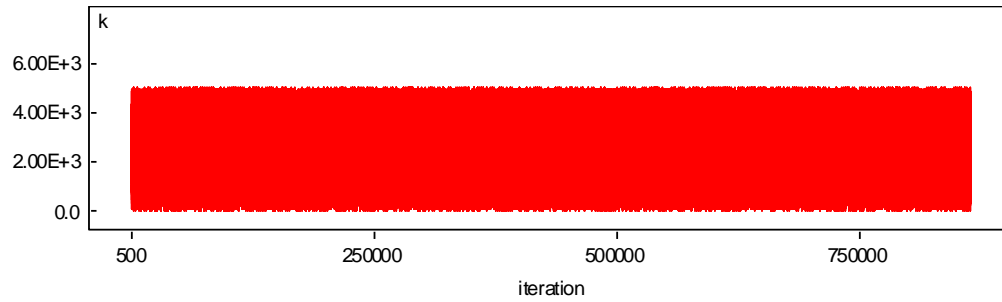
## Appendix D-III: WINBUGS Chain History for Orr-Sherby Dorn Model Parameters



## Appendix D-IV: WINBUGS Chain History for Manson Haferd Model Parameters



## Appendix D-V: WINBUGS Chain History for Wilshire Model Parameters



## Bibliography

A.S.T.M., “Symposium on the Effect of Cyclic Heating and Stressing on Metals at Elevated Temperatures,” (Special Tech. Publ. No.165), Philadelphia, Pa. (Amer. Soc. Test. Mat.), 1954.

Anon. Code Case N-47, ASME boiler and pressure vessel code, “Criteria for design of elevated temperature,” Class 1 Components in section III, division 1, *American Society of Mechanical Engineers*, 1976.

Asayama, T. and Tachibana, Y., “Collect Available Creep-Fatigue Data and Study Existing Creep-Fatigue Evaluation Procedures for Grade 91 and Hastelloy XR,” DOE/ASME Generation IV Materials Project, Japan Atomic Energy Agency, September 30, 2007.

ASTM Standard E2714-09e1, “Standard test method for creep-fatigue testing,” ASTM International, West Conshohocken, PA, 2009, DOI: 10.1520/E2714-09EOI, [www.astm.org](http://www.astm.org).

ASTM Standard E407-07, “Standard practice for microetching and alloys,” ASTM International, West Conshohocken, PA, 2007, DOI: 10.1520/E0407-07, [www.astm.org](http://www.astm.org).

ASTM Standard E606/E606M, “Standard Test Method for Strain-Controlled Fatigue Testing,” ASTM International, West Conshohocken, PA, 2012, DOI: 10.1520/E0606-04E01, [www.astm.org](http://www.astm.org).

ASTM Standard E8/E8M-11, “Standard test methods for tension testing on metallic materials,” ASTM International, West Conshohocken, PA, 2011, DOI:10.1520/E0008\_E0008M-11, [www.astm.org](http://www.astm.org).

Baker and Cane model: Baker AJ, O'Donnell MP. R5 high temperature structural integrity assessment of a cracked dissimilar metal weld vessel test. In: Proceedings of second international conference on integrity of high temperature welds, London, 10–12 November 2003.

Banerjee, A., Koul, A., Kumar, A. and Goel, N., “Physics based Prognostics of Solder Joints in Avionics,” Annual Conference of the Prognostics and Health Management Society, 2011.

BJF-model: Jones, D.I.G, French, R.M. and Bagley, R.L.; A Renewal Theory of Inelastic Thermo-Mechanical Behavior of Metal Alloys; ASME AD-Vol. 50, Fatigue and Fracture at Elevated Temperatures, A. Nagar and S. Mall, ed.; Book No. H01013 1995.

Brinkman, C.R., “High temperature time-dependent fatigue behavior of several engineering structural alloys,” *International Metal Reviews*, Vol.30, Issue 5, pp:235-258, 1985.

Brinkman, C.R.; Booker, M.K.; and Ding, J.L.: Creep and Creep-Rupture Behavior of Alloy 718. Proceedings of the International Symposium on the Metallurgy and Applications of Superalloys 718, 625, and Various Derivatives, Minerals, Metals & Materials Society, Warrendale, PA, 1991.

Burt, H. and Wilshire, B., *Metall. Mater. Trans. A* 35A, pp. 1691–1701, 2004.

Burt, H. and Wilshire, B., *Metall. Mater. Trans. A* 36A (2005), pp. 1219–1227, 2005.

Carden, A.E., McEvily, A. and Wells, C.H., *Fatigue at elevated temperatures*, American Society for Testing and Materials, 1974.

Chen, J. and Young, B., “Stress-strain curves for stainless steel at elevated temperatures,” *Engineering Structures*, Vol.28, pp: 229-239, 2006.

Chrzanowski, M., “Use of the damage concept in describing creep-fatigue interaction under prescribed stress,” *International Journal of Material Sciences*, Vol.18, Issue 2, pp.69-73, 1976.

Coffin, L.F., “Methods for predicting life in fatigue,” *American Society of Mechanical Engineers*, pp:1-24, New York, 1979.

Coffin, L.F., “Fatigue at high temperature – prediction and interpretation,” *Inst MechEng*, Vol.188 9, Issue 74, pp.109-127, 1974.

Diercks, D.R. and Raske, D.T., “A statistical analysis of elevated temperature, strain controlled fatigue data on type 304 stainless steel,” *ASME Annual Winter Meeting*, New

York, December 5-10, 1976.

Eno, D.R., and Young, G.A., "A unified view of engineering creep parameters," *Proceedings of PVP2008, ASME Pressure Vessels and Piping Division Conference*, July 21-31, Chicago, Illinois, 2008.

Evans, J.L. and Saxena, A., "Modeling Creep Fatigue," In. Furrer D.U. and Semiatin, S.L. (Eds.), *ASM Handbook*, Vol.22A: Fundamentals of Modeling for Metals Processing, pp:419-428, 2009.

Evans, R. W. and Wilshire, B., *Introduction to Creep*, The Institute of Materials, London 1993.

Evans, R.W., and Wilshire, B. "Creep of Metals and Alloys", The Institute of Metals, London, 1985.

Faridani, M.N, and Modarres, M., "A probabilistic model of creep failure mechanism for structural reliability assessment with applications," 2012.

Faridani, M.N. and Modarres, M., "Classification and probabilistic model development for creep failures of structures: study of X-70 carbon steel and 7075-T6 aluminum alloys," Thesis, In partial fulfillment of the requirements of the degree of Master of Science, Fall 2011.

Fatemi, A. and Yang, L., "Cumulative fatigue damage and life prediction theories: a survey of the state of the art for homogenous materials," *International Journal of Fatigue*, Vol.20, Issue: 1, pp:9-34, 1998.

Frith, P.H., "Properties of Wrought and Cast Aluminum and Magnesium Alloys at Room and Elevated Temperatures," London (H.M. Stationery Office), 1956.

Goswami, T. and Hanninen, H., "Dwell effects on high temperature fatigue behavior Part I," *Materials and Design*, Vol.22, pp:199-215, 2001.

Goswami, T., "Creep-fatigue life prediction of Cr-Mo steel alloys," In. Laiw, P.K., Bunchanan, R.A., Klarstrom, D.L., Wei, R.P., Harlow, D.G., Tortorelli, P.F. (Eds.), *Material lifetime science and engineering*, pp.43-50, 2003.

Goswami, T., "Development of generic creep-fatigue life prediction models," *Materials and Design*, Vol.25, pp.277-288, 2004.

Goswami, T., "Low-cycle fatigue life prediction - a new model," *International Journal of Fatigue*, Vol. 19, Issue 2, pp:109-115, 1997.

Graham, A. and Walles, K.F.A. ; NGTE Reports Nos.R.100(1952), R.137 (1953), R.189 and R.190 (1956); J. Iron and steel Inst.179,105, 1955.

Haford, G.R., Saltsman, J.F., and Hirschberg, M.H., "Ductility normalized strainrange-partitioning life relations for creep-fatigue life predictions," Conference on Environmental Effects and Degradation of Engineering Materials, Virginia, October 10-12, 1977.

Halford, G.R., Saltsman, J.F. and Hirschberg, M.H., "Ductility normalized strain range partitioning life relations for creep-fatigue life predictions," NASA Report TMX 67838, 1971.

He, X., "Statistical thermal fatigue-creep modeling of stainless steel materials," fatigue endurance," *Metals Technology*, pp:297-305,1981.

He, X., Li, G. and Ding, Y., "Statistical thermal creep-fatigue modeling of 316 stainless steel materials," *Scientific Research Essays*, Vol.6, Issue 20, pp:7172-7178, 19 September, 2011.

Hempel, H. and Krug, H., *ibid.*, Vo.24, Issue:77, 1942.

Hempel, M. and Ardelt, F., *ibid.*, Vol.21, Issue:115, 1939.

Hempel, M. and Tillmanns, H.E., *Mitt. K.-W.Inst.Eisenforsch*, Vol.18, Issue:163, 1936.

Holdsworth, S.R. and Davies, R.B., "A recent advance in the assessment of creep rupture data," *Nuclear Engineering and Design*, Vol.190, pp:287-296, 1999.

Holdsworth, S.R., "Component Assessment Data Requirements from Creep-Fatigue Tests," *Journal of ASTM International*, 2011, [www.astm.org](http://www.astm.org).

Holdsworth, S.R., Gandy, D., "Towards a standard for creep-fatigue testing," *Advances in Materials Technology for Fossil Power Plants Proceedings from the Fifth International Conference*, In. Viswanathan, R., Gandy, D., and Coleman, K. (Eds.), pp: 689-701, 2008.

Holdsworth, S.R., Merckling, G., "ECCC developments in the assessment of creep rupture data," In: Proceedings of sixth international Charles Parsons Conference on engineering issues in turbine machinery, power plant and renewable, Trinity College Dublin, 16-18 September, 2003.

Holmstörn, S. and Auerkari, P., "A robust model for creep-fatigue life assessment," *Materials Science & Engineering A*, Vol. 559, pp.333-335, 2013.

Holmstrom, S., "Engineering Tools for Robust Creep Modeling," PhD Dissertation, *VTT Publications 728*, The Faculty of Engineering and Architecture, The Aalto University School of Science and Technology, Espoo, Finland, 2010.

Huang, R., *Turbine Technol.* 43, pp: 9–13, 2001.

Jaske, C.E., Mindlin, H., and Perrin, J.S., "Combined Low-Cycle Fatigue and Stress Relaxation of Alloy 800 and Type 304 Stainless Steel at Elevated Temperatures," *Fatigue at Elevated Temperature*, ASTM STP 520, American Society for Testing Materials, pp:365-376, 1973.

Jeong, C.Y. and Nam, S.W., "Stress dependence on stress relaxation creep rate during tensile holding under creep-fatigue interaction in 1Cr-Mo-V steel," *Journal of Materials Science*, Vol.34, pp:2513-2517, 1999.

Johnson, G.R.; Cook, W.H., "A constitutive model and data for metals subjected to large strains, high strain rates and high", 1983.

Johnson, G. R., Cook, W.H. ; Fracture characteristics of three metals subjected to various strain rates, temperatures and pressures, *Eng. Fracture Mechanics*, Vol.21, Issue:1, pp:31-48, 1985.

Kachanov, L. M., *Izv. AN SSSR, OTN* 8, pp. 26–31, 1958.

Kachanov, L. M., *The Theory of Creep*, British Library, Boston Sp, Wetnerley, 1960.

Kennedy, A.J., "Proceedings of the International Conference on Fatigue of Metals," p:401, London(Inst. Mech. Eng.), 1956.

Lafen, J.H. and Jaske, C.E., "Cyclic relaxation response under creep-fatigue conditions," *Stress Relaxation Testing, ASTM STP 676*, pp:182-206, 1976.

Lafen, J.H. and Jaske, C.E., "Cyclic relaxation response under creep-fatigue conditions," *Stress Relaxation Testing, ASTM STP 676*, pp:182-206, 1976.

Langer, B.F., "Design of pressure vessels for low-cycle fatigue," *J Basic Eng*, Vol.84, Issue 3, pp.389-402, 1962.

Larson, F.R., Miller, E.J., "Time-temperature relationship for rupture and creep stresses," *Trans. ASME*, vol.74, p.765-775, 1952.

Larson, F.R., Miller, J., "A time-temperature relationship for rupture and creep stress," *Trans. ASME*, Vol.74, p:765, 1952.

Li, J. and Dasgupta, A., "Failure mechanisms and models for creep and creep rupture," *IEEE Transactions on Reliability*, Vol.42, No.3, 1993.

Lin, J., Kowalewski, Z. L. and Cao, J., *Int. J. Mech. Sci.* 47, pp. 1038–1058, 2005.

Ling, X., Zheng, Y. Y. and You, Y. J., *Int. J. Pressure Vessels Piping* 84 (2007), pp:304-309, 2007.

Lloyd, G.J. and Wareing, J., "Life prediction methods for combined creep rupture," *IEEE Transactions on Reliability*, Vol.42, No.3, 1993.

Maiya, P.S., "Effects of wave shape and ultrahigh vacuum on elevated temperature low cycle fatigue in type 304 stainless steel," *Material Science and Engineering*, Vol.47, pp.13-21, 1981.

Majumdar, S., Maiya, P.S., "Wave shape effects in elevated temperature low-cycle fatigue of type 304 stainless steel," *ASME/CSME Pressure Vessel and Piping Conference*, PVP-PB 028, 1978.

Manson, S.S. and Muralidharan, U., "Analysis of creep-rupture data for five multi-heat alloys by the minimum commitment method using double heat term centering," *Progress in Analysis of Fatigue and Stress Rupture MPC-23*, ASME, pp:43-60, 1984.

Manson, S.S., "A complex subject – some simple approximations," *Experimental Mechanics*, Vol.5, Issue 7, pp:193-326, 1965.

Manson, S.S., Haferd, A.M., "A linear time-temperature relation for extrapolation of creep and stress rupture data," *NASA TN*, 2890, 1953.

Manson, S.S., Halford, G.R. and Hirschberg, M.H., "Creep-fatigue analysis by strain-range partitioning," *1<sup>st</sup> National Pressure Vessel and Piping Conference Sponsored by the American Society of Mechanical Engineers*, pp: 12-24, New York, 1971.

Manson, S.S., *Thermal stress and low cycle fatigue*, McGraw-Hill, p:171, New York, 1966.

Mao, H., Mahadevan, S., "Reliability analysis of creep-fatigue failure," *International Journal of Fatigue*, Vol.22, pp:789-797, 2000.

Maruyama, K. et al. ; Long-term creep curve prediction based on the modified  $\theta$  projection concept. *J. Pressure Vessel Technol.*, 112, 1990.

Meleka, A.H., "Combined creep and fatigue properties," *Metallurgical Reviews*, Vol.7, Issue:25, 1962.

Modarres, M., Kaminskiy, M, Krivtsov, V., *Reliability Engineering and Risk Analysis, A Practical Guide*, CRC Press, 2<sup>nd</sup> Edition, 2010.

Modified Theta model in: R.W. Evans and B. Wilshire, *Creep of metals and alloys*, Institute of Metals, 1985.

Moles, M. D. C. and Westwood, H. J.; "Residual life estimation of high temperature superheater and reheater tubing, CER RP, 78-66, Final report of Ontario Hydor Research Dev., Toronto, for the Canadian Electrical Assn., Montreal, pp: 67-82, Mar. 1982.

Ntzoufras, I., *Bayesian Modelling Using WinBUGS*, In. Giudici, P., Givens, G.H. and Mallick, B.K. (Eds.), John Wiley & Sons, Inc., Canada, 2009.

Orr, R.L., Sherby, O.D., Dorn, J.E., "Correlation of rupture data for metals at elevated temperatures," *Trans. ASM*, Vol:46, p:113, 1954.

Ostergren, W. J., "A Damage Function and Associated Failure Equations for Predicting Hold Time and Frequency Effects in Elevated Temperature, Low Cycle Fatigue," *Journal of Testing and Evaluation*, JTEVA, Vol. 4, No.5, pp.327-339, Sept. 1976.

Ostergren, W.J., "A damage function and association failure equations for predicting hold time and frequency effects in elevated temperature, low cycle fatigue," *Journal of Testing and Evaluation*, Vol.4, Issue 5, pp. 327-339, 1976.

Prager, M. 'Development of the MPC Omega method for life assessment in the creep range', *ASME J. Pressure Vessel Technology*, 117, May, 95-103, 1995.

Rabotnov, Y. N. ; On the equation of state of creep, *ASME/ASTM/IMEchE Proceedings Conference on creep*, Inst. Mech. E., New York/London, 1963.

Rabotnov, Y. N., *Creep Problems in Structural Members*, Amsterdam, North-Holland 1969.

Rabotnov, Y.N. ; Some problems of the theory of creep, *NACA., TM*, 1353, 1953.

Seruga, D. and Nagude, M., "Uniform of the most commonly used time-temperature creep parameters," *Material Science and Engineering A*, Vol.528, pp:2804-2811, 2011.

Sonoya, K., Nonaka, I. and Kitagawa, M., "Prediction of creep-fatigue lives of Cr-Mo steels with Direcks Eq.," *ISIJ International*, Vol. 1, No.12, pp.1424-1430, 1991.

Steel, R. G. D. and Torrie, J. H., *Principles and Procedures of Statistics*, New York: McGraw-Hill, pp:187-287, 1960.

Sun, G., Chen, Z., Liu, Z., "Analytical and Experimental Investigation of Thermal Expansion Mechanism of Steel Cables," *Journal of Materials in Civil Engineering*, Vol.1017, July 2011.

Syn, C.K., Lesueur, D.R., Sherby, O.D., Taleff, E.M., "Stress-strain rate relations in ultrahigh carbon steels deformed in the ferrite range of temperature," *Materials Science Forum*, Vol.426-432, pp:853-858, 2003.

Takagi, Y., Otsuki, S., "Creep-fatigue characteristics of partial repair welds and full repair welds on aged 2.25Cr-1Mo Steel," *CMMI*, Vol.3, Issue:1, 2004.

Takahashi, Y., Shibamoto, H. and Inoue, K., "Study on creep-fatigue life prediction methods for low-carbon nitrogen-controlled 316 stainless steel (316FR)," *Nuclear Engineering and Design*, Vol.238, pp:322-335, 2008.

Takashi, Y., Shibamoto, H., Inoue, K., "Long-term creep rupture behavior of smoothed and notched bar specimens of low-carbon nitrogen-controlled 316 stainless steel (316 FR) and their evaluation," *Nuclear Engineering and Design*, Vol.238, pp:310-321, 2008.

Tapsell, H.J., "Symposium on High-Temperature Steels and Alloys for Gas Turbines" (Special Rep. No.43), p:169, London (Iron and Steel Inst.), 1952.

Tapsell, H.J., Forrest, P.G., and Tremain, G.R., *Engineering*, Vol.170, Issue:189, 1950.

The Engineering Toolbox, *Coefficients of Thermal Expansion*. [available online: [http://www.engineeringtoolbox.com/linear-expansion-coefficients-d\\_95.html](http://www.engineeringtoolbox.com/linear-expansion-coefficients-d_95.html)]

Toland, J. and Goswami, T., "General creep-fatigue life prediction models," *Journal of the Mechanical Behavior of Materials*, Vol.15, Issue 1-2, 2004.

Truman, R.S. et al., "Elevated-temperature tensile, creep and rupture properties of 18%Cr-8%Ni, 18%Cr-12%Ni-Mo, 18%Cr-10%Ni-Ti, and 18%Cr12%Ni-Nb steels," *Proceedings of Joint Conference Organizaed by the British Iron and Steel Research Association and the Iron and Steel Institute*, pp:265-300, Eastbourne, UK, 1966.

Trunin, I.I., Golobova, N.G., Loginov, E.A., "New method of extrapolation of creep test and long time strength results," *In: Proceedings of the Fourth International Symposium on Heat-Resistant Metallic Materials*, Mala Fatra, CSSR, p:168,1971.

Wendell, F., *A Handbook on Accelerated Testing*, In Fulfillment of the Scholarly Paper Requirement for the Degree of Master of Science in Reliability Engineering, Modarres,

M. (Adv.), Department of Mechanical Engineering, University of Maryland, College Park.

Wilshire, B., Scharning, P.J. and Hurst, R., “A new approach to creep data assessment,” *Material Science and Engineering A*, Vol.510-511, pp:3-6, 15 June 2009.

Wilshire, B., Scharning, P.J., Hurst, R., “A new approach to creep data assessment,” *Materials Science and Engineering A*, Vol:3, Issue:6, pp:510-511, 2009.

Zhao, Bin, et.al., “Experiment and simulation of creep damage for duralumin alloy” 2A12, *Material Science and Engineering A* 513-514, 91-95, 2009.